PETROLOGY OF THE TACONIAN-ACADIAN OVERLAP ZONE, HARTLAND BELT, WESTERN CONNECTICUT

Peter Welch

Thesis submitted to the faculty of

Virginia Polytechnic Institute and State University

in Partial fulfillment of the requirements for the degree of

Master of Science

in Geological Sciences

Robert J. Tracy, Chairman
Robert J. Bodnar
James R. Craig

May 1999
Blacksburg, Virginia

Keywords: Metamorphic Petrology, Garnet zoning, Hartland Belt, Cameron's Line

PETROLOGY OF THE TACONIAN-ACADIAN OVERLAP ZONE, HARTLAND BELT, WESTERN CONNECTICUT

By
Peter Welch

Committee Chairman: Robert J. Tracy
Geological Sciences

ABSTRACT

Cameron's Line in western Connecticut and its equivalents in western Massachusetts and Vermont mark a major tectonic boundary in the New England Appalachians and are considered by many to delineate the trace of the Taconian suture zone. The Cambro-Ordovician Ratlum Mountain and Rowe Formations lie to the east of Cameron's Line in western Connecticut. Mineral equilibria and compositional zoning studies for pelitic units of the Ratlum Mountain and Rowe Formations indicate that garnet porphyroblast rims equilibrated with matrix minerals at P-T conditions that are consistent with an Acadian (Devonian) metamorphic field gradient for this area. P-T conditions were calculated by simultaneously solving for a geothermometer and a geothermobarometer in low-variance assemblages. All of the possible equilibria for each sample were then calculated using an internally consistent thermodynamic database with the software TWEEQU (thermobarometry with estimations of equilibria). Both of these methods produced consistent results with peak P-T conditions of 575-650 ˚ C and 6-9 kbars.

Wavelength dispersive X-ray compositional images (WDS images) along with quantitative traverses for major (Fe, Mg, Mn and Ca) elements were collected for garnet porphyroblasts in each of the samples. Trace (Y, P, Sc, Ti and Cr) element WDS images and quantitative traverses were then collected for representative samples. Petrographic observations coupled with WDS compositional imaging show that early garnet porphyroblasts have been modified either by overgrowths of biotite and chlorite or by a second phase of garnet growth. For those garnets that show two phases of growth, compositional images reveal patchy Ca content in rounded overgrowths surrounding more homogeneous euhedral cores. This is consistent with a second phase of growth of garnet at higher pressure accompanied by anorthite breakdown. Yttrium compositional images for these sample show a very narrow band of Y enrichment that lies just inside these high-Ca overgrowths. Garnets that have been overgrown by biotite have compositional images and quantitative traverses indicative of continuous prograde growth with minor resetting of chemistry along garnet rims. These overgrowths are thought to be the result of the compositionally complex continuous reaction,

Grt + Ms → An + Bt.

Although Y images for these samples show a similar narrow band of Y enrichment, in these samples this band of enrichment lies within a few microns of the garnet rim. Biotite overgrowths truncate compositional zoning for both major and trace elements and therefore postdates porphyroblast growth. Compositional images for these samples generally show euhedral zoning patterns suggesting that diffusion was very limited both during and after growth.

Peak P-T conditions are consistent with previously documented conditions for this region in that they suggest a predominantly Acadian metamorphic signature. There is strong evidence that garnet porphyroblast cores predate these overgrowth textures and thus may represent a resetting of Taconian garnet cores with matrix minerals during the Acadian. Maximum P-T conditions (600 ˚ C and 9 kbars) were obtained from a sample collected in close proximity to Cameron's Line. If these P-T conditions represent the thermal maximum accompanying Acadian metamorphism then there is likely also some resetting of mineral assemblages to the west of Cameron's Line.

ACKNOWLEDGEMENTS

My time in Blacksburg and at Virginia Tech has been successful and pleasant due in large part to unending support of many people. First and foremost, I would like to extend thanks to my family for their support and encouragement in every project I have undertaken however foolish they may have been. I should also offer special thanks (or blame) to my two sisters, Kathy and Sue, for first introducing me to idea of pursuing studies in the geological sciences.

Many thanks are also due to may advisor, Robert Tracy, for acting as both friend and mentor. He has been a pleasure to work with and I have learned a great deal about petrology as well as other more important things under his tutelage. The rest of faculty in the Dept. of Geological Sciences have also been very supportive of my effort. Special thanks are extended to my committee members James Craig and Robert Bodnar as well as to the dept. chairman Cahit Çoruh. Credit is also due to Todd Solberg for his many hours of assistance collecting microprobe data. Every graduate student I have known during my stay here (which has been a long one) would not have made it without the support and help of the staff and many thanks are due to them as well.

My friends within the group of graduate students in this dept are many. I have spent many long hours of misery and pleasure since the days of Theoretical Petrology with Dr Hewitt. I would like to extend thanks to my friends for those many hours of discussion of the periodic table, geology, fishing ,….. Mona, Court ,Jun, Max, Sven, Adam, Maria, Eric, Jim, Luca, Jay and especially to Rhonda.

I have enjoyed my time here and will miss Blacksburg very much.

TABLE OF CONTENTS

LIST OF FIGURES

LIST OF TABLES

INTRODUCTION

The Appalachian orogen is an elongate tectonic region that spans most of the east cost of North America from Alabama to Newfoundland (Hatcher 1989). It is the culmination of the tectonometamorphic processes of four major collision events and one major rifting event generally younging from west to east: Grenville (≈ 1100-1000 Ma), rifting of the Laurentian margin (≈ 800-575 Ma), Taconic (≈475-445 Ma), Acadian (≈415-380 Ma) and Alleghenian (≈300-275 Ma). Although these events may be considered to be discrete events in time, the areas affected by both older and younger events may show changes in mineralogy, mineral chemistry, textures and structures superimposed by the younger event on those same features produced in an older event. And by the nature of orogenesis, each individual event may be further complicated by involvement of multiple phases of metamorphism and deformation.

Cameron's Line in western Connecticut and its equivalents in western Massachusetts and Vermont mark a major tectonic boundary in the New England Appalachians and are considered by many to delineate the trace of the Taconian suture zone (Zen, 1972; Stanley and Ratcliffe, 1985; Amenta and Mose, 1985). It marks the easternmost exposure of Grenville age (> 900 Ma) basement gneisses and associated cover rocks (Merguerian 1983) and the westernmost occurrence of the distal facies of metasediments in the Taconic thrust slices. In western Connecticut, it separates the Cambro-Ordovician miogeoclinal sequence of (Zen , 1972) from the eugeoclinal sequence of the Iapetos Ocean to the east.

The Cambro-Ordovician Ratlum Mountain and Rowe Formations lie to the east of Cameron's Line in western Connecticut and consist of quartzites, schists and amphibolites that have been metamorphosed to amphibolite grade (Rodgers, 1985). Argon isotopic thermochronologic work by Sutter and others (1985) has assigned an Acadian age to the peak metamorphism to this region. A northeast-trending belt

(≈ 4 km wide) of Acadian (390 Ma) metamorphic overprinting of Taconian (450 Ma) mineral assemblages was clearly documented by Hames and others (1991) in the Everett and Canaan Mountain Taconic allochthons in northwestern Connecticut and eastern New York. This belt of overprinting coincides with an area identified by Agar (1932) as a the "zone of retrogression" and contains textures very similar to those identified in the Ratlum Mountain and Rowe schists east of Cameron's line in western Connecticut.

There has been no detailed petrologic investigation of the mineral assemblages in rocks east of Cameron's Line since the work of Gates (1952) and thus none involving modern quantitative petrologic techniques. One of the key aspects in understanding the complex history of polymetamorphic terranes is to be able to distinguish the effects of progressive changes in metamorphic assemblages produced in a single event from those changes that may be the result of superimposed metamorphism in a later event. The goals of this study were to establish to what extent Acadian metamorphic overprinting of Taconian metamorphic mineral assemblages can be recognized in this area and to distinguish between those features caused by prograde Taconic metamorphism and those changes induced in the Acadian overprint.

This was done through a careful examination of mineral textures, chemical analysis of mineral compositions and garnet zoning, mineral exchange thermobarometry, and calculations of mineral equilibria. Detailed analysis of garnet zoning was undertaken by collecting analog composition maps (wavelength dispersive X-ray images) along with quantitative analysis traverses on the electron microprobe. This combination of techniques provided very detailed information about the extent to which zoning in garnets has been produced during growth and modified later. Because growth zoning in garnets is very commonly preserved in amphibolite grade rocks, careful areal analysis of zoning patterns provided insights into perturbations from later events superimposed on preexisting crystals. Microprobe point analyses of

garnet and matrix minerals were then collected in appropriate locations on crystals for calculations of mineral equilibria and determination of peak temperature and pressure. Estimated conditions of metamorphism were then compared to those east and west of Cameron's Line that have been determined in previous studies in order to place peak metamorphic conditions for this study area into the tectonic framework for western Connecticut and adjacent New York.

GEOLOGIC SETTING

The Connecticut Valley synclinorium (CVS) extends over 1000 km from the Gaspé Peninsula southwestward across Quebec and western Maine, across northern New Hampshire, eastern Vermont, western Massachusetts and Connecticut, to Long Island Sound (Hatch, 1988). The CVS is composed of Lower to Middle Paleozoic metasedimentary, and to a lesser extent metavolcanic, rocks of the former Iapetos Ocean. In western Connecticut, the CVS is bounded to the west by Cameron's Line and to the east by the eastern Border Fault (Rodgers 1985) of the Mesozoic Connecticut Valley graben (Hartford Basin).

The CVS is a narrow belt approximately 10 km wide at the Connecticut-Massachusetts border which broadens to a maximum width in west-central Connecticut of 40 km at the latitude of the Waterbury Dome (Dietsch, 1988). Rodgers (1985) divided the rocks of the CVS in western Connecticut into three groups, the Hartland Belt, the Gneiss Dome Belt and the Orange-Milford Belt. He grouped the Cambro-Ordovician metasedimentary and metavolcanic rocks of the Iapetos Ocean have been grouped as the Hartland Belt (Rodgers, 1985). This group extends from Cameron's Line eastward to a north-south trending belt of domes (called the Gneiss Dome Belt) just to the west of the Western Border Fault. The Gneiss Dome Belt comprises those rocks exposed in the shallow domal structures and the contiguous units that flank them Dietsch, 1989). The Silurian-Devonian age Straits Schist is thought to overlie both the Hartland and Gneiss Dome belts and is considered to be structurally involved with both of them (Dietrich, 1968). The third belt, the Orange-Milford belt, lies just to the north and west of New Haven, Connecticut. The Orange-Milford belt is separated from the Hartland and Gneiss Dome belts by the northeast-trending East Derby fault and is bounded to the east by the Mesozoic Hartford Basin. This belt consists of greenschist through amphibolite facies metasedimentary and metavolcanic rocks of Ordovician through Devonian ages.

The Hartland Belt forms the crystalline terrain of the western Highlands of Connecticut east of Cameron's Line (Merguerian, 1983). The Hartland Formation of Gates (1952) was subdivided into upper and lower members by Merguerian (1983) and then renamed as the Ratlum Mountain and Rowe Formations by Rodgers (1985). This belt of Cambro-Ordovician metasedimentary and metavolcanic rocks forms a roughly continuous belt along the eastern flank of the Berkshires and Green Mountains from Connecticut northward to Massachusetts and Vermont. The Ratlum Mountain and Rowe Schists in Connecticut are thought to be correlative with Savoy and Rowe Schists in Massachusetts of Zen and others (1983) and the Moretown Formation in Vermont (Rodgers, 1985).

Figure 1 Generalized geologic map of western Connecticut after Dietsch (1988) and Rodgers (1985). Boxed area shows approximate outline of Figure 2 with detailed sample locations.

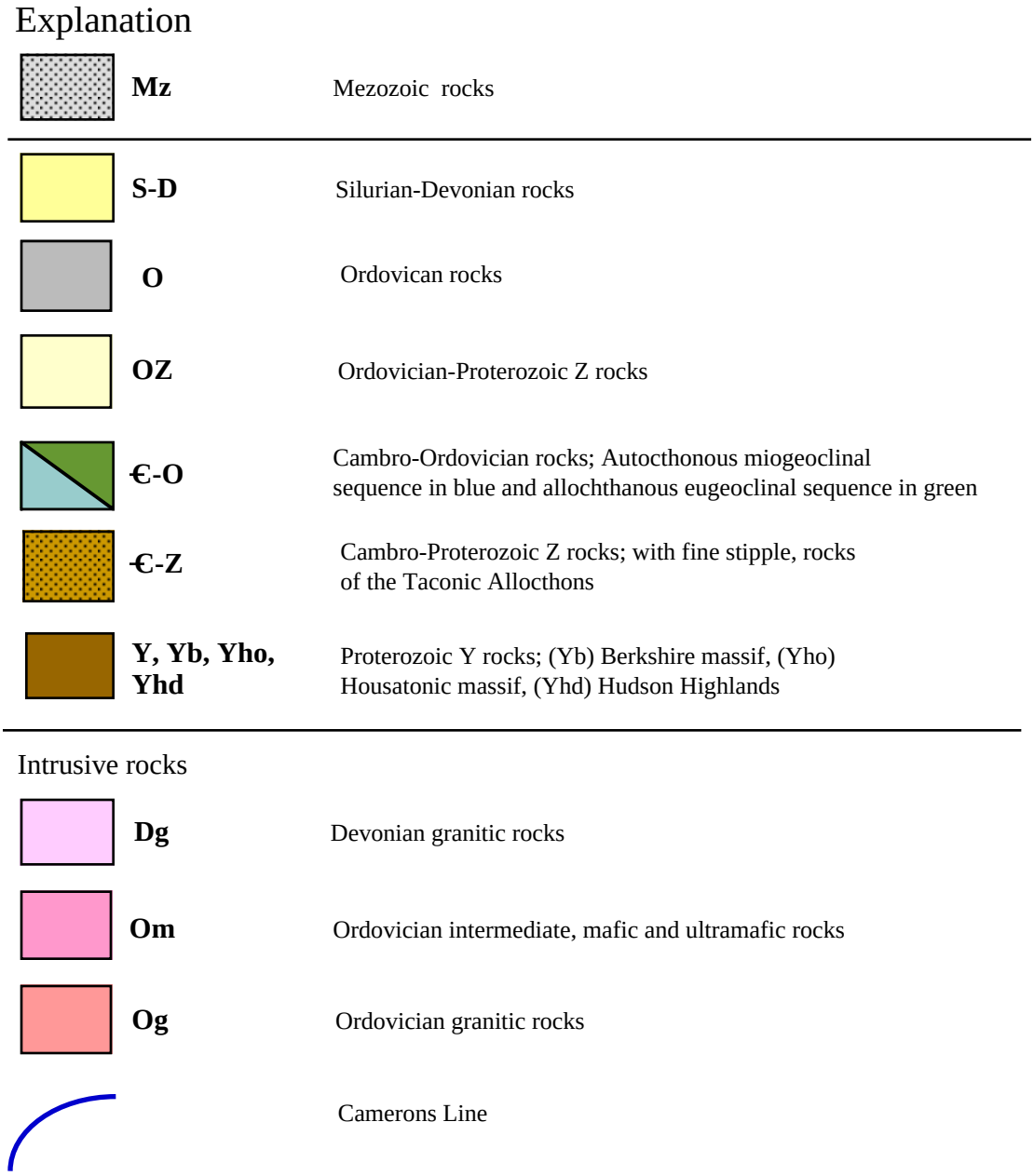

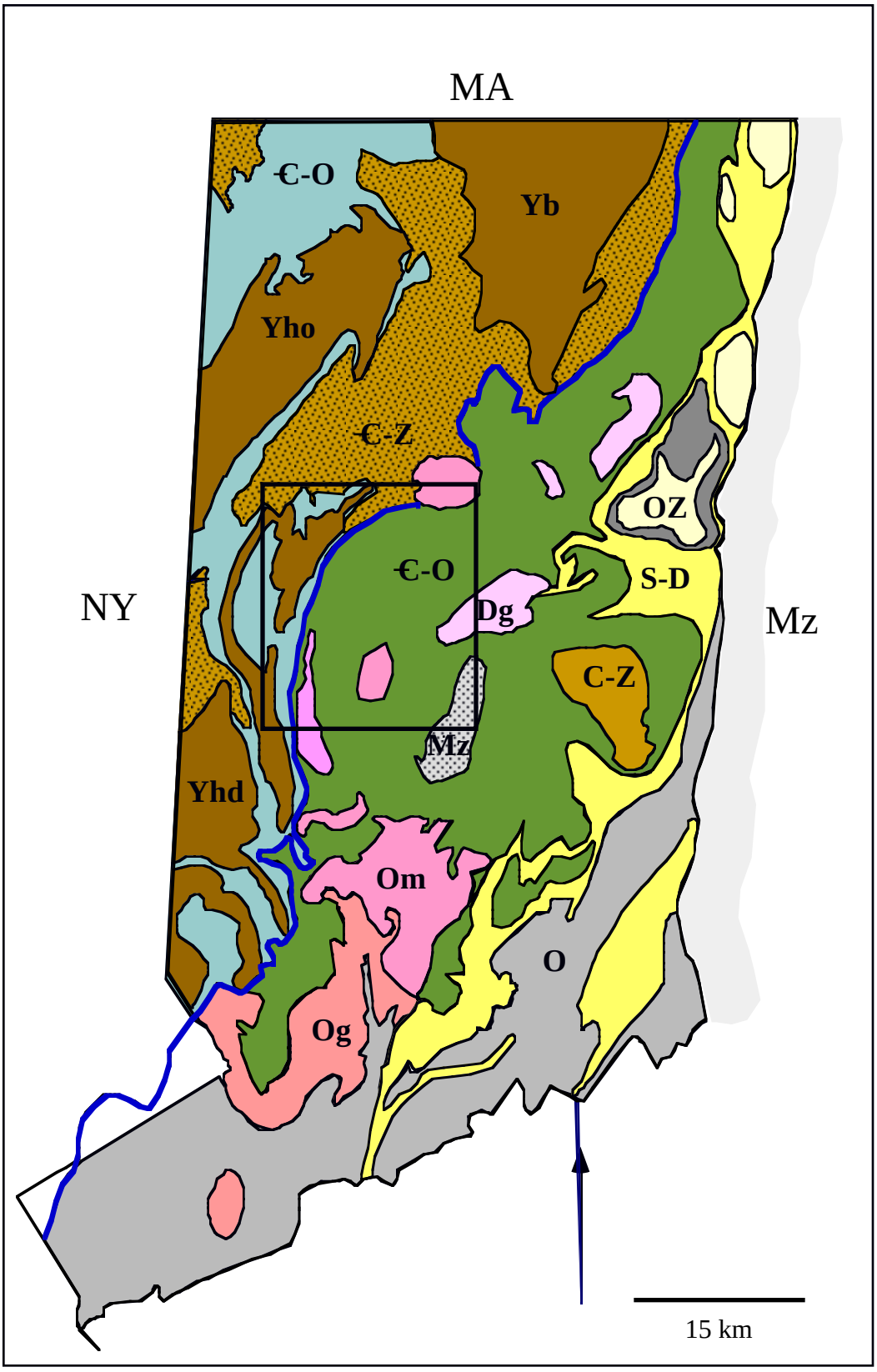
MA
NY
Mz
Є-O
Yb
Yho
Є-Z
OZ
Є-O
S-D
Dg
C-Z
Mz
Yhd
Om
O
Og
15 km

Figure 2 Geologic map of study area showing New Preston and Roxbury quadrangles after Rodgers (1985) with sample locations for detailed microprobe analysis.

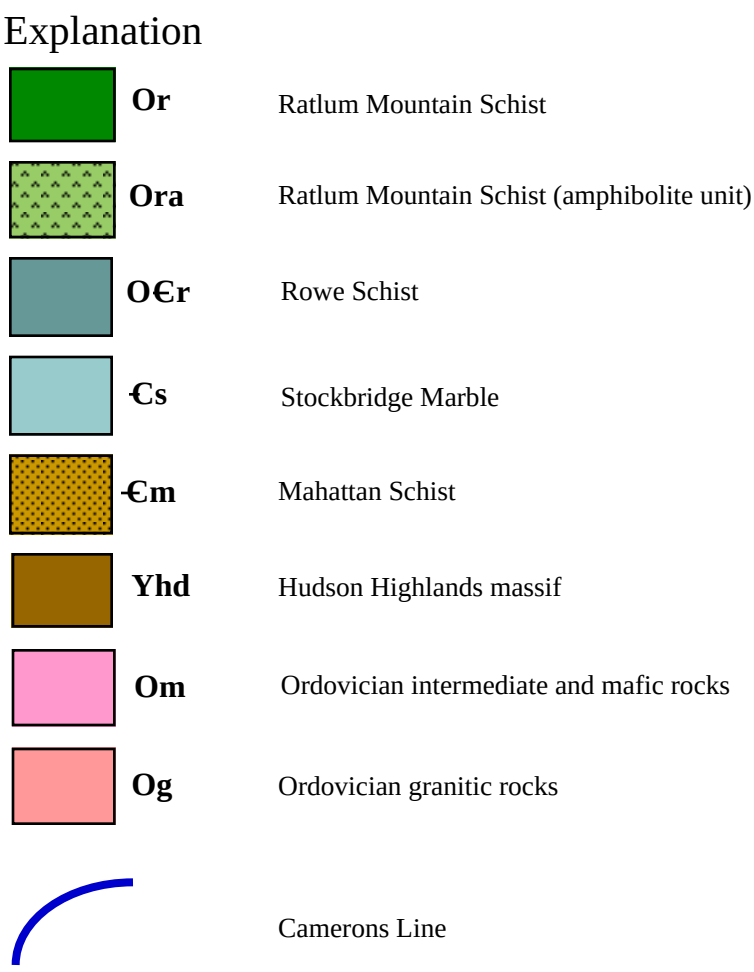

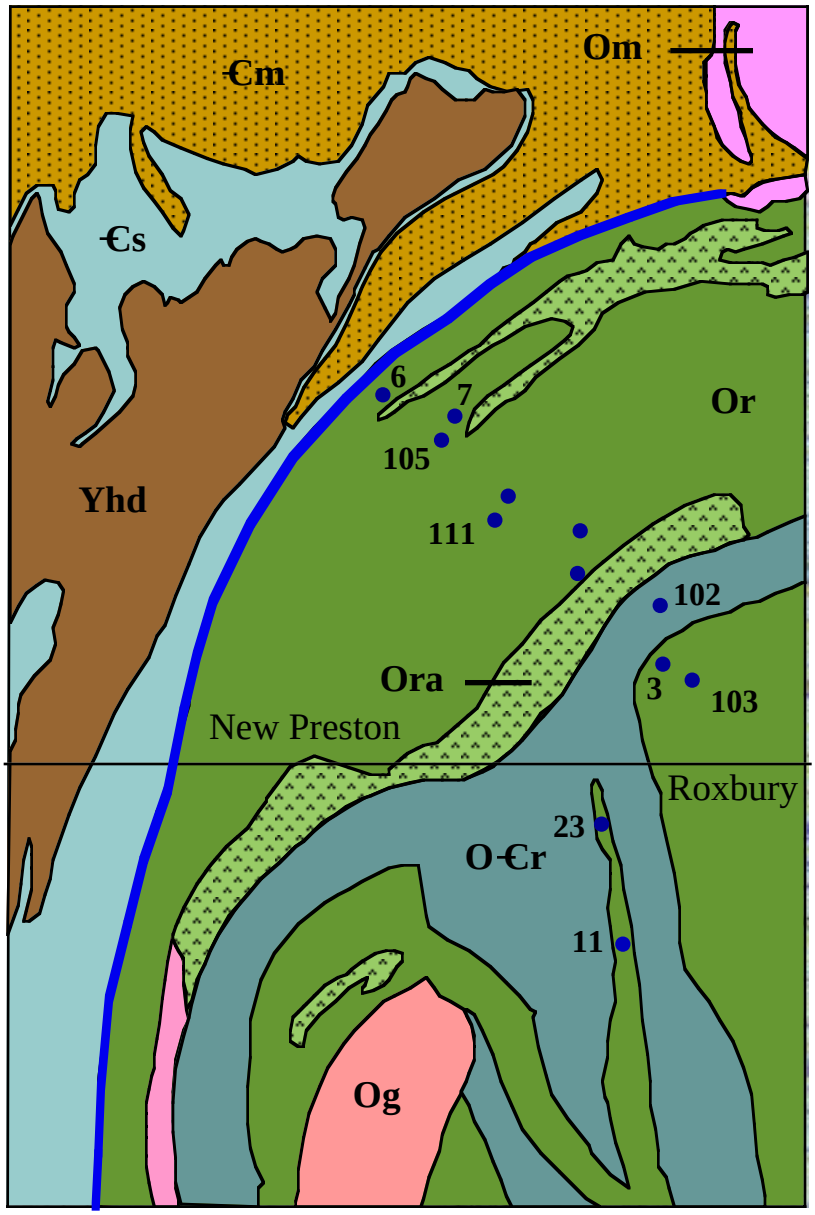
Om
Cm
Cs
6
7
105
Or
Yhd
111
102
Ora
3
103
New Preston
Roxbury
23
O-Cr
11
Og

TIMING AND STYLES OF METAMORPHISM

Gates (1952) reported that the Hartland Belt within the New Preston quadrangle had undergone a relatively simple set of changes. The metamorphic grade is consistent across the New Preston quadrangle reaching a maximum of staurolite grade. He noted that the Hartland Belt has undergone only one major episode of regional folding, with only localized crenulation development and only minor pegmatite and granite intrusions.

Sutter and others (1985) provided a very detailed synthesis of the tectonometamorphic evolution of western New England. Only a brief synopsis of their interpretations for western Connecticut and New York will be presented here. The area extending from New York City northeastward through Dutchess county and then through to the Berkshire massif in western Massachusetts (T-3 domain, or youngest Taconian metamorphism) reached a maximum of sillimanite grade during the Taconian. The T-3 metamorphic assemblages are considered to be Taconian with no significant Acadian overprinting effects. This area is characterized by a steep metamorphic gradient that coincides with maximum crustal thickening from imbricate thrusting (Stanley and Ratcliffe, 1985). East of the Berkshire massif in Massachusetts and east of Cameron's line in Connecticut the metamorphic thermal maximum occurred during the Devonian (Acadian). Sutter and others (1985) proposed that in this region the two metamorphic events have undergone very different cooling/uplift paths based on hornblende and biotite $^{40}Ar/^{39}Ar$ and K-Ar ages. Post Taconian uplift/cooling was slow (5-10 ˚C /m.y.) whereas the uplift/cooling rates for the Acadian infrastructure were very fast (25 ˚C/ m.y.). Figure 3 modified from Sutter and others (1985) shows the positions for both Taconian and Acadian isograds for western Connecticut and adjacent New York.

Figure 3 Isograd map for western Connecticut and eastern New York state after Sutter and others (1985) Taconian isograds are shown in solid lines and Acadian isograds are shown in dashed lines.

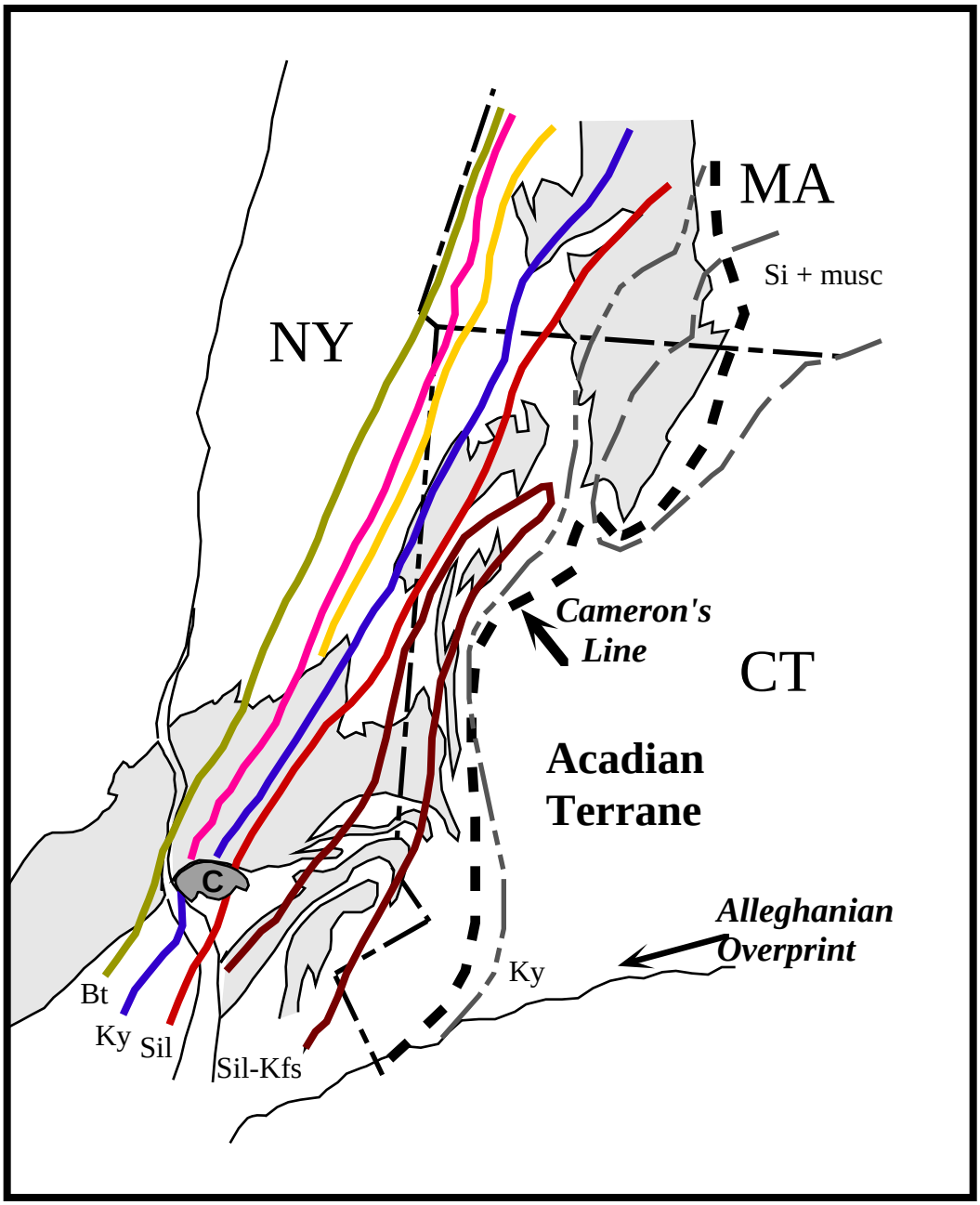

Taconian metamorphic grade progressively increases from west to east, from greenschist facies at the Hudson River to Sil-Kfs grade in eastern Westchester County, NY and westernmost CT, with a thermal maximum (from west to east) of 400 to 600 ˚C and pressures ranging from 4 to 6 kbars (Armstrong and others 1992). To the east, the Acadian overprint is characterized by significantly higher temperatures ranging from 600 to as high as 725 ˚C and pressures of 6.5 to 10 kbars (Miller 1990). Along the western edge of the Acadian metamorphic overprint the P-T conditions were similar to those of the Taconian and the timing of metamorphism can only be identified by $^{40}Ar/^{39}Ar$ ages and textural evidence (Sutter and others 1985).

PETROGRAPHY

Samples used in this study were in part collected by R. J. Tracy in 1987 and 1988 and in part by the author in 1996. Petrography was done on standard thin sections and those that contained suitable mineral assemblages were polished for microprobe analysis. The examined samples lie on a roughly northwest-southeast transect within the New Preston and Roxbury quadrangles (Figure 2).

The Ratlum Mountain and Rowe Schists are generally fine to medium-grained quartzites and mica schists with minor interbedded amphibolites. The emphasis for this study was on the more pelitic layers because the mineral assemblages are more suitable for thermobarometry. The predominant assemblage within the pelitic layers is quartz, muscovite, biotite, chlorite, plagioclase, garnet, and ilmenite with minor apatite and tourmaline. Staurolite is also present in more muscovite-rich samples and kyanite was not observed in any of the samples.

The schistosity is generally defined by alignment of both muscovite and biotite. Chlorite rarely lies within the dominant foliation plane. Some samples are crenulated with schistosity tightly folded.

Garnet porphyroblasts are ubiquitous and range in size from 1mm to greater than 1cm in diameter. They are generally euhedral but commonly have embayed edges where chlorite or biotite has replaced garnet. In many samples biotite is pseudomorphically replacing garnet with single biotite crystals replacing garnet edges (Figure 4 F). The most common solid inclusions in garnet are ilmenite and quartz, however several samples also contain porphyroblasts in which garnet cores have apparently been partially replaced by coarse-grained biotite, chlorite, plagioclase and quartz (Figure 4 A and B). These samples tend to have a much finer-grained matrix with a similar assemblage. The porphyroblasts range from relatively inclusion-free to containing abundant quartz inclusions that commonly define a preexisting foliation. Sample Np6 contains porphyroblasts with abundant quartz inclusions in the cores,

and with rims that contain numerous micron size apparent fluid inclusions. These inclusion are rounded, non-birefrigent and may have discernible vapor bubbles (Figure.4 E.). Hames (1991) reported similar textures in the Walloomsac Formation in northwestern Connecticut.

Staurolite, where present, occurs as porphyroblasts up to 1.5 cm with a variety of textures, from large, inclusion-free euhedral crystals to poikiloblastic crystals. In sample Np111a porphyroblasts are euhedral and inclusion-free and have overgrown and surrounded rounded garnet grains. In sample Np105 staurolite porphyroblasts are anhedral and surrounded by fine-grained muscovite. Sample Np111b also contains staurolite with abundant quartz inclusions and in this sample staurolite growth appears to post-date formation of crenulation cleavage. Np105 and 111b, which are the most aluminous samples also contain optically zoned plagioclase porphyroblasts that contain abundant muscovite and quartz inclusions

Chlorite porphyroblasts are ubiquitous. They occur most commonly as radiating aggregates of crystals that crosscut foliation.
(Figure 4J).Chlorite is also very commonly associated with garnet overgrowths.

Table 1. Abbreviations for minerals used in photomicrographs (Kretz, 1983).

Mineral	**Symbol**
Garnet	Grt
Biotite	Bt
Muscovite	Ms
Chlorite	Chl
Plagioclase	Pl
Staurolite	St
Ilmenite	Ilm
quartz	Qtz

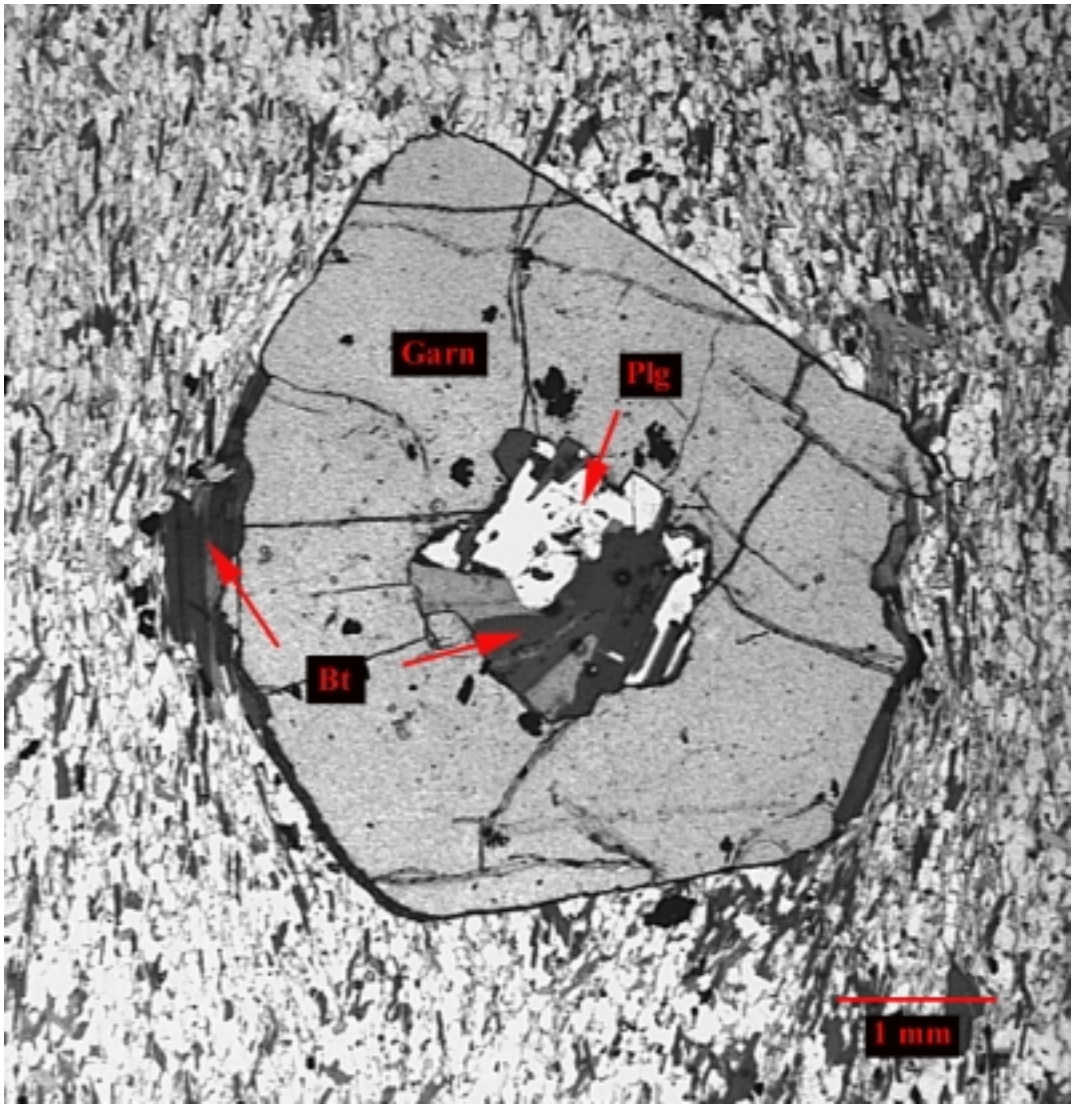

Figure 4 A. Photomicrograph of garnet porphyroblast with fine grained matrix of muscovite, biotite. quartz and plagioclase. The core of the grain has apparently been replaced with coarse grained biotite, chlorite, plagioclase and quartz and the rim partially replaced by biotite.

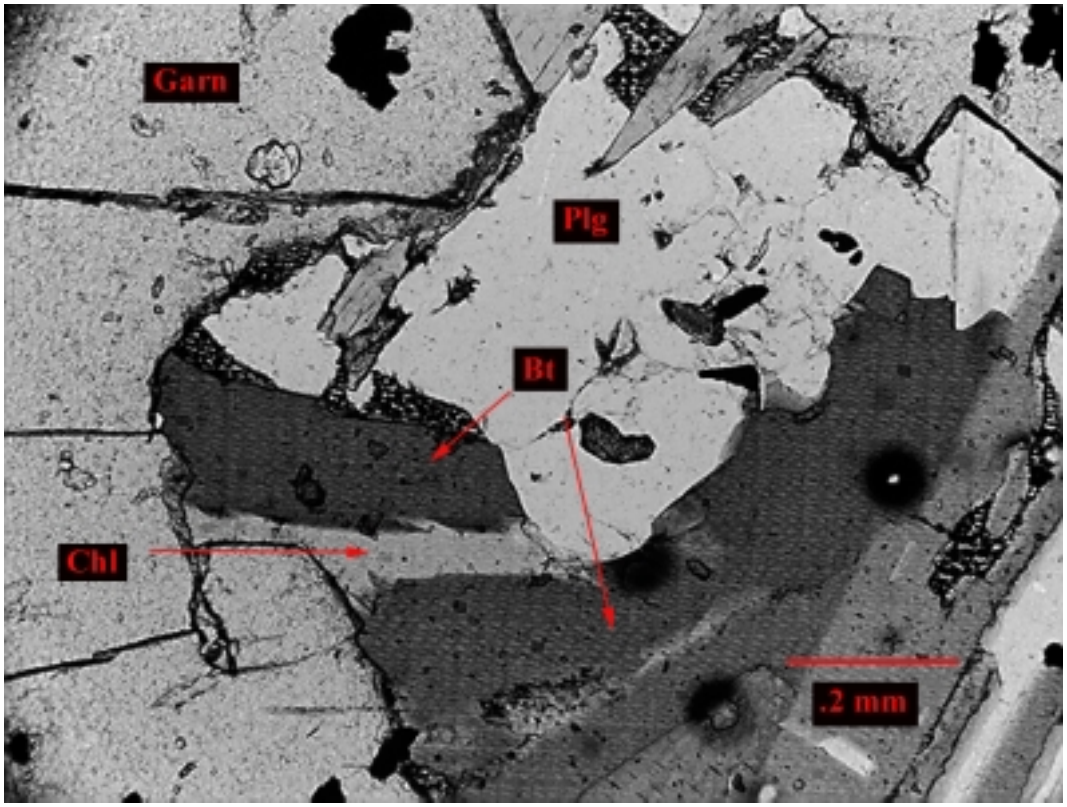

Figure 4 B. Photomicrograph of the core of the garnet in Figure 4 A showing intergrown biotite and chlorite.

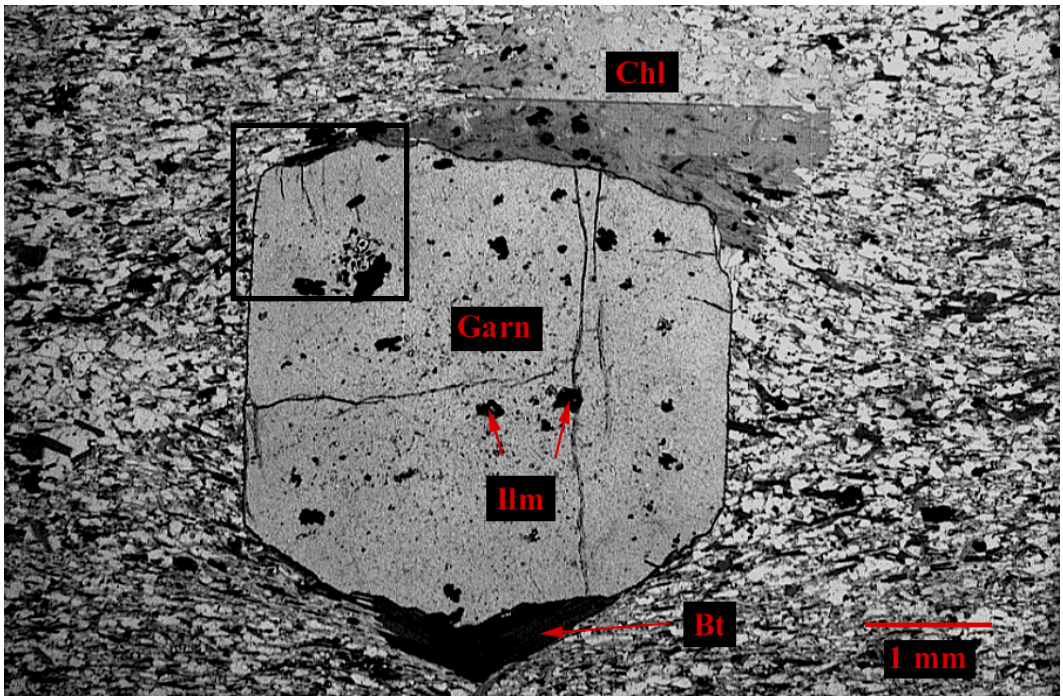

Figure 4C. Photomicrograph of a garnet porphyroblast with ilmenite inclusions. The edge of the grain has been overgrown by biotite and porphyroblastic chlorite. Boxed area shows location of Figure 4D and high resolution compositional imaging (Figure 14).

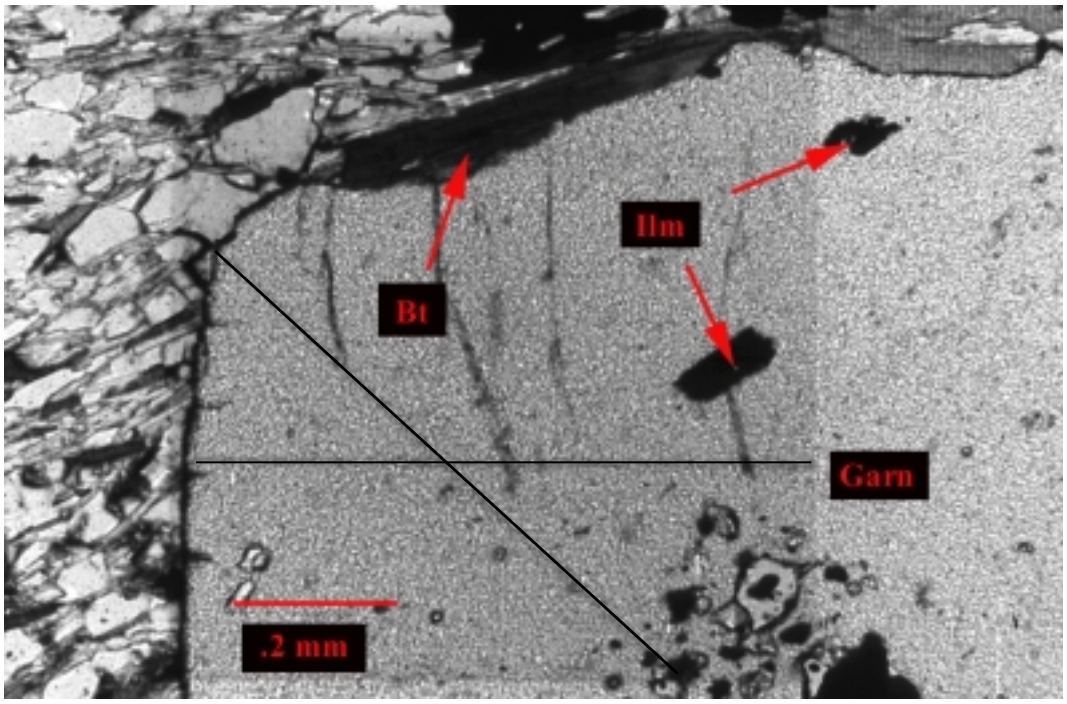

Figure 4D Photomicrograph of boxed area shown in Figure 4 C. Darker area marks exact area of detailed compositional imaging. Lines within this area mark positions of quantitative traverses for major and trace elements.

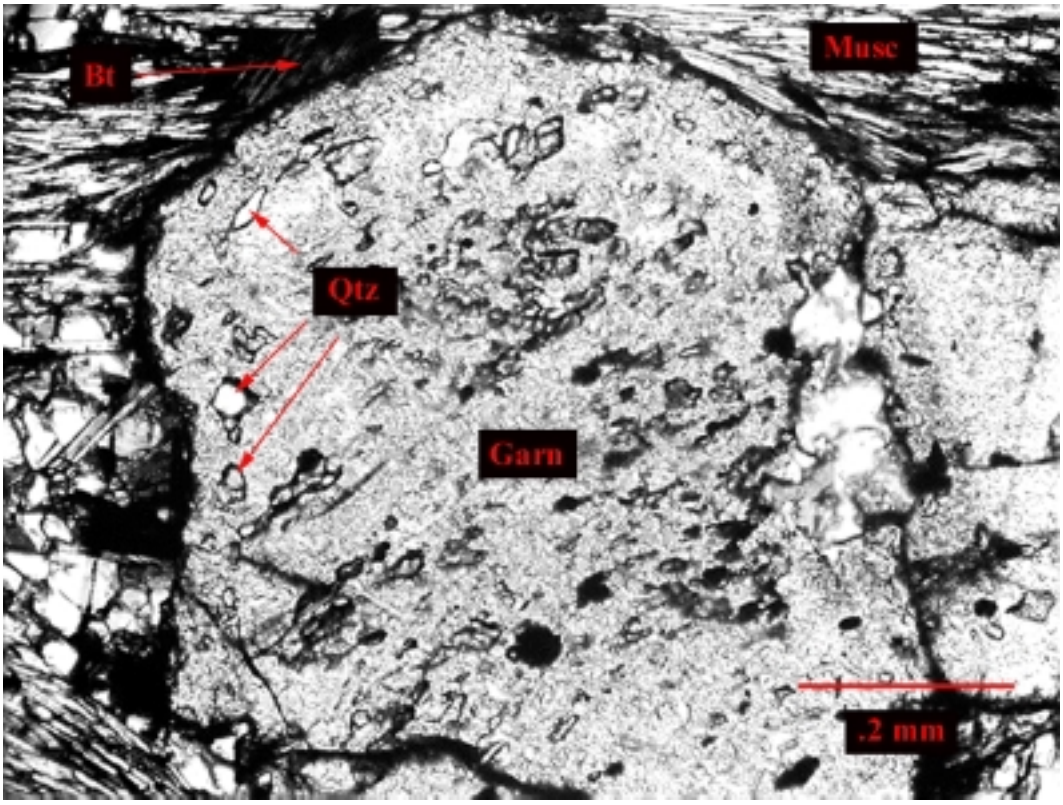

Figure 4E. Photomicrograph of garnet porphyroblast from sample Np6. The core of the porphyroblast contains numerous inclusions of quartz that appear to be aligned in a foliation different from that in the matrix. Notice the dusty appearance of the rim of the grain, particularly in the upper right corner. Along the interior of this dusty rim there is another set of quartz inclusions that roughly parallel the shape of the grain.

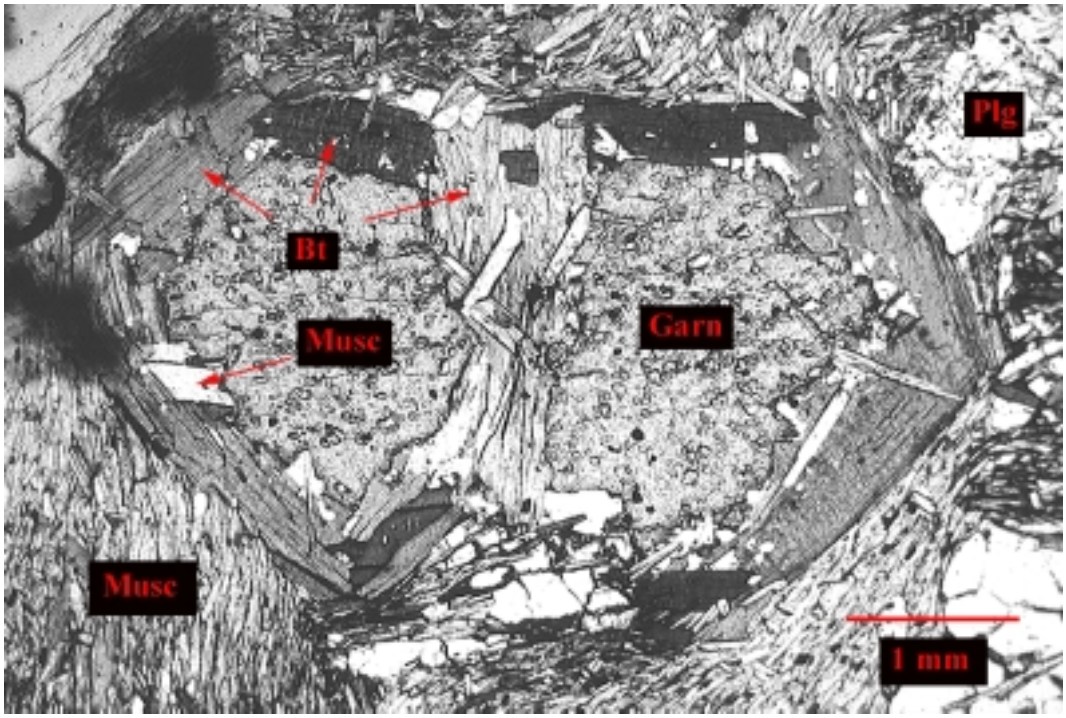

Figure 4F. Photomicrograph of a broken and partially resorbed garnet porphyroblast from Np111b that has been completely overgrown by biotite. Notice that several large grains of biotite show cleavage traces that are parallel to the edges of the garnet porphyroblast.

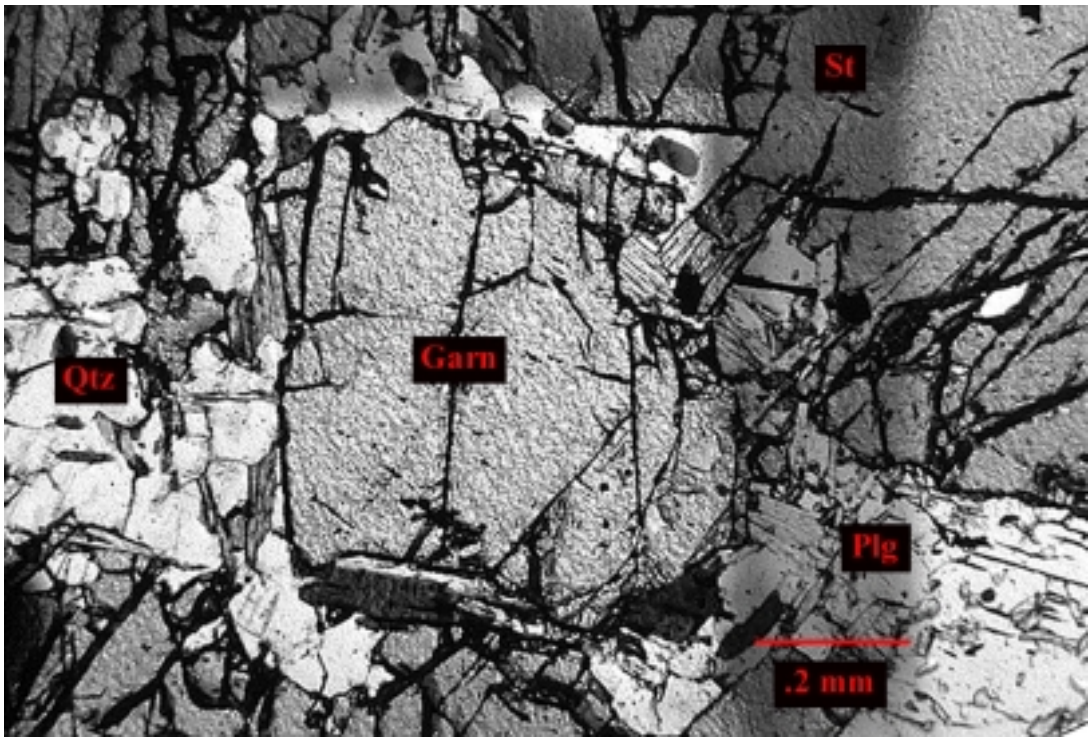

Figure 4G. Photomicrograph of an anhedral garnet porphyroblast from sample Np111a with quartz and plagioclase that is completely surrounded by a large staurolite porphyroblast.

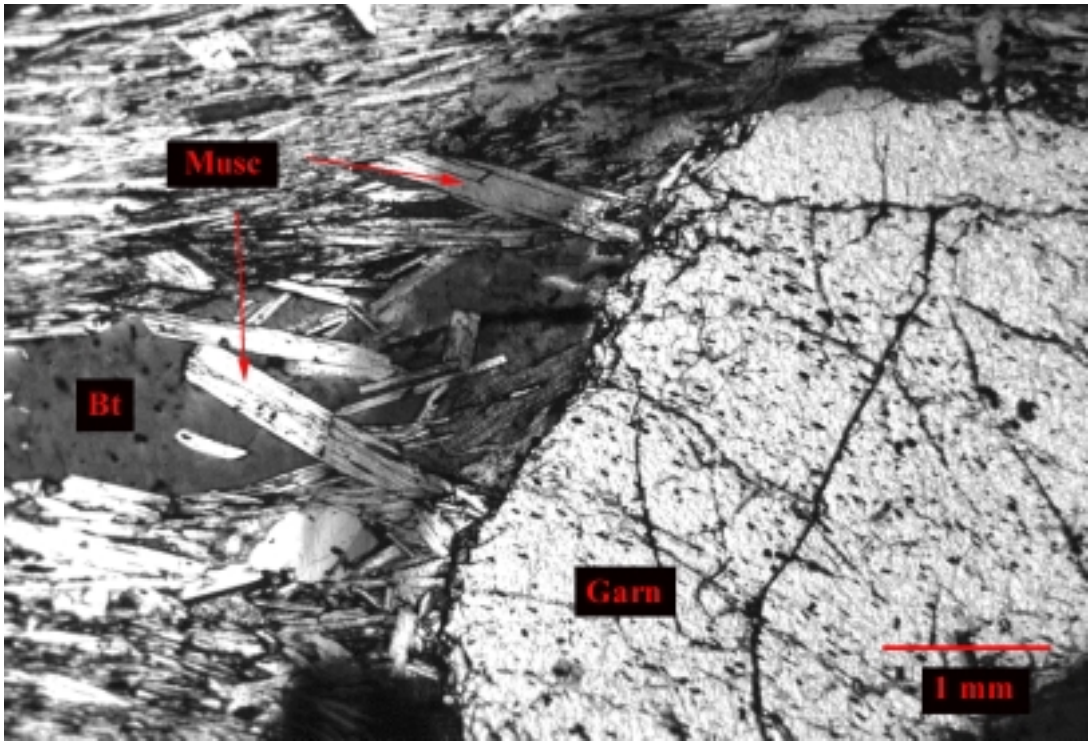

Figure 4H. Photomicrograph of a garnet porphyroblast from sample Np102 with coarse-grained muscovite and biotite growing at the garnet rim in a fine-grained matrix of muscovite.

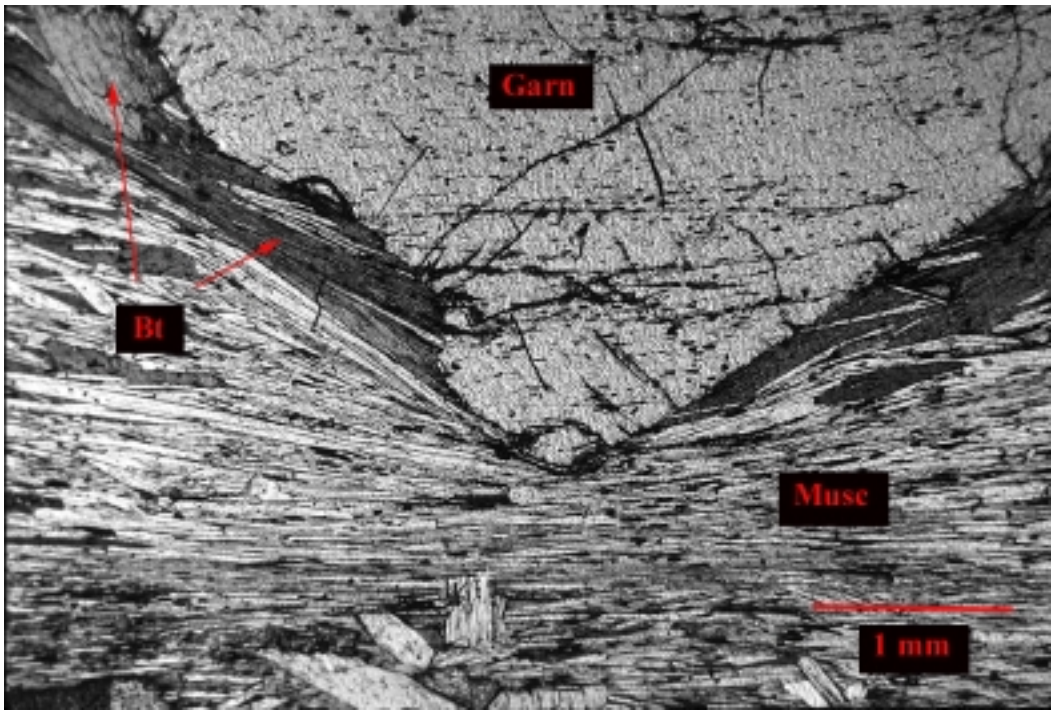

Figure 4I. Photomicrograph of the termination of a garnet porphyroblast from sample Np102 with small embayment on the left being replaced by biotite. Around the embayment biotite has grown along a sharp garnet face.

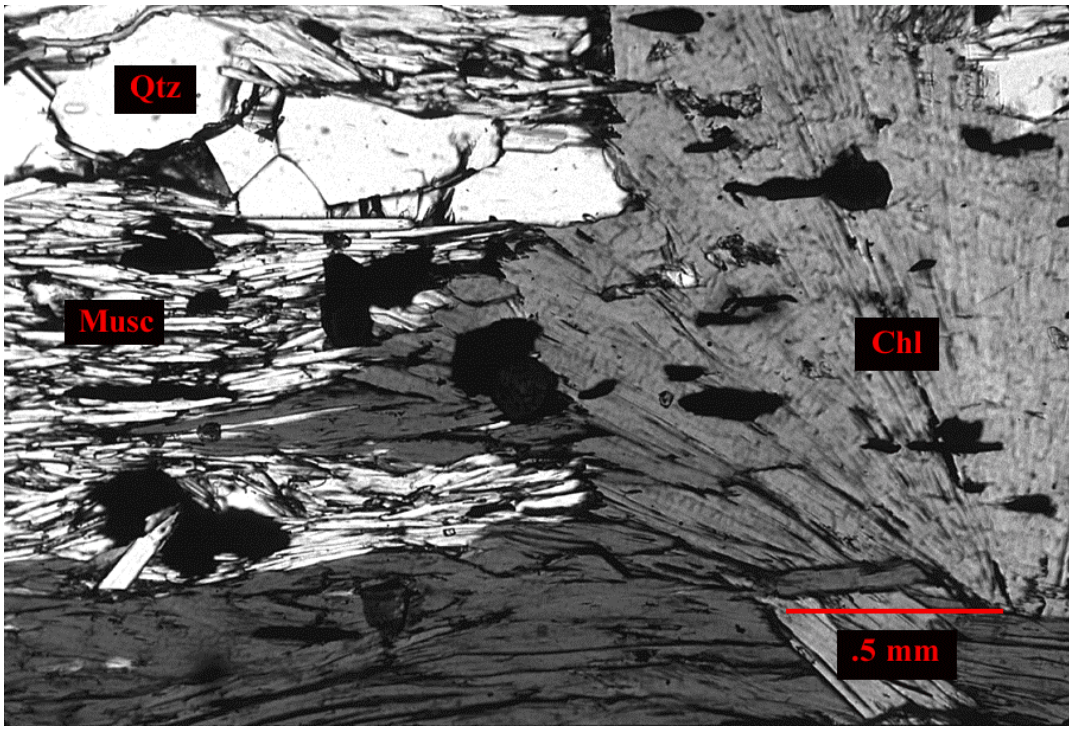

Figure 4J. Photomicrograph of a cross-cutting chlorite porphyroblast overgrowing foliation of quartz and muscovite.

ANALYTICAL METHODS

All of the mineral compositional data for this study were collected on the fully automated Cameca SX-50 electron microprobe at Virginia Polytechnic Institute and State University. Quantitative point analyses were collected for thermobarometric calculations and estimations of mineral equilibria. Quantitative traverses as well as qualitative wavelength dispersive X-ray images (WDS images or analog compositional images or maps) were obtained for both major and trace elements in order to assess chemical variability and zoning of porphyroblastic minerals. Generally, reconnaissance WDS images were collected on several garnet porphyroblasts per thin section before locations for point analyses were selected.

Beam conditions of 15 keV acceleration potential and 20 nA sample current were used for point analyses and major element traverses. A 1 micron spot was used for garnet, staurolite and ilmenite analyses and a 10-micron rastered beam was used for muscovite, biotite, chlorite and plagioclase. WDS images were collected using beam conditions of 25 keV and 40 nA for major elements and 25 keV and 100-500 nA for trace elements. For trace element images several passes were made over a given grain and then the images were added or "stacked" in order to improve counting statistics. Oxides or simple silicates were used for microprobe calibration and compositions were obtained using the ZAF data reduction scheme outlined in Heinrich (1981).

MINERAL CHEMISTRY

In order to calculate temperatures and pressures of metamorphism, it is essential to obtain chemical data that that are representative of equilibrium assemblages, that is, mineral compositions in a low-variance assemblage that formed at a unique P-T condition. This is often a difficult task for samples that may have undergone multiple episodes of metamorphic mineral growth. Electron microprobe point analyses were collected for garnet, staurolite, muscovite, biotite, chlorite, plagioclase and ilmenite at locations within a thin section where mineral assemblages suitable for thermobarometry appeared to be in textural equilibrium. Individual points were then chosen where mineral grains were in close mutual contact when possible. If this was not feasible, grains in close proximity within the matrix were chosen, as was often the case for muscovite and plagioclase. For garnet grains that are partially replaced by biotite or chlorite, analyses were collected at the interior portion of the garnet grain that was in direct contact with the replacement mineral as well as areas along the rim of a given grain. Short core-to-rim traverses were also collected for garnet porphyroblasts. Individual grains within the matrix were analyzed to test for chemical variability between reacted areas and matrix.

Representative microprobe analyses are listed in the following tables.

Table 2. Idealized garnet endmember formulas and abbreviations

mineral	Abbreviation	formula
pyrope	Prp	$Mg_3Al_2Si_3O_{12}$
Grossularite	Grs	$Ca_3Al_2Si_3O_{12}$
Spessartine	Sps	$Mn_3Al_2Si3O_{12}$
Almandine	Alm	$Fe_3Al_2Si_2O_{12}$

GARNET
Table 3 A.

	np7		np6			np111b	
	rim	core	rim	int	core	rim	core
Analysis #	10	15	1	2	3	67	76
SiO2	37.41	38.10	37.65	38.01	37.74	38.73	38.02
Al2O3	22.11	22.05	20.50	20.84	20.64	20.94	20.83
TiO2	0.01	0.10	0.04	0.04	0.09	0.11	0.04
FeO	37.77	33.96	34.30	33.97	31.65	35.65	33.37
MnO	0.71	4.18	3.06	6.41	7.65	0.49	2.14
MgO	2.21	1.64	2.35	2.26	1.84	2.64	2.27
CaO	2.70	3.73	3.30	0.84	2.09	4.83	4.94
Total	102.91	103.74	101.20	102.37	101.70	103.39	101.61
Formulas on the basis of 12 oxygens							
Si	2.948	2.975	3.014	3.020	3.019	3.018	3.015
Al	2.053	2.029	1.934	1.952	1.946	1.923	1.947
Ti	0.000	0.006	0.002	0.002	0.005	0.006	0.002
Fe	2.489	2.217	2.296	2.257	2.117	2.323	2.213
Mn	0.047	0.276	0.207	0.431	0.518	0.032	0.144
Mg	0.259	0.190	0.280	0.268	0.219	0.307	0.268
Ca	0.228	0.312	0.283	0.072	0.179	0.403	0.420
Total cations	8.025	8.005	8.017	8.002	8.003	8.014	8.009
Almandine	82.3	74.0	74.9	74.5	69.8	75.8	72.7
Grossular	7.5	10.4	9.2	2.4	5.9	13.2	13.8
Pyrope	8.6	6.4	9.1	8.8	7.2	10.0	8.8
Spessartine	1.6	9.2	6.8	14.2	17.1	1.1	4.7
Fe/(Fe+Mg)	0.91	0.92	0.89	0.89	0.91	0.88	0.89

	np111a rim	core	np106 small garn	np103 rim	np105 rim	np102 rim	core
Analysis #	109	110	104	94	29	77	103
SiO2	38.54	38.39	37.87	37.71	39.26	38.15	38.32
Al2O3	20.84	20.35	20.09	21.03	21.31	21.12	20.78
TiO2	0.01	0.07	0.00	0.07	0.01	0.02	0.14
FeO	32.70	29.41	27.86	38.24	35.02	35.76	28.5
MnO	5.61	9.14	10.51	1.79	0.35	0.46	7.83
MgO	3.72	2.56	2.96	2.17	2.80	2.82	0.77
CaO	1.77	3.32	2.81	1.68	4.68	3.49	6.61
Total	103.19	103.24	102.10	102.69	103.43	101.82	102.95
Formulas on the basis of 12 oxygens							
Si	3.013	3.019	3.012	2.992	3.040	3.014	3.020
Al	1.920	1.886	1.883	1.967	1.945	1.966	1.930
Ti	0.001	0.004	0.000	0.004	0.001	0.001	0.008
Fe	2.138	1.934	1.853	2.538	2.268	2.362	1.878
Mn	0.372	0.609	0.708	0.120	0.023	0.031	0.523
Mg	0.434	0.300	0.351	0.257	0.323	0.332	0.090
Ca	0.148	0.280	0.239	0.143	0.388	0.295	0.558
Total cations	8.026	8.033	8.047	8.020	7.987	8.002	8.007
Almandine	69.2	61.9	58.8	83.0	75.5	78.2	61.6
Grossular	4.8	9.0	7.6	4.7	12.9	9.8	18.3
Pyrope	14.0	9.6	11.1	8.4	10.8	11.0	3.0
Spessartine	12.0	19.5	22.5	3.9	0.8	1.0	17.1
Fe/(Fe+Mg)	0.83	0.87	0.84	0.91	0.88	0.88	0.95

BIOTITE
Table 3 B.

	np7			np6		np111b
	bt rim	bio at int	bt matrix	bt rim	bt matrix	bt rim
analysis#	21	4	12	17	42	31
SiO2	35.74	35.94	33.94	36.27	35.89	35.95
Al2O3	20.02	20.22	19.90	17.95	17.95	18.51
TiO2	1.28	1.43	1.55	1.70	1.95	1.50
FeO	21.96	22.34	23.72	21.86	21.82	20.53
MnO	0.00	0.05	0.03	0.07	0.22	0.06
MgO	8.15	7.81	8.90	8.97	9.04	10.15
CaO	0.01	0.05	0.11	0.00	0.03	0.07
Na2O	0.23	0.10	0.13	0.07	0.07	0.36
K2O	8.57	8.44	7.03	9.02	8.88	7.88
F	0.12	0.15	0.12	0.27	0.29	0.26
Total	96.08	96.52	95.43	96.19	96.16	95.27
Formulas on the basis of 22 oxygens						
Tetrahedral						
Si	5.422	5.428	5.212	5.528	5.478	5.467
Al	2.578	2.572	2.788	2.472	2.522	2.533
	8.000	8.000	8.000	8.000	8.000	8.000
Octahedral						
Al	1.002	1.027	0.814	0.752	0.707	0.784
Ti	0.146	0.162	0.179	0.195	0.224	0.172
Fe	2.786	2.821	3.046	2.786	2.786	2.611
Mn	0.000	0.007	0.004	0.008	0.029	0.008
Mg	1.843	1.758	2.038	2.037	2.057	2.301
	5.777	5.775	6.082	5.778	5.803	5.875
A site						
Ca	0.002	0.007	0.018	0.000	0.005	0.011
Na	0.066	0.028	0.037	0.022	0.021	0.106
K	1.659	1.627	1.378	1.753	1.729	1.529
	1.727	1.662	1.434	1.775	1.756	1.646
Fe/(Fe+Mg)	0.60	0.62	0.60	0.58	0.58	0.53
Mg/(Mg+Fe)	0.40	0.38	0.40	0.42	0.42	0.47

	np111a	np6	np105	np103	np102	
	bt matrix	bt matrix	bio	bio	bio at rim	bio g.m.
analysis#	103	109	60	103	91	100
SiO2	35.72	36.58	35.18	35.72	36.40	35.99
Al2O3	18.88	16.72	26.96	18.88	18.72	18.21
TiO2	1.55	1.38	0.13	1.55	1.37	1.84
FeO	23.73	17.83	14.35	23.73	22.09	20.74
MnO	0.14	0.27	0.22	0.14	0.06	0.12
MgO	7.14	13.32	9.10	7.14	9.05	9.44
CaO	0.03	0.05	0.04	0.03	0.05	0.04
Na2O	0.07	0.08	0.62	0.07	0.37	0.25
K2O	8.49	8.89	3.76	8.49	8.58	8.81
F	0.15	0.49	0.26	0.15	0.23	0.20
Total	95.90	95.61	90.62	95.90	96.92	95.64
Formulas on the basis of 22 oxygens						
Tetrahedral						
Si	5.485	5.527	5.265	5.485	5.490	5.485
Al	2.515	2.473	2.735	2.515	2.510	2.515
	8.000	8.000	8.000	8.000	8.000	8.000
Octahedral						
Al	0.902	0.505	2.020	0.902	0.818	0.755
Ti	0.179	0.157	0.015	0.179	0.155	0.211
Fe	3.047	2.253	1.796	3.047	2.786	2.643
Mn	0.018	0.035	0.028	0.018	0.008	0.015
Mg	1.634	3.001	2.030	1.634	2.035	2.145
	5.781	5.950	5.888	5.781	5.803	5.769
A site						
Ca	0.005	0.008	0.006	0.005	0.008	0.007
Na	0.021	0.023	0.180	0.021	0.108	0.074
K	1.663	1.714	0.718	1.663	1.651	1.713
	1.689	1.745	0.904	1.689	1.767	1.793
Fe/(Fe+Mg)	0.65	0.43	0.47	0.65	0.58	0.55
Mg/(Mg+Fe)	0.35	0.57	0.53	0.35	0.42	0.45

MUSCOVITE
Table 3 C.

	np7 matrix	np6 matrix	rim	np111b matrix	np111a matrix	para inc	inc
analysis#	22	22	33	75	75	115	71
SiO2	46.73	46.73	46.68	47.69	46.88	46.94	47.50
Al2O3	34.57	34.57	34.30	34.37	33.95	38.69	34.69
TiO2	0.55	0.55	0.41	0.56	0.37	0.06	0.27
FeO	1.59	1.59	1.78	1.99	2.08	1.23	1.96
MnO	0.00	0.00	0.00	0.00	0.04	0.00	0.00
MgO	0.60	0.60	0.78	0.67	0.47	0.12	0.54
CaO	0.00	0.00	0.01	0.01	0.04	0.25	0.01
Na2O	1.30	1.30	1.19	1.53	2.23	6.09	2.43
K2O	9.07	9.07	9.08	8.06	7.56	2.13	7.49
Total	94.42	94.42	94.26	94.88	93.62	95.51	94.89
Formulas on the basis of 22 oxygens							
Tetrahedral							
Si	6.243	6.243	6.253	6.310	6.295	6.035	6.283
Al	1.757	1.757	1.747	1.690	1.705	1.965	1.717
	8.000	8.000	8.000	8.000	8.000	8.000	8.000
Octahedral							
Al	3.687	3.687	3.669	3.669	3.668	3.898	3.691
Ti	0.055	0.055	0.041	0.056	0.037	0.006	0.027
Fe	0.178	0.178	0.199	0.220	0.234	0.132	0.217
Mn	0.000	0.000	0.000	0.000	0.005	0.000	0.000
Mg	0.120	0.120	0.157	0.132	0.094	0.023	0.106
	4.039	4.039	4.066	4.077	4.038	4.059	4.041
A site							
Ca	0.000	0.000	0.002	0.001	0.006	0.034	0.001
Na	0.336	0.336	0.308	0.392	0.581	1.518	0.623
K	1.547	1.547	1.551	1.360	1.295	0.349	1.264
	1.88	1.88	1.86	1.75	1.88	1.90	1.89

	np105 matrix	inc	inc	np103 matrix	np102 rim	matrix
analysis#	56	65	66	100	86	99
SiO2	45.87	46.67	46.39	47.29	44.46	47.01
Al2O3	33.28	33.55	34.04	35.36	31.50	34.41
TiO2	0.41	0.30	0.36	0.10	0.68	0.59
FeO	2.42	3.26	3.35	1.25	6.26	1.71
MnO	0.04	0.00	0.03	0.00	0.04	0.03
MgO	0.69	0.57	0.60	0.55	2.28	0.63
CaO	0.02	0.01	0.01	0.05	0.03	0.00
Na2O	1.75	1.74	1.90	1.68	1.21	1.35
K2O	8.45	8.18	8.04	7.92	8.65	9.07
Total	93.03	94.28	94.72	94.20	95.11	94.80
Formulas on the basis of 22 oxygens						
Tetrahedral						
Si	6.253	6.276	6.215	6.273	6.075	6.259
Al	1.747	1.724	1.785	1.727	1.925	1.741
	8.000	8.000	8.000	8.000	8.000	8.000
Octahedral						
Al	3.600	3.594	3.591	3.802	3.147	3.659
Ti	0.042	0.030	0.036	0.010	0.070	0.059
Fe	0.276	0.367	0.375	0.139	0.715	0.190
Mn	0.005	0.000	0.003	0.000	0.005	0.003
Mg	0.140	0.114	0.120	0.109	0.464	0.125
	4.063	4.105	4.125	4.059	4.401	4.037
A site						
Ca	0.003	0.001	0.001	0.007	0.004	0.000
Na	0.463	0.454	0.494	0.432	0.321	0.349
K	1.470	1.403	1.374	1.340	1.508	1.541
	1.93	1.86	1.87	1.78	1.83	1.89

PLAGIOCLASE
Table 3 D

	np7		np6		np111b		np111a
	plag in core	matrix plag	plag at rim	plag in p.s.	rim	matrix plag	plag core
analysis#	9	13	14	27	49	57	69
SiO2	65.36	66.04	66.14	65.61	64.56	64.10	68.18
Al2O3	22.40	22.52	21.98	21.73	23.29	23.55	20.83
TiO2	0.00	0.00	0.00	0.03	0.00	0.00	0.00
FeO	0.10	0.05	0.02	0.15	0.01	0.31	0.00
MnO	0.00	0.00	0.00	0.00	0.02	0.00	0.00
MgO	0.00	0.02	0.00	0.00	0.01	0.02	0.01
Cr2O3	0.00	0.00	0.00	0.00	0.00	0.00	0.00
CaO	2.48	2.86	2.85	2.90	4.62	4.88	1.99
Na2O	10.25	10.16	10.20	10.14	9.10	9.11	10.64
K2O	0.08	0.02	0.02	0.02	0.06	0.05	0.04
Total	100.67	101.66	101.21	100.59	101.67	102.02	101.69
Formulas on the basis of 8 oxygens							
Si	2.856	2.858	2.874	2.872	2.805	2.784	2.938
Al	1.154	1.149	1.125	1.121	1.192	1.205	1.058
Ti	0.000	0.000	0.000	0.001	0.000	0.000	0.000
Fe	0.004	0.002	0.001	0.006	0.000	0.011	0.000
Mn	0.000	0.000	0.000	0.000	0.001	0.000	0.000
Mg	0.000	0.001	0.000	0.000	0.001	0.001	0.001
Cr	0.000	0.000	0.000	0.000	0.000	0.000	0.000
Ca	0.116	0.132	0.132	0.136	0.215	0.227	0.092
Na	0.869	0.852	0.860	0.861	0.767	0.767	0.889
K	0.005	0.001	0.001	0.001	0.003	0.003	0.002
Total cations	5.00	4.99	4.99	5.00	4.98	5.00	4.98
Mole% Ab	87.8	86.5	86.5	86.2	77.8	76.9	90.4
Mole% An	11.7	13.4	13.3	13.6	21.8	22.8	9.3
Mole% Or	0.5	0.1	0.1	0.1	0.3	0.3	0.2
	100	100	100	100	100	100	100

	np111a		np106	np105	np103	np102
	plag rim	plag inc	plag	plag blast	plag	plag blast
analysis#	72	118	108	61	107	98
SiO2	67.61	68.68	65.06	62.81	66.49	63.53
Al2O3	20.39	19.54	21.94	23.45	20.97	23.88
TiO2	0.00	0.00	0.00	0.00	0.00	0.00
FeO	0.00	0.11	0.11	0.03	0.00	0.04
MnO	0.00	0.01	0.00	0.02	0.00	0.01
MgO	0.01	0.04	0.02	0.02	0.01	0.01
Cr2O3	0.00	0.00	0.00	0.00	0.00	0.00
CaO	1.39	0.48	4.23	5.81	2.18	5.67
Na2O	10.96	11.45	9.27	8.47	10.55	8.31
K2O	0.04	0.02	0.07	0.07	0.07	0.12
Total	100.40	100.33	100.70	100.68	100.27	101.57
Formulas on the basis of 8 oxygens						
Si	2.949	2.991	2.851	2.767	2.912	2.769
Al	1.048	1.003	1.133	1.217	1.082	1.227
Ti	0.000	0.000	0.000	0.000	0.000	0.000
Fe	0.000	0.004	0.004	0.001	0.000	0.001
Mn	0.000	0.000	0.000	0.001	0.000	0.000
Mg	0.001	0.003	0.001	0.001	0.001	0.001
Cr	0.000	0.000	0.000	0.000	0.000	0.000
Ca	0.065	0.022	0.199	0.274	0.102	0.265
Na	0.927	0.967	0.787	0.723	0.896	0.702
K	0.002	0.001	0.004	0.004	0.004	0.007
Total cations	4.99	4.99	4.98	4.99	5.00	4.97
Mole% Ab	93.2	97.6	79.5	72.2	89.4	72.1
Mole% An	6.5	2.3	20.1	27.4	10.2	27.2
Mole% Or	0.2	0.1	0.4	0.4	0.4	0.7
	100	100	100	100	100	100

STAUROLITE
Table 3 E.

	np111b st	np111a st at garn	np105 st blast	np102 staur rim	staur int
analysis#	91	112	52	93	94
SiO2	28.69	28.90	28.92	28.28	28.13
Al2O3	52.47	52.50	53.95	53.12	53.56
TiO2	0.54	0.56	0.44	0.52	0.64
FeO	15.37	14.31	9.7	13.69	14.02
MnO	0.09	0.39	0.59	0.09	0.11
MgO	2.00	2.43	1.07	1.58	1.51
ZnO	0.27	0.02	2.48	0.59	0.61
CaO	0.00	0.03	0.01	0.02	0
Total	99.43	99.14	97.16	97.89	98.58
Formulas on the basis of 23 oxygens					
Si	3.950	3.970	4.006	3.927	3.887
Al	8.513	8.500	8.807	8.694	8.722
Ti	0.056	0.058	0.046	0.054	0.067
Fe	1.769	1.644	1.124	1.590	1.620
Mn	0.010	0.045	0.069	0.011	0.013
Mg	0.410	0.498	0.221	0.327	0.311
Zn	0.029	0.002	0.270	0.064	0.066
Ca	0.000	0.004	0.001	0.003	0.000
Total cations	14.74	14.72	14.54	14.67	14.69
Fe/(Fe+Mg)	0.81	0.77	0.84	0.83	0.84

CHLORITE

Table 3 G.

	np7		np6	np111b		np111a
	chl core	chl rim	chl blast	matrix chl	rim chl	chl inc
analysis#	18	29	26	60	69	123
SiO2	24.21	25.09	24.88	25.30	24.85	24.93
Al2O3	23.37	23.81	21.99	22.64	22.94	22.87
TiO2	0.07	0.07	0.08	0.03	0.08	0.14
FeO	32.04	28.66	27.29	25.78	26.58	24.29
MnO	0.26	0.04	0.13	0.08	0.07	0.51
MgO	10.35	12.38	13.35	15.47	14.73	16.20
CaO	0.04	0.01	0.00	0.01	0.01	0.05
Total	90.35	90.04	87.71	89.31	89.26	88.99
Formulas on the basis of 14 oxygens						
Si	2.561	2.606	2.647	2.617	2.584	2.577
Al	2.914	2.913	2.757	2.760	2.811	2.786
Ti	0.006	0.005	0.006	0.002	0.006	0.011
Fe	2.835	2.488	2.428	2.230	2.311	2.100
Mn	0.023	0.003	0.012	0.007	0.006	0.045
Mg	1.632	1.916	2.118	2.385	2.283	2.496
Ca	0.005	0.001	0.000	0.001	0.001	0.006
Total cations	9.98	9.93	9.97	10.00	10.00	10.02
Fe/(Fe+Mg)	0.63	0.57	0.53	0.48	0.50	0.46

	np106 chl	np105 chl blast	chl matrix	np103 chl	np102 chl blast
analysis#	113	59	64	104	87
SiO2	26.46	25.42	25.75	26.12	24.99
Al2O3	21.44	22.51	22.14	21.76	22.29
TiO2	0.04	0.01	0.02	0.09	0.13
FeO	21.98	22.32	23.01	32.99	27.46
MnO	0.49	0.29	0.32	0.23	0.10
MgO	17.99	17.17	17.36	9.00	13.81
CaO	0.03	0.02	0.01	0.04	0.02
Total	88.43	87.74	88.61	90.23	88.80
Formulas on the basis of 14 oxygens					
Si	2.713	2.633	2.649	2.768	2.626
Al	2.591	2.748	2.685	2.718	2.760
Ti	0.003	0.001	0.002	0.007	0.010
Fe	1.885	1.933	1.980	2.924	2.413
Mn	0.043	0.025	0.028	0.021	0.009
Mg	2.750	2.651	2.663	1.422	2.163
Ca	0.003	0.002	0.001	0.005	0.002
Total cations	9.99	9.99	10.01	9.87	9.98
Fe/(Fe+Mg)	0.41	0.42	0.43	0.67	0.53

GARNET ZONING

In recent years, WDS images have proven to be an essential tool in understanding the growth and post-growth histories of zoned minerals. Garnet is an important mineral in both igneous and metamorphic rocks and is a common constituent of pelitic assemblages from greenschist through granulite facies rocks. Because of its nearly ubiquitous occurrence in pelitic assembles and its ability to preserve a record of compositional change it is potentially the most important mineral used for thermobarametric calculations in these rocks. It is also commonly zoned in amphibolite or lower grade rocks due to low diffusion rates for major and trace cations (Tracy 1982) and it is therefore essential to assess the chemical variability of garnet porphyroblasts in order to interpret the growth history as well as understand the effect of zoning on thermobarometric calculations . Collecting point analyses without an understanding of the 2-D or 3-D chemical variability of zoned mineral will likely produce spurious results. The extent to which compositional growth zoning is preserved provides useful information about the thermal maximum and subsequent cooling history experienced by a rock. Modifications of growth zoning, such as truncations of chemical zoning can also be used to infer relative timing of metamorphic mineral growth.

A detailed investigation of garnet zoning was undertaken before point analyses were collected. Major element (Mg, Ca, Mn, Fe) WDS images were collected for all of the analyzed thin sections. Detailed major element and trace element images (Y, Sc, P, Ti, and Cr) were collected for samples Np6 and Np7. Quantitative traverses were also collected for imaged grains. Compositional images for several of the analyzed grains are presented here as false color images showing relative elemental concentrations.

Figure 5. False color scale used for wavelength-dispersive X-ray compositional images. Red represents highest relative concentration and violet represents the lowest concentration.

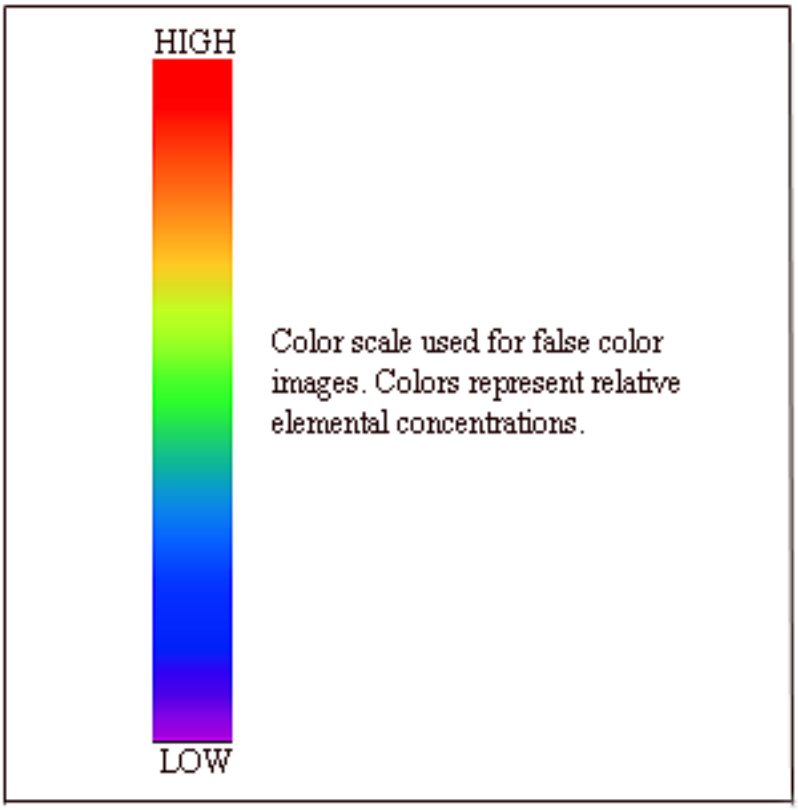

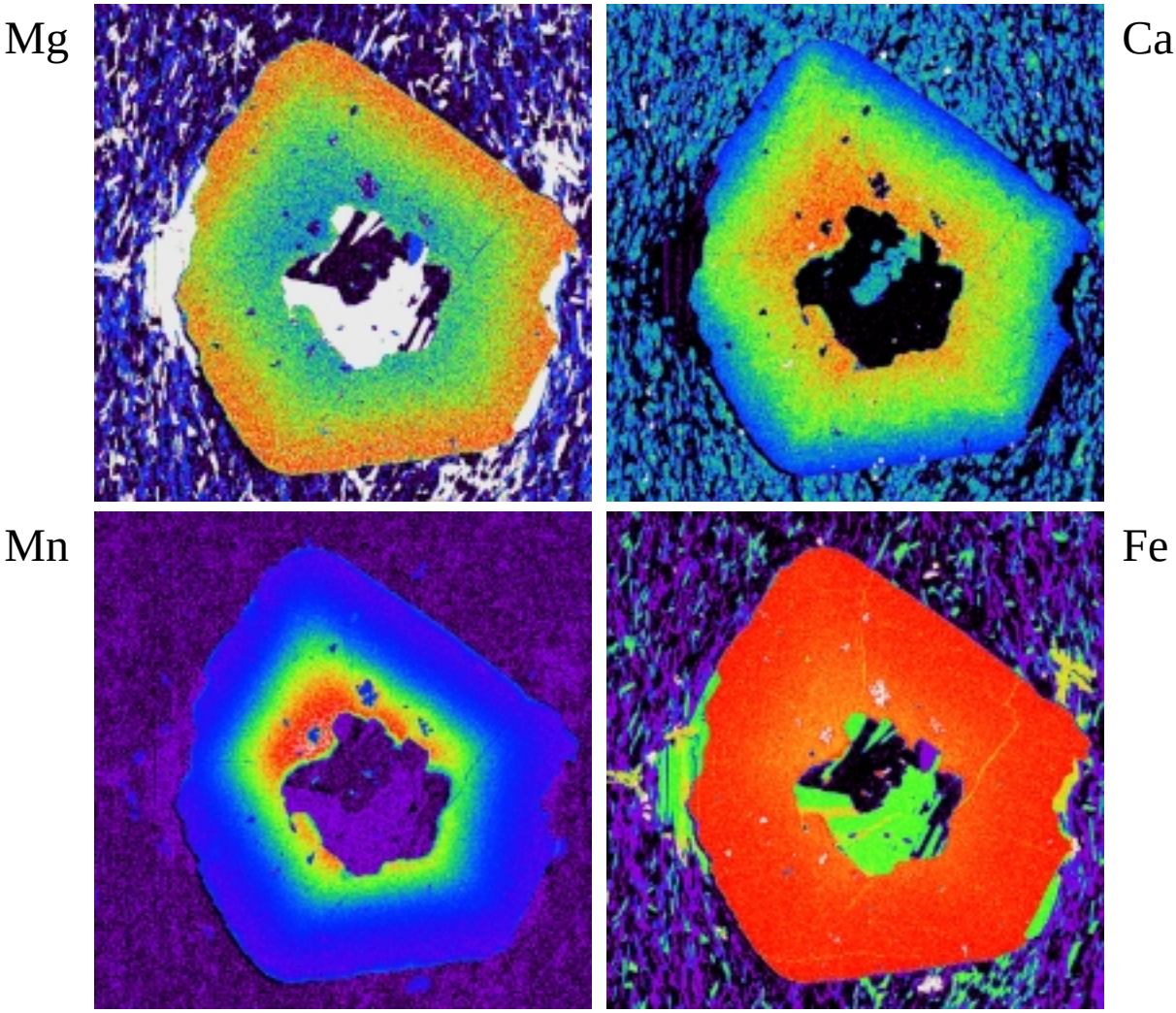

Figure 6 A. Field of view =4100 μm
Np7 major element compositional images of garnet porphyroblast in a fine-grained matrix. Garnet core has apparently been replaced by coarse grained biotite, chlorite, quartz and plagioclase. Garnet rims have been partially replaced by biotite shown in white false color in Mg image. Major element zoning patterns are euhedral and are truncated by both the coarse replacement in the core as well as well as biotite overgrowths at the rim. Again, zoning shows normal prograde patterns with Mn and Ca decreasing toward the rim and Fe and Mg increasing to the rim.

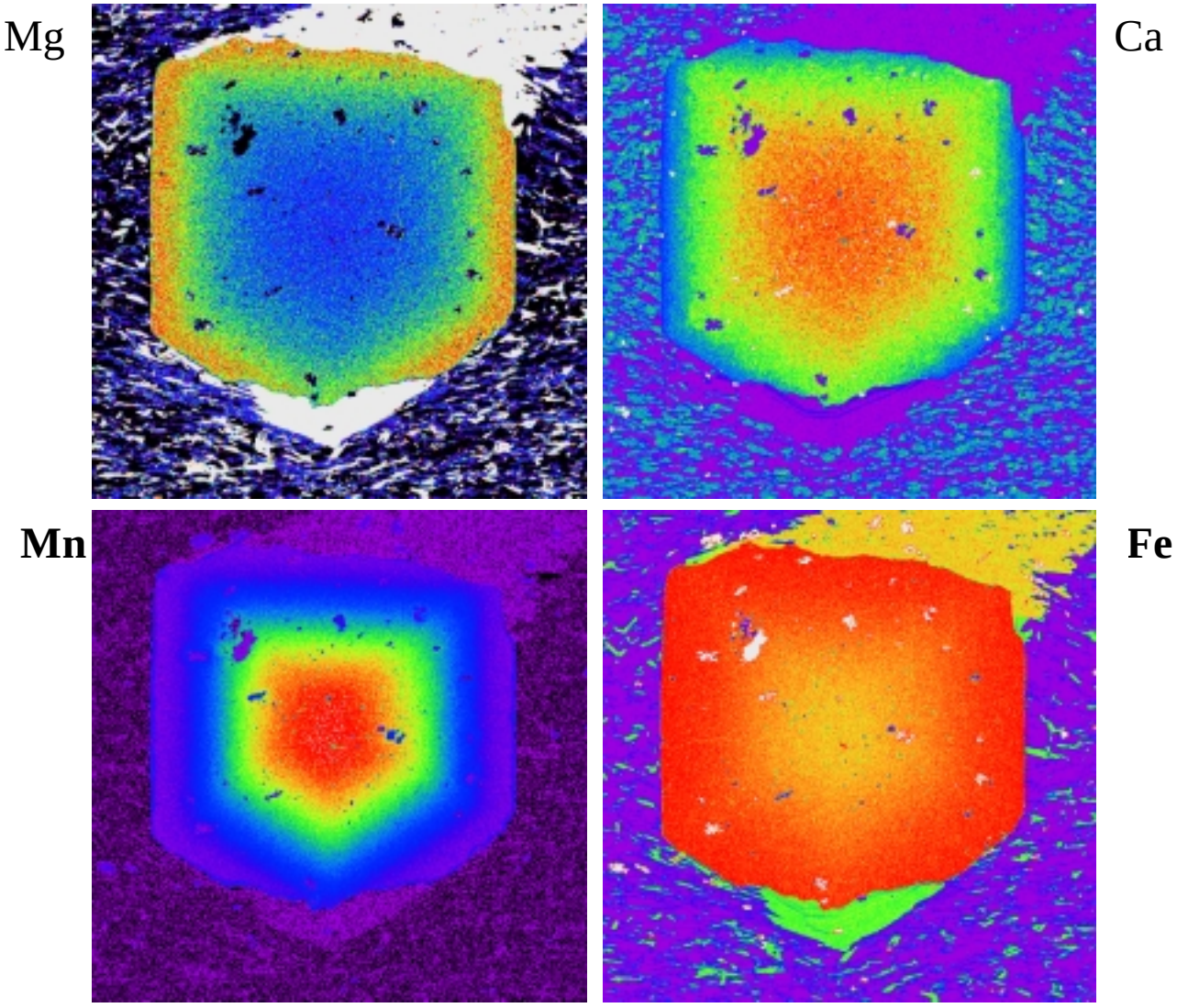

Figure 6 B. Field of view = 4100 μm.
Np7 major element compositional images from the same thin section as Figure 4 C. Porphyroblast rim is partially overgrown by both chlorite and biotite shown in yellow and green false colors, respectively, in Fe image. Both biotite and chlorite overgrowths truncate compositional zoning.

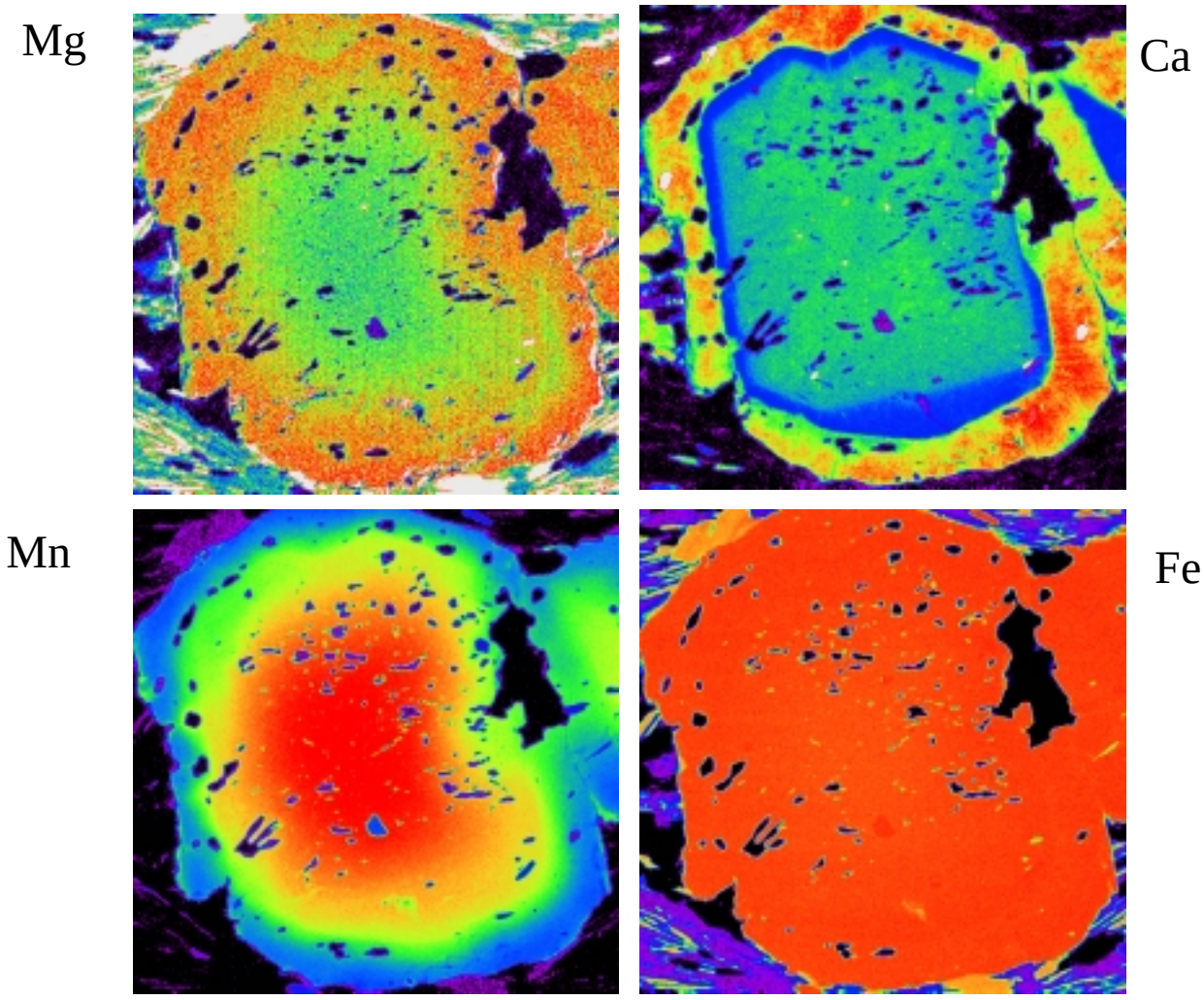

Figure 7. Horizontal field of view = 1024 μm.
Np6 major element compositional images for garnet grain in figure 4 E showing patchy high calcium overgrowth on low calcium garnet. Inside this overgrowth calcium content sharply decreases and then increases toward the core. This overgrowth is not as well preserved in Mn and Fe images. Mg content decreases from core to rim and then shows a slight decrease where calcium content steps up and then increases again to the rim. Mn content shows no compositional inflection and decreases from core to rim.

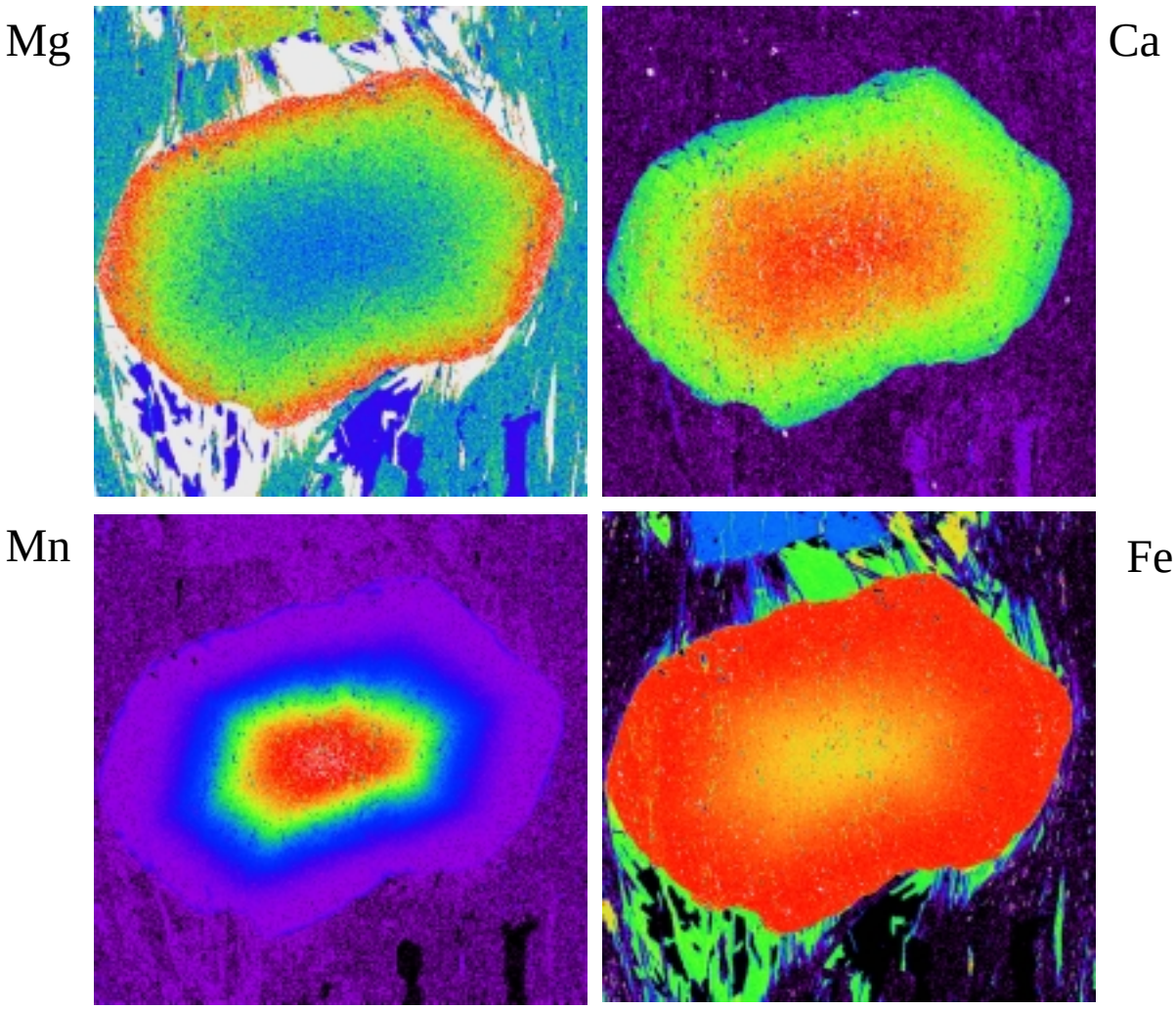

Figure 8. Field of view = 7200 μm
Np102 major element compositional images. Mn and Ca content decrease from core to rim and Fe and Mg increase from core to rim. Mn shows euhedral zoning pattern form the core to rim. Fe, Mg and Ca strongly preserve zoning but do not show the same sharp euhedral patters. Biotite grains , white false color grains in Mg image, growing along the edge of the garnet porphyroblast do not significantly truncate zoning.

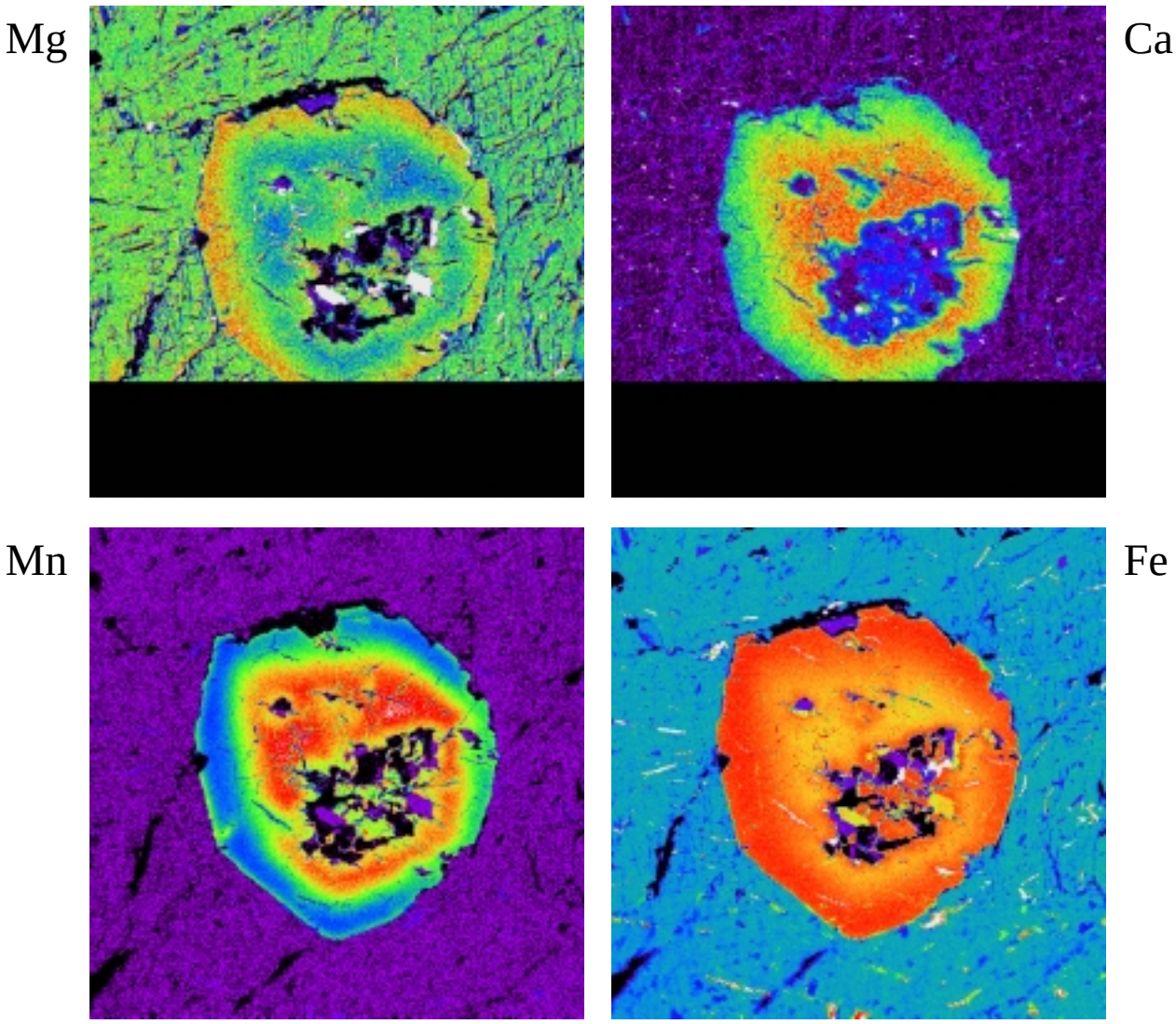

Figure 9 A. Field of view = 7200 μm
Np111a major element compostional image for a garnet grain completely surrounded by a staurolite porphyroblast. Black areas Mg and Ca images was caused by two spectrometers that stopped collecting during scans. The garnet core has been partially replaced by plagioclase, quartz, chlorite and paragonite. The zoning otherwise shows nearly euhedral pattern with Mn and Ca content decreasing from core to rim and Fe and Mg increasing from core to rim. Staurolite grain shows no zoning and does not appear to have reacted significantly with this garnet grain.

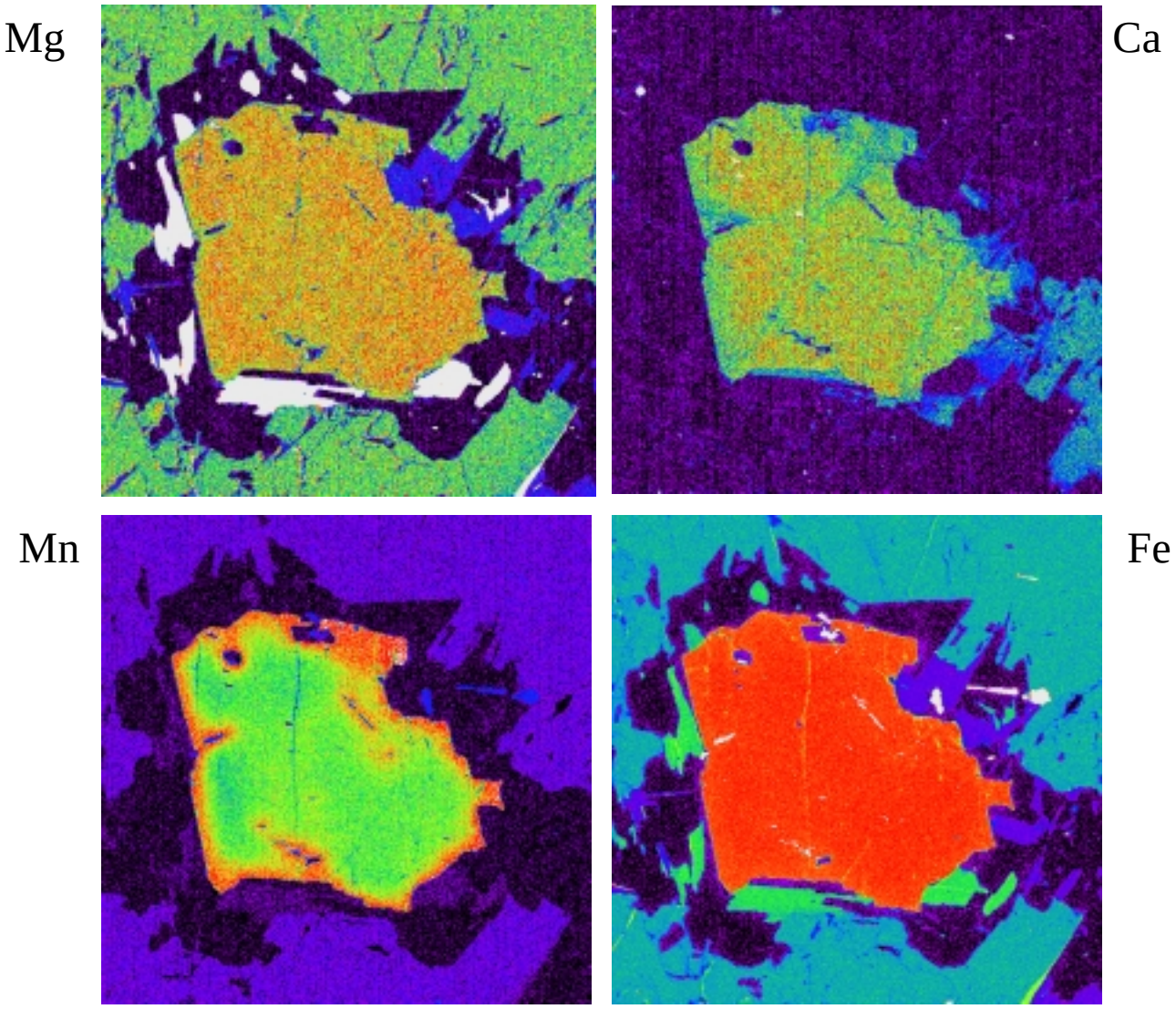

Figure 9 B. Field of view = 3600 μm
Np111a major element compositional images for a garnet grain surrounded by plagioclase, biotite muscovite and staurolite. Mg, Ca and Fe images do not preserve compositional zoning. Mn content is homogeneous in the core and sharply increases along the rim of the grain in contrast to all of the other examined thin sections where Mn content decreases from core to rim.

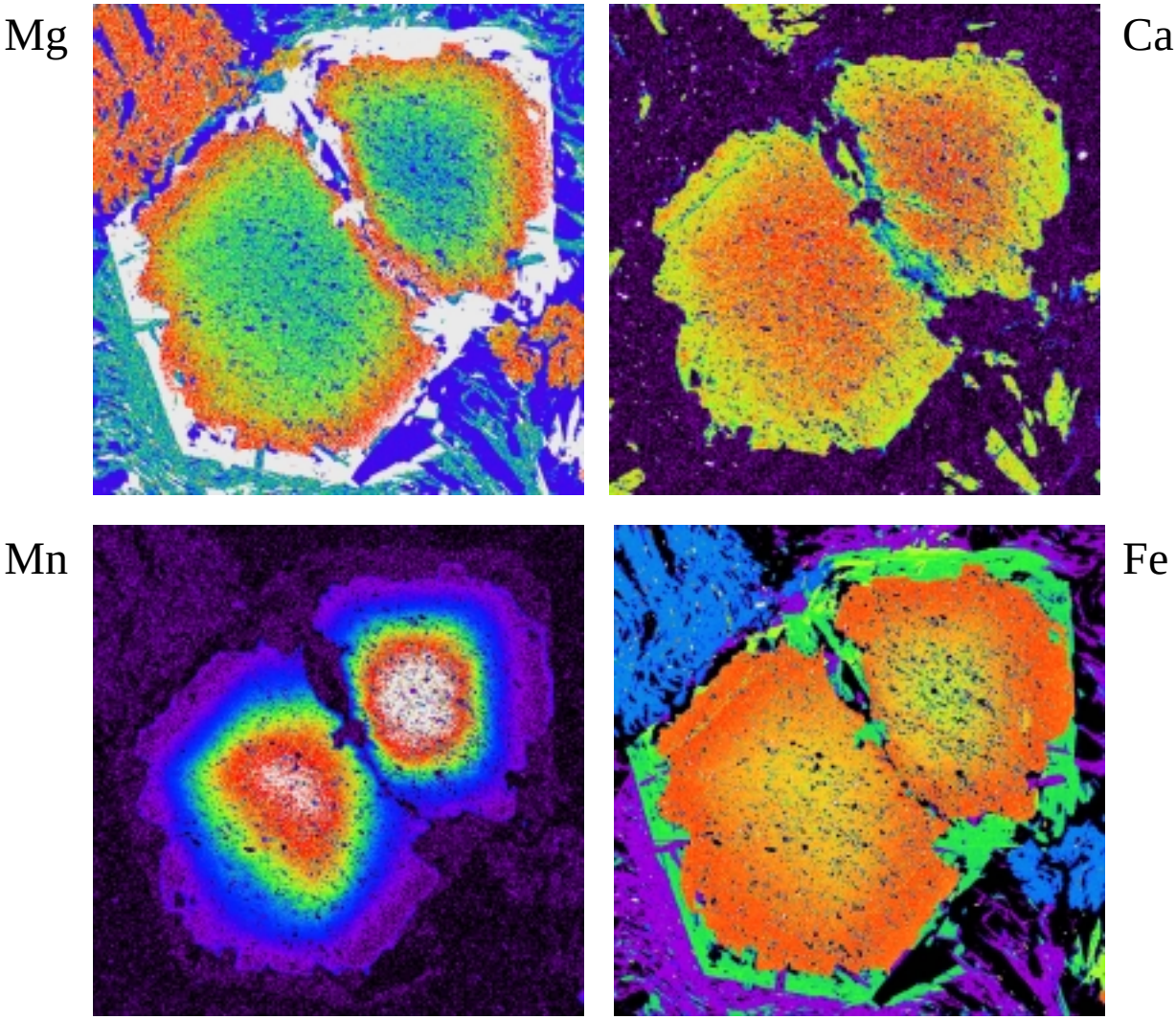

Figure 10. Field of view = 8200 μm
Np111b major element compositional images of a large garnet porphyroblast that has been overgrown by biotite shown in white false color in Mg image. The grain is cut by a fracture filled with biotite, chlorite, quartz and muscovite. Zoning patterns show slightly rounded zoning patterns in the core that become more euhedral at the rims. Mn and Ca content decrease from core to rim and Fe and Mg content increase from core to rim.

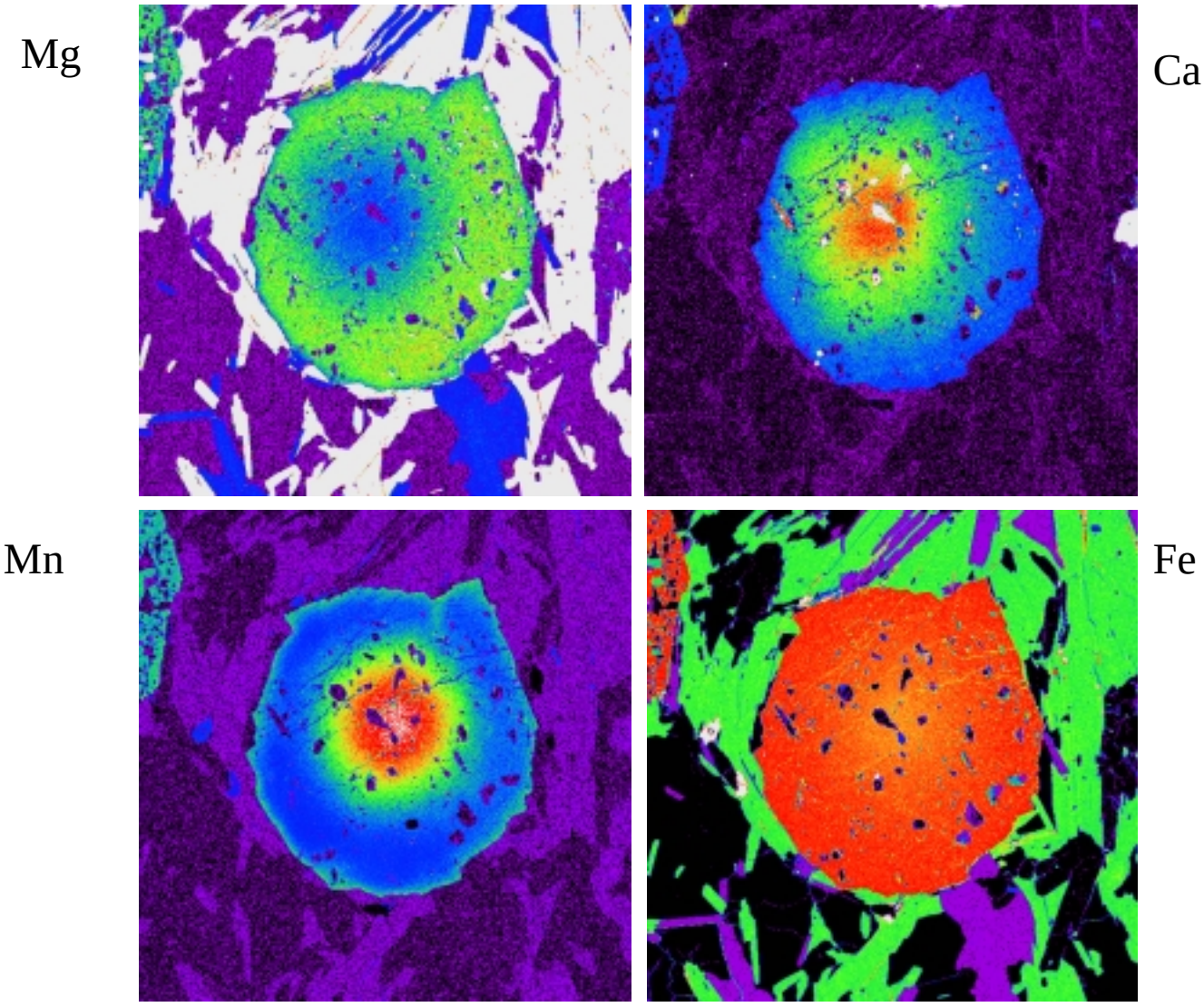

Figure 11. Field of view = 7200 μm
Sby1 major element compositional images for a garnet porphyroblast from the Straits Schist. In contrast to garnets from Ratlum Mountain and Rowe Schists, porphyroblasts from the Straits Schists have much more rounded or "bullseye" patterns to zoning. Elemental trends are the same with Mn and Ca decreasing from core to rim and Fe and Mg increasing from core to rim.

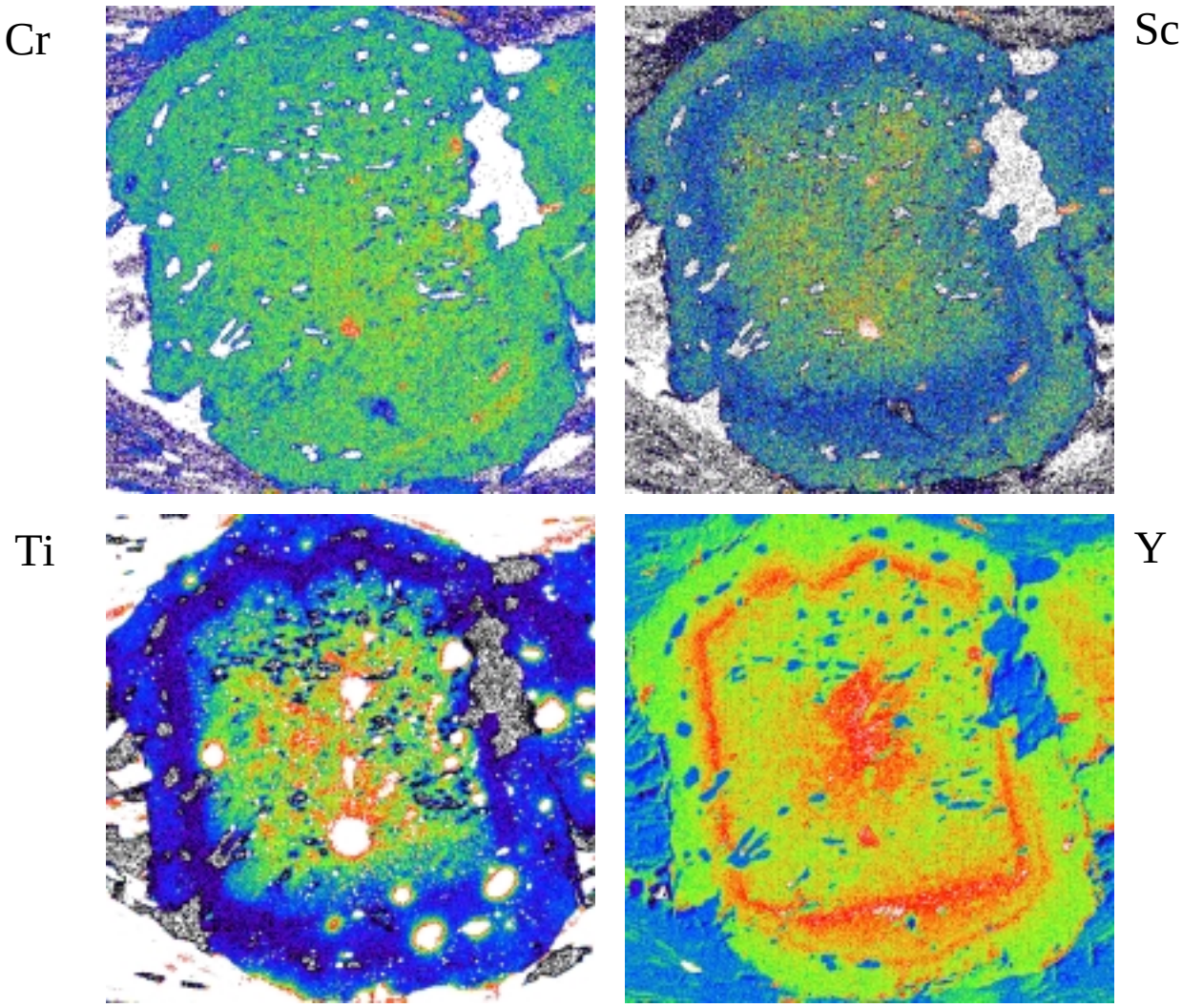

Figure 12. Field of view = 1024 µm
Np6 trace element compositional images for the same garnet grain shown in figure 7. White spots in the Ti image are ilmenite inclusions. Ti content is highest in the core and decreases outward towards the rim and shows lowest concentration along the edge of the relict core grain. Y content decreases from the core toward the rim as well to a point where it shows sharp increase along a narrow band and then and then sharply decreases again out to the rim. This narrow band roughly coincides with the same area that shows a sharp drop in Ca. Sc decreases from core to rim and shows a broad band of depletion that coincides with Y enrichment.

Ca 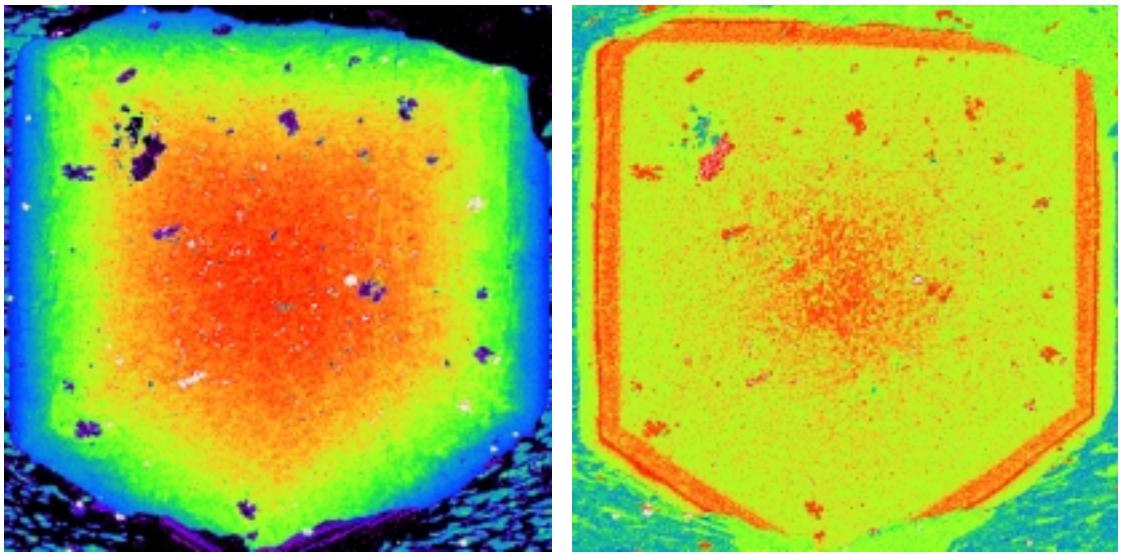 Y

Figure 13. Field of view = 3600 μm
Np7 Ca and Y compositional images shown for comparison. Ca image shows sharp composition zoning with Ca content decreasing from core to rim characteristic of prograde growth zoning. In contrast Y shows an irregular enrichment pattern in the core that decreases outward to a narrow band of enrichment just inside the rim that parallels crystal faces.

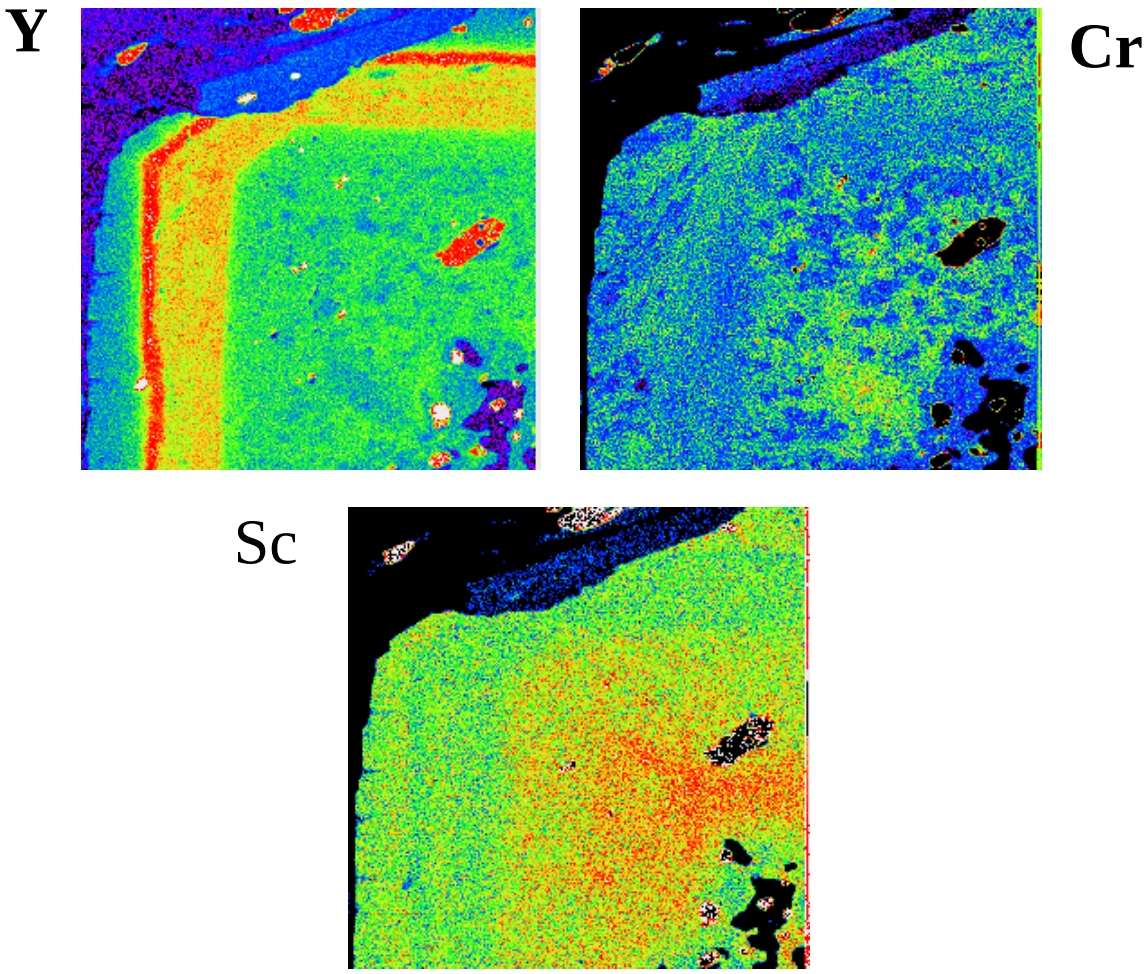

Figure 14. Field of view =770 μm
High resolution trace element images for sample Np7. Y concentration is patchy in the core outward to a very sharp band enrichment. Y content steps up sharply in the band shown in orange and then increases along a very narrow band (aprrox. 10 μm wide) before dropping of sharply along the rim of the grain. Cr content is patchy throughout the imaged area. Sc content shows inverse concentrations to Y although the patterns are not nearly as pronounced.

Ca 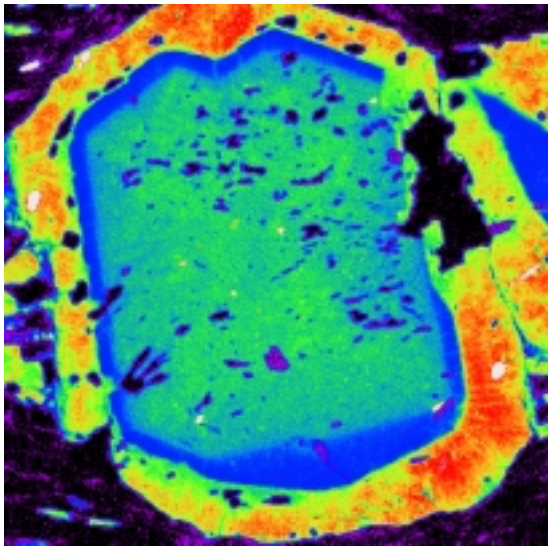 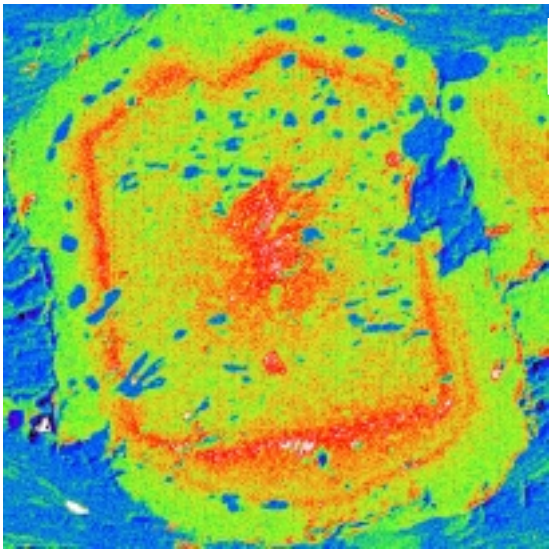 **Y**

F**igure 15.** Field of view = 1024 μm
Np6 Ca and Y compositional images shown for comparison. Ca image clearly shows a euhedral core grain with low Ca content that has been overgrown by high Ca Garnet.. Around the rim of the core grain there is a sharp drop in Ca content that roughly corresponds to the narrow band of Y enrichment.

Quantitative compositional profiles must be used in conjunction with compositional images. Images provide a great deal of detail about the elemental distributions within a given grain but do not provide exact elemental concentrations. Quantitative traverses were collected from rim to rim and are presented as concentration (end-member % for major elements and in ppm for trace elements) vs. distance.

Figure 16 A.

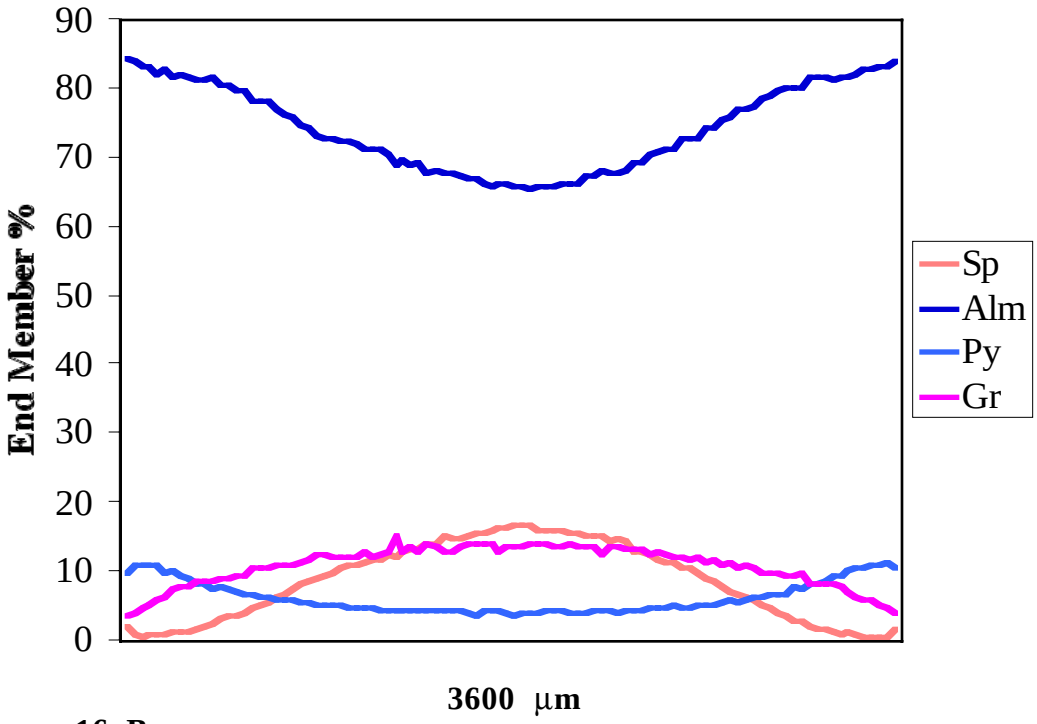

Figure 16 B.

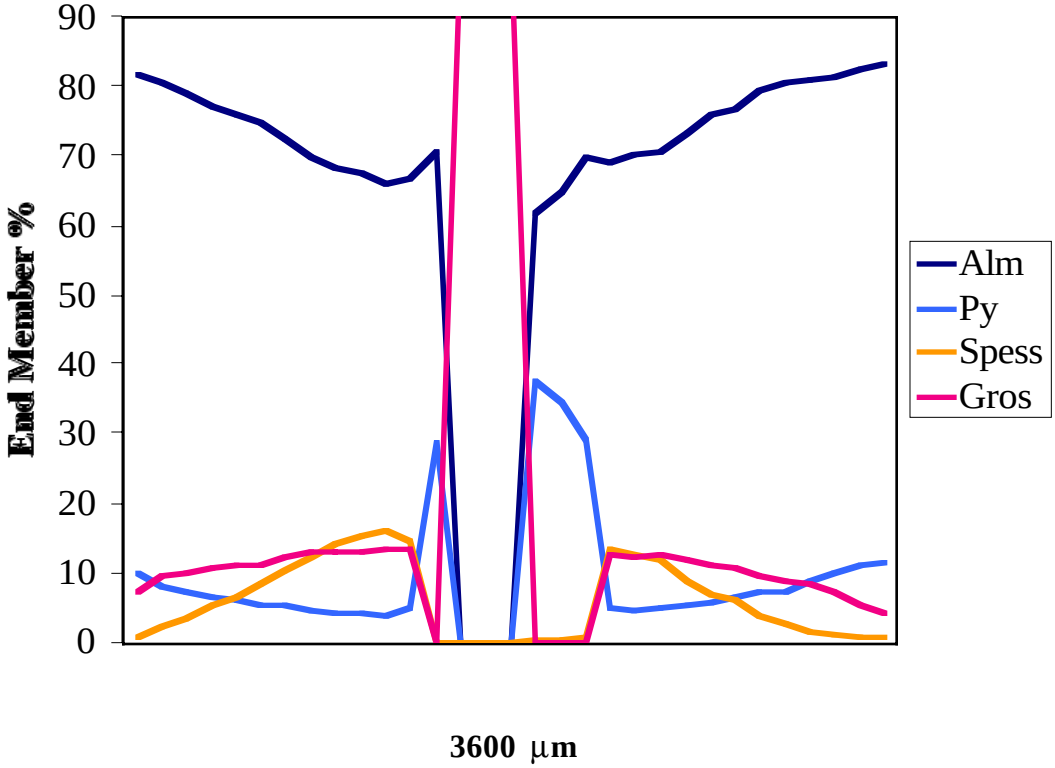

Figure 16 C.

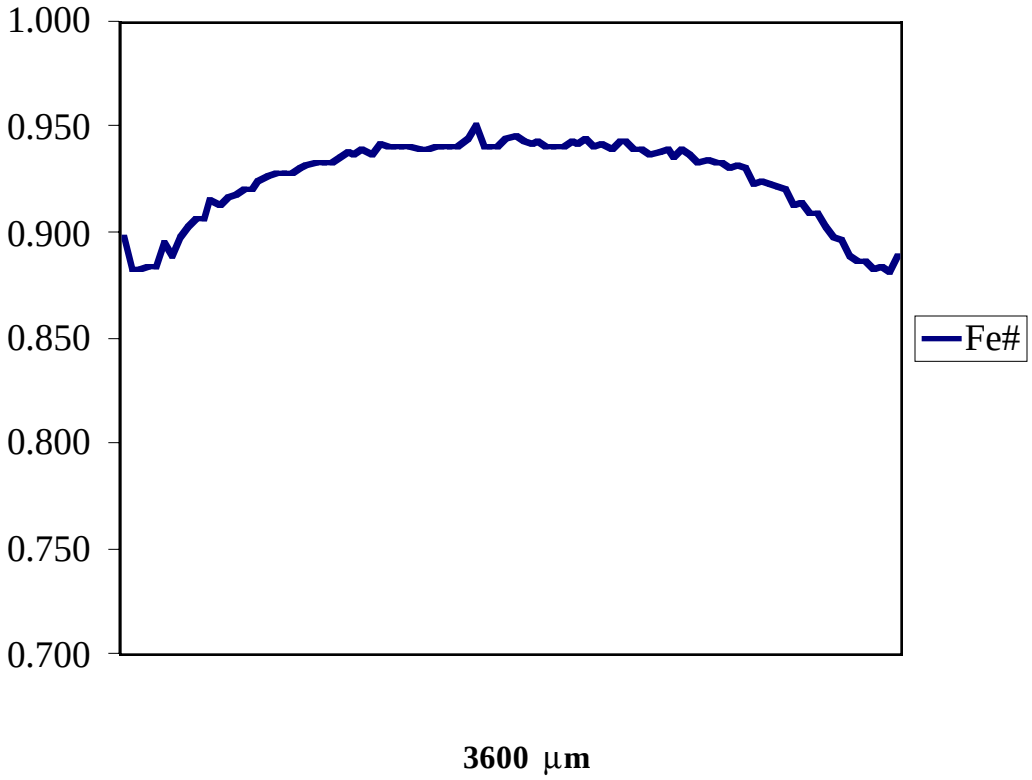

Figures 16 A-C. Compositional profiles for two grains from Np7 with Fe# plotted for first compostional profile. Figure B shows compositional profile for a grain that has the core replaced by bt, chl, qtz and plg.

Figure 17 A.

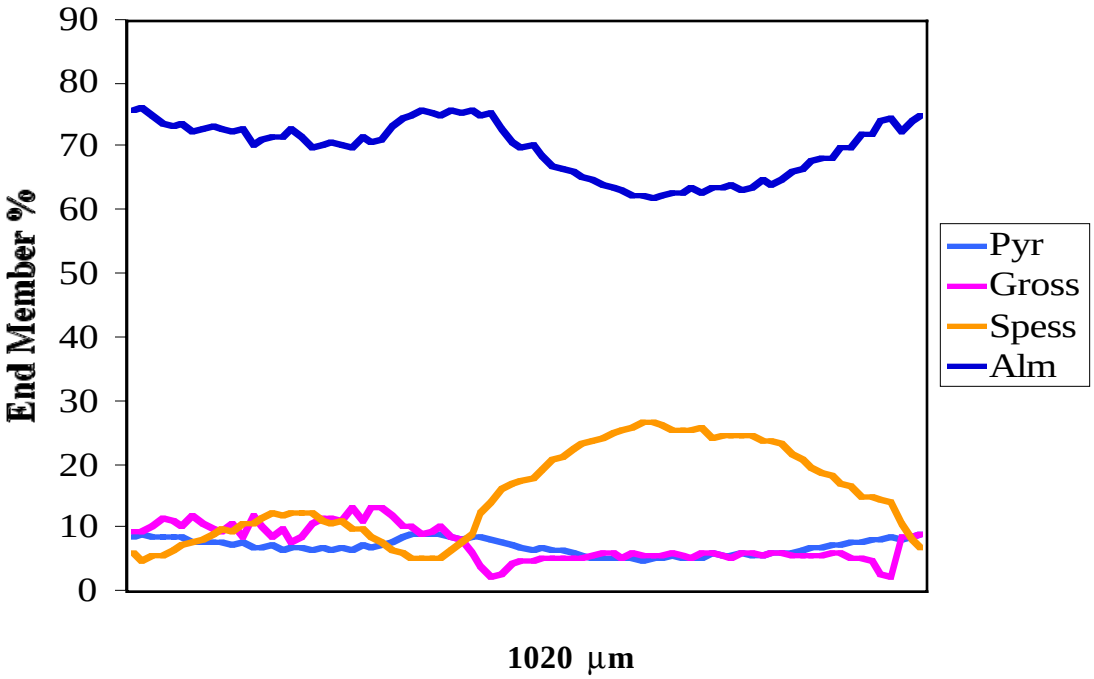

Figure 17 B.

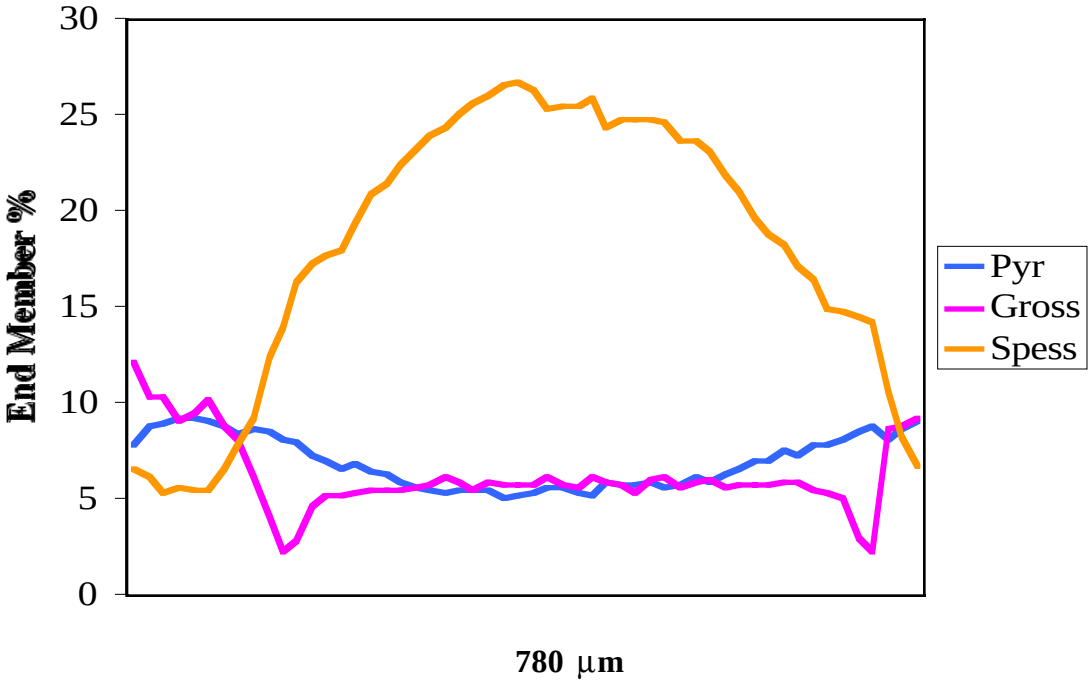

Figure 17 C.

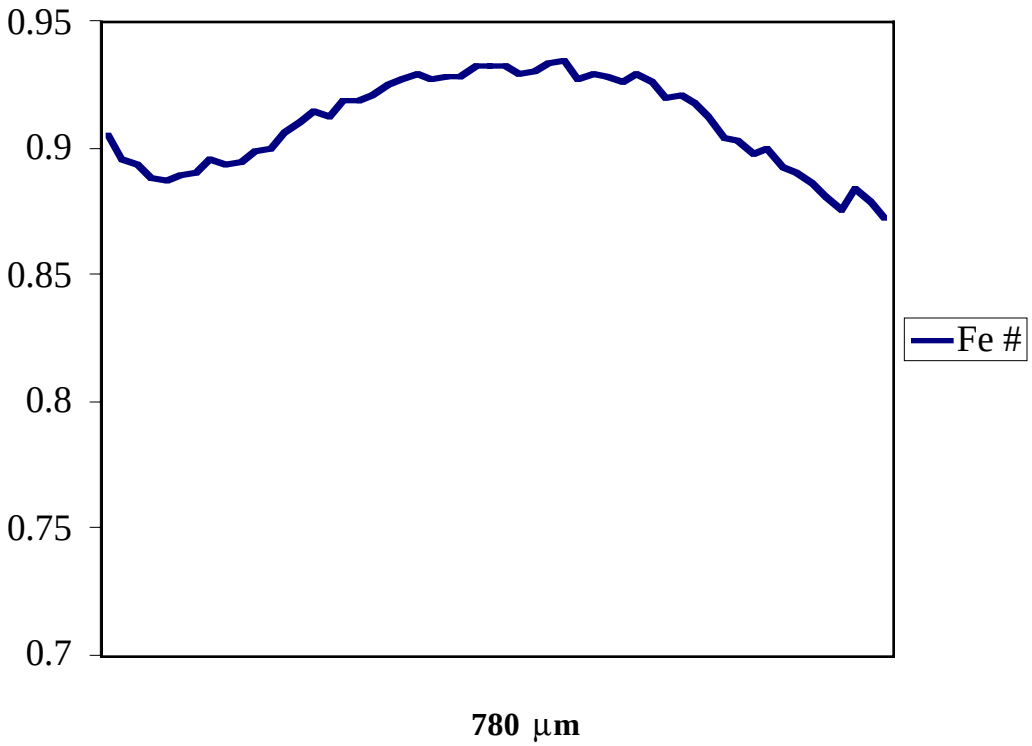

Figure 17 A- C. Compositional profiles Figure B shows enlargement of symmetrically zoned portion of Figure A. Figure C shows Fe# profile for Figure 17B.

Figure 18 A.

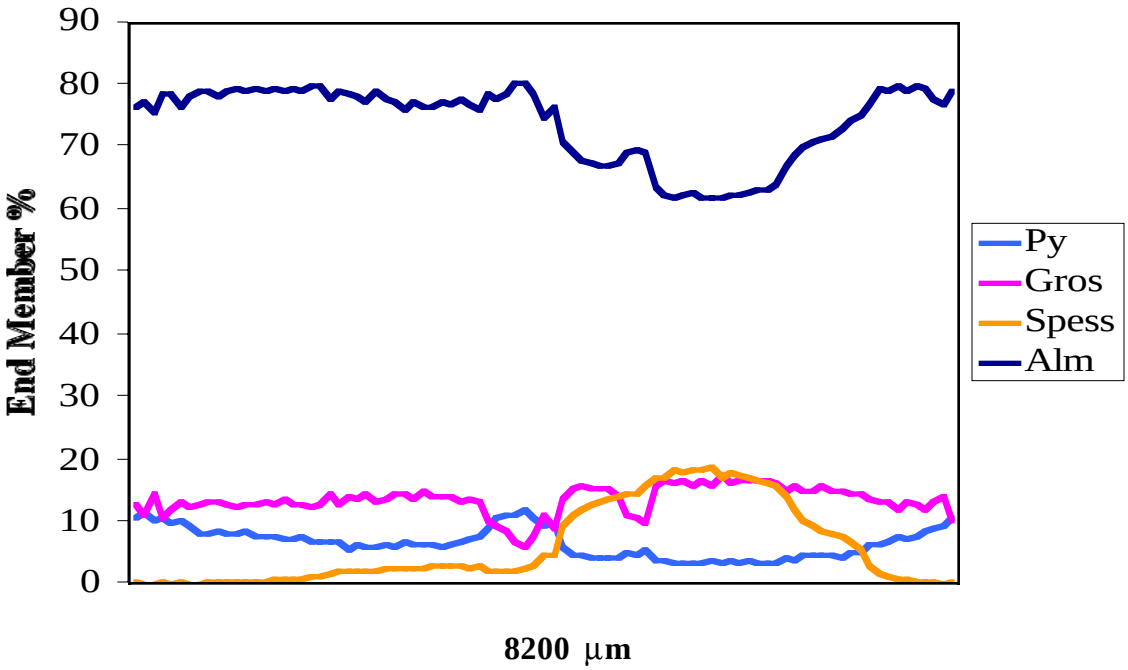

Figure 18 B.

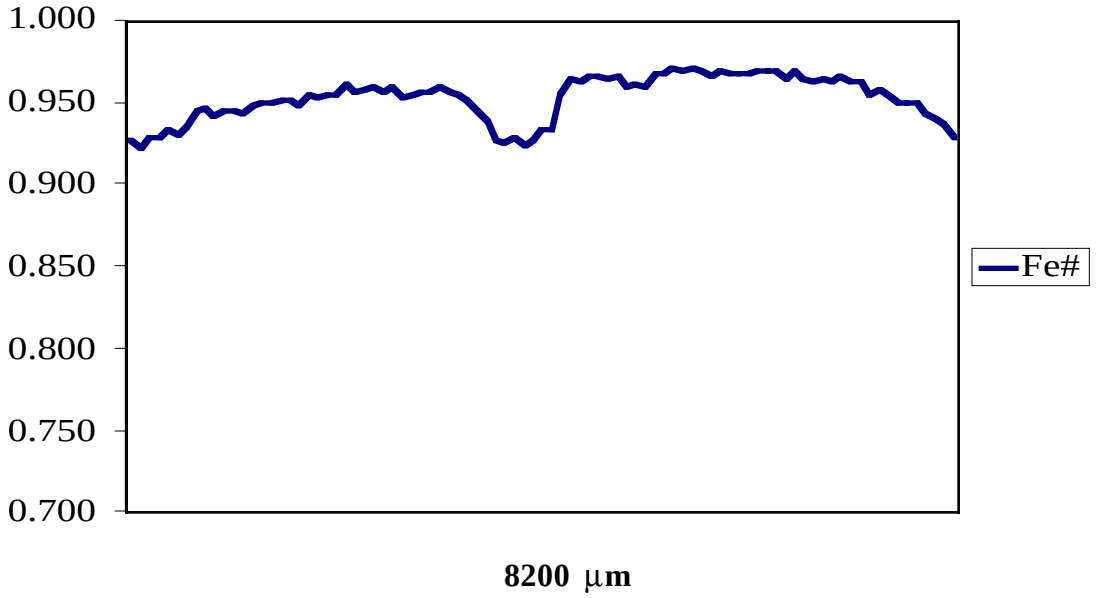

Figure 18 A and B. Compositional profile and Fe# profile for large broken grain from sample Np111b.

Figure 19 A.

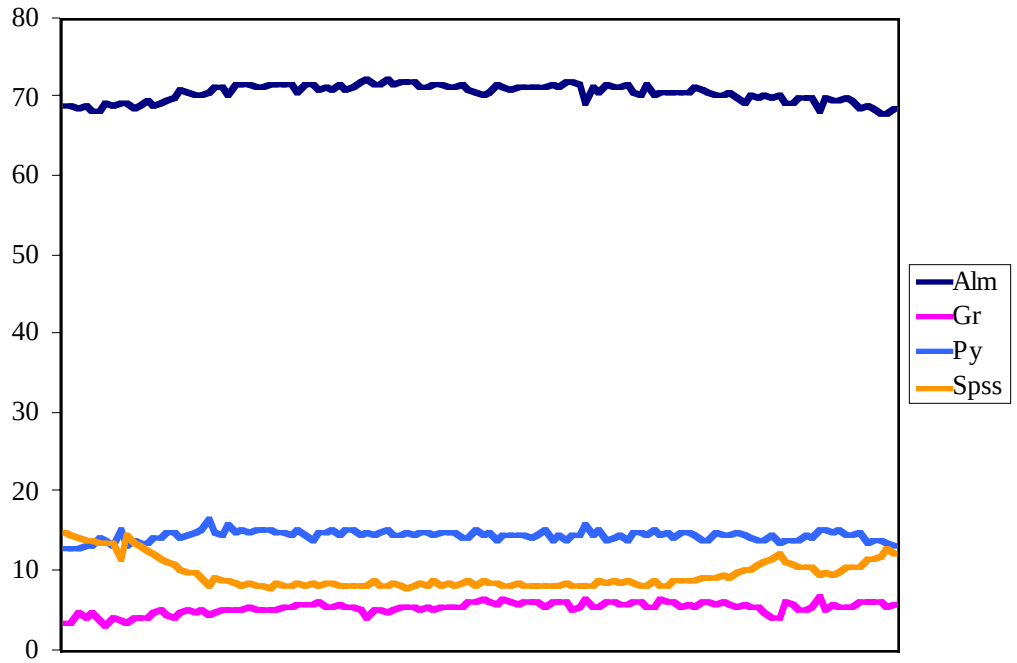

Figure 19 B.

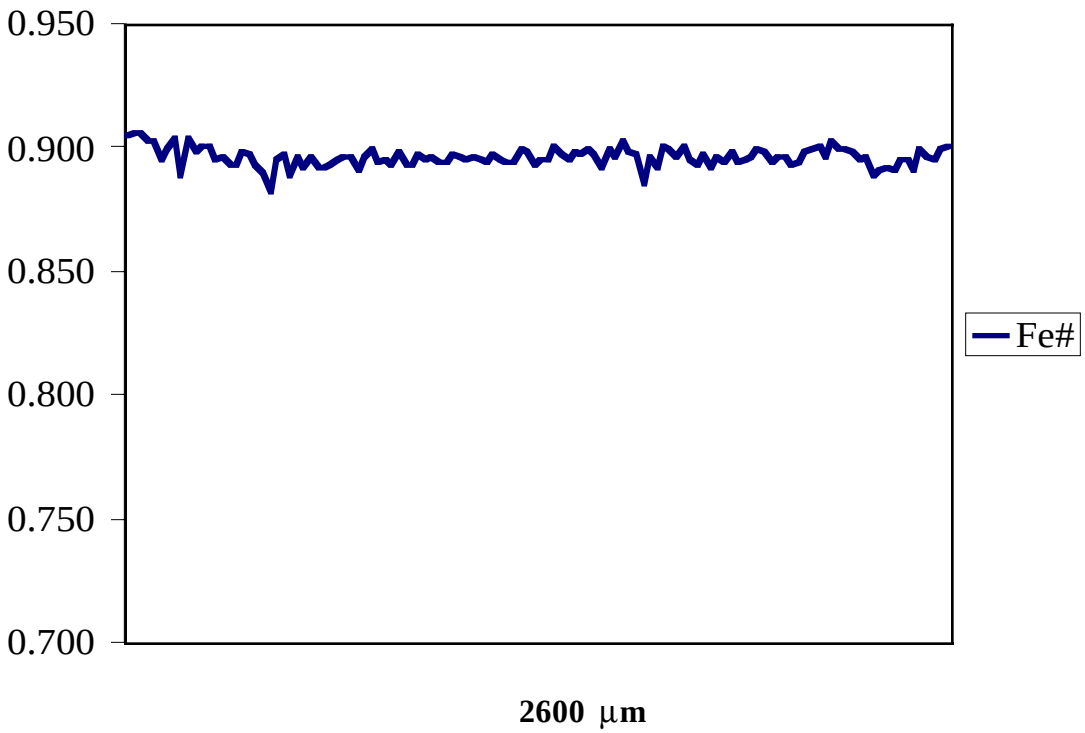

Figure 19 A and B. Compositional profile and Fe# profile for garnet grain in sample Np111a that has been overgrown by staurolite.

Figure 20 A.

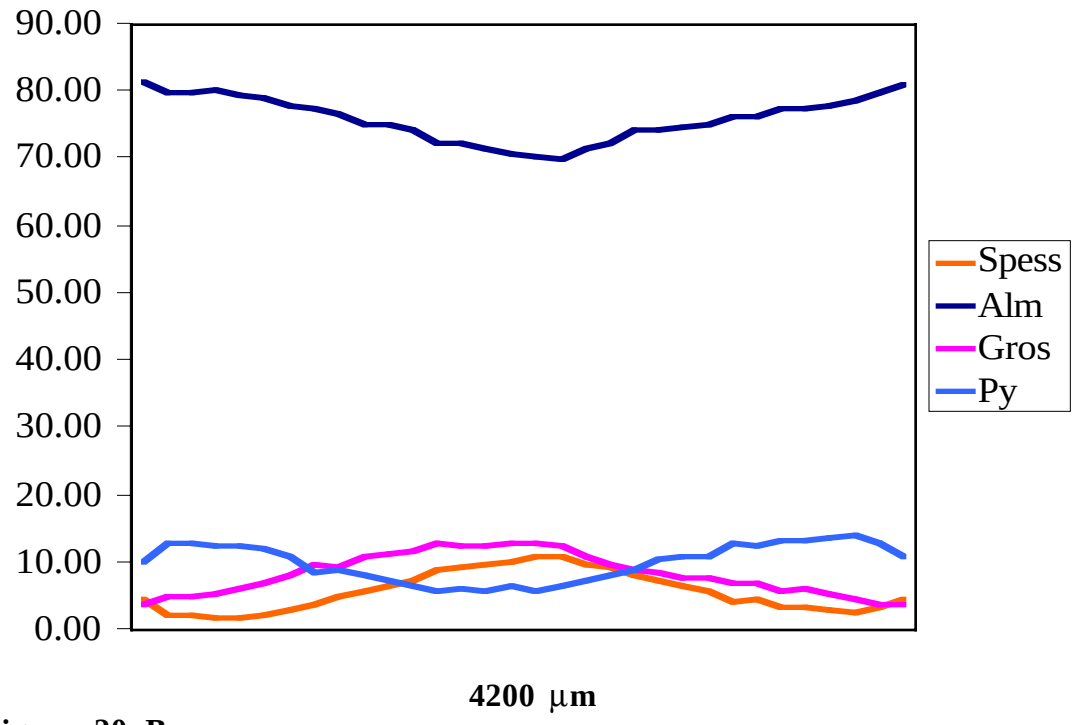

Figure 20 B.

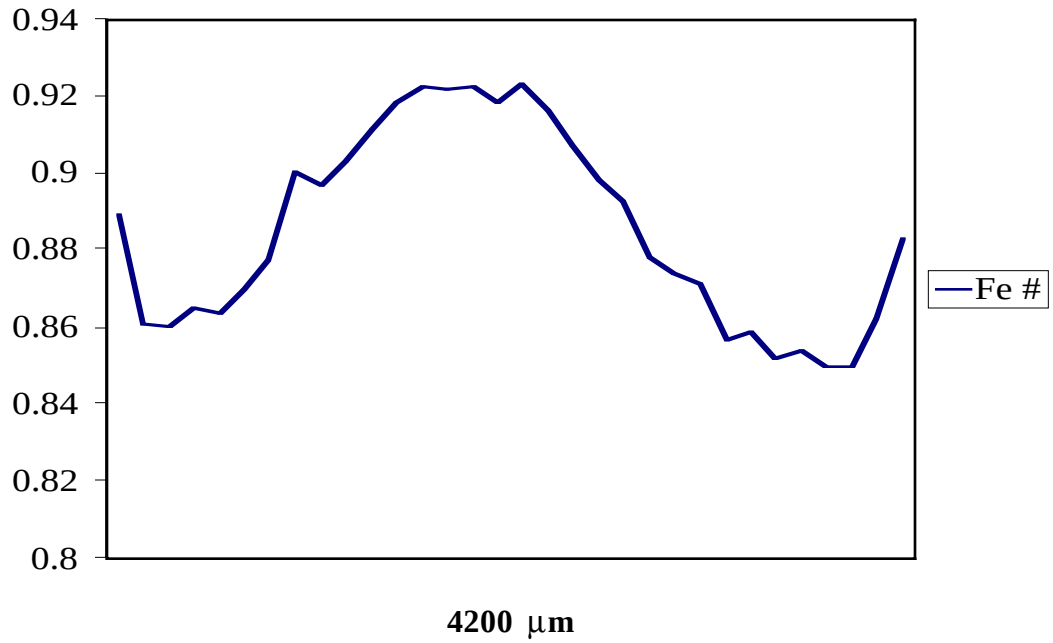

Figure 20.A and B. Compositional profile and Fe# profile for by from the Straits schist.

Figure 21 A

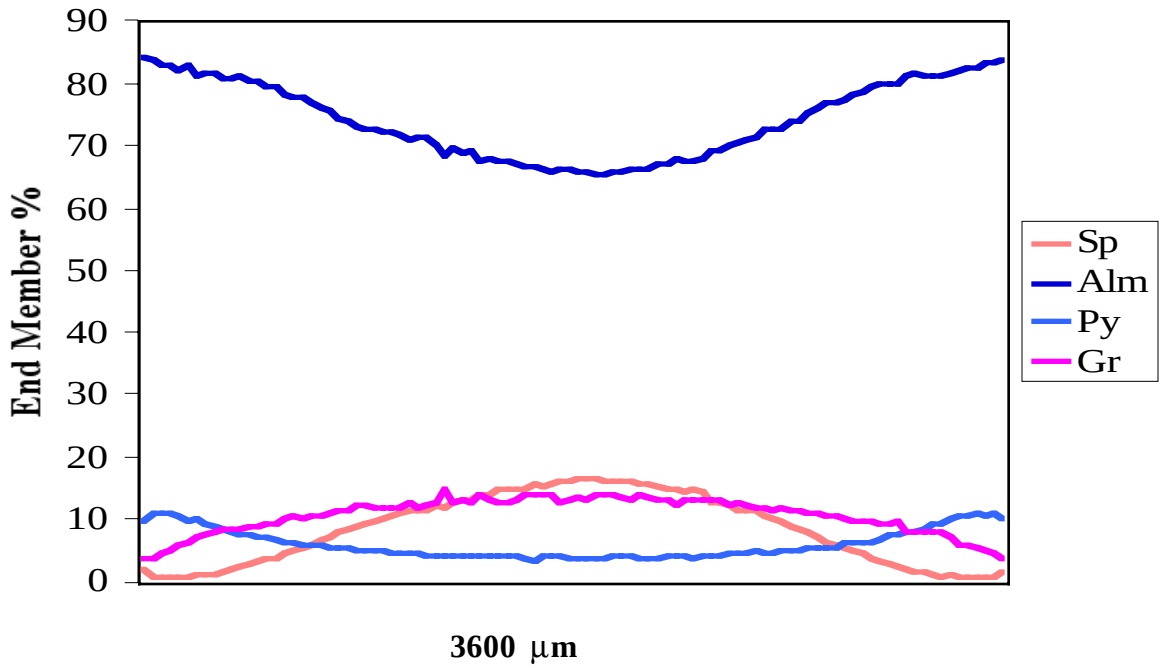

Figure 21 B.

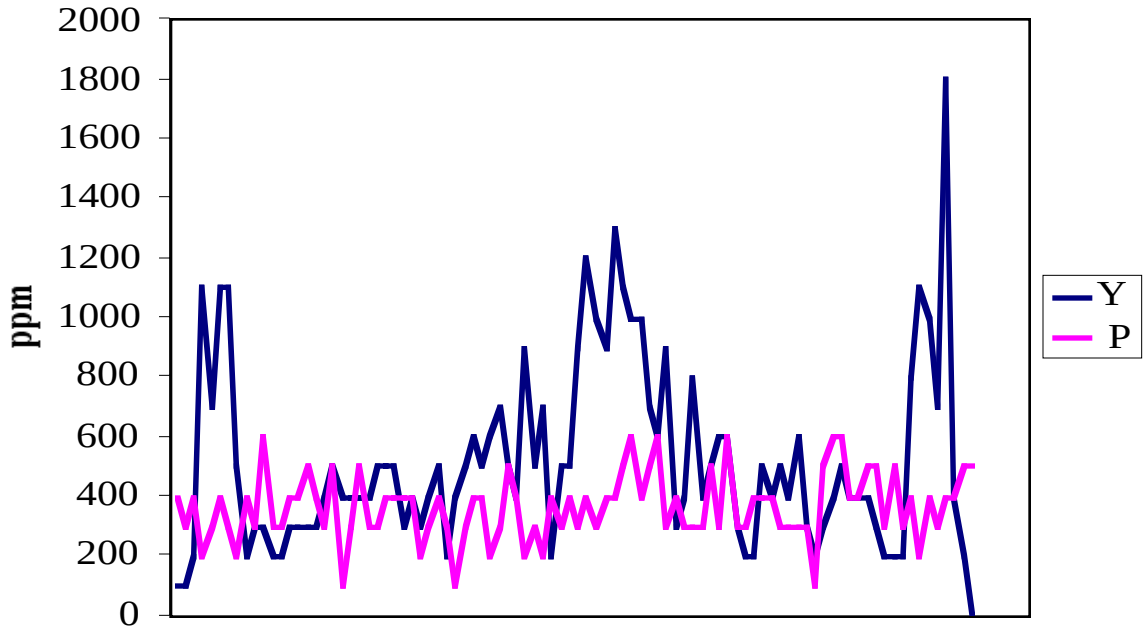

Figure 21 A-B. Major element compositional profile for sample Np7. Figure 21B Trace element profile for same grain as Figure 21A showing trends of Y and P content.

Figure 22 A

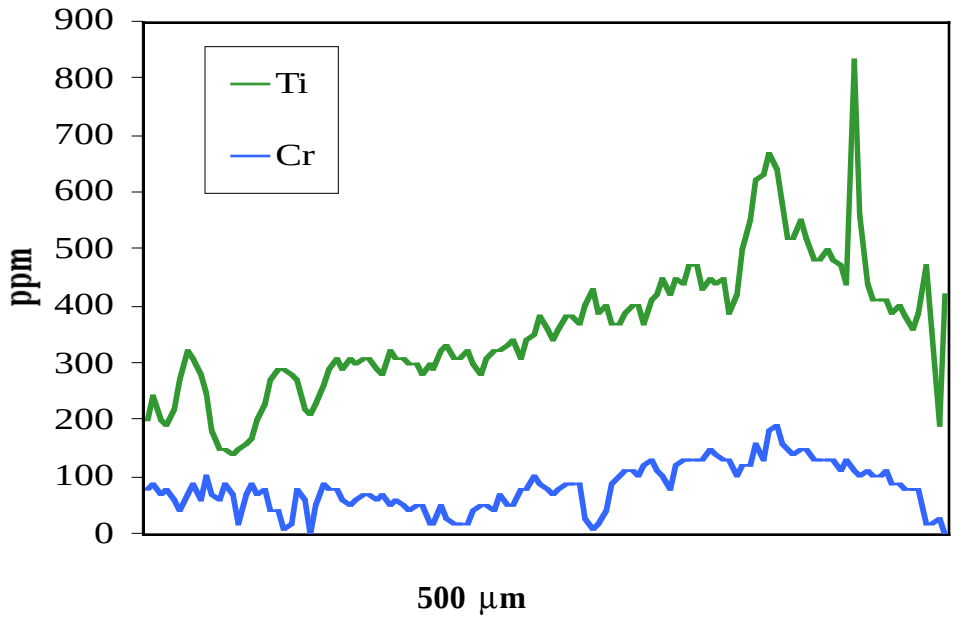

Figure 22 B.

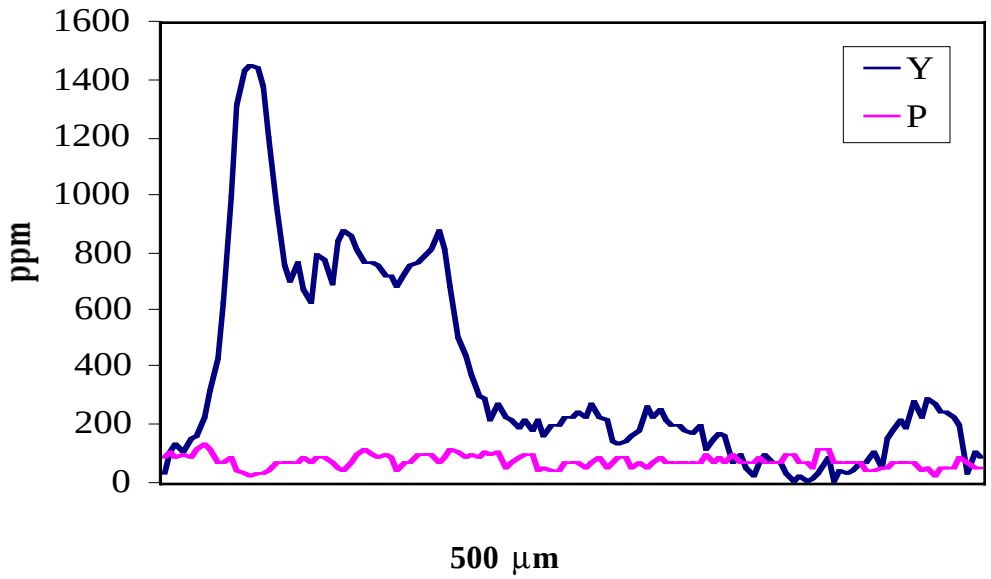

Figure 22 C.

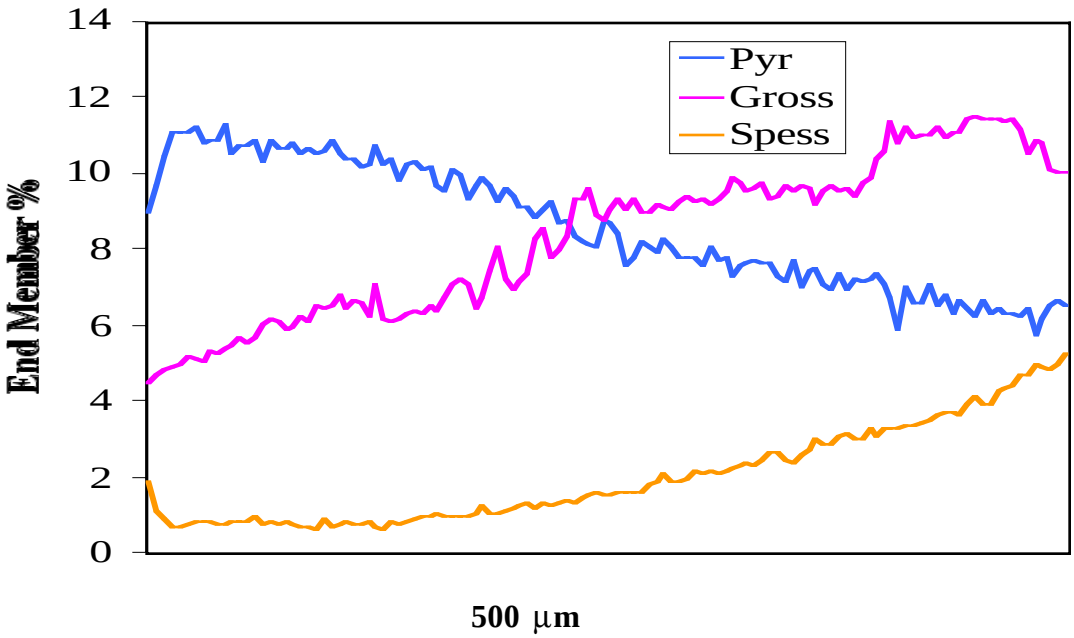

Figure 22 A-C. High resolution major and trace element profiles for corner of a garnet porphyroblast from sample Np7. Photomicrograph for the imaged area as well as the position for compositional profiles is shown in Figure 4D

Mechanisms for Mineral Zoning

The chemical zoning that may be preserved in a mineral is the result of two major processes: growth zoning and post-growth modifications caused by diffusion (Tracy, 1982). Growth zoning occurs when material being added to the rim of a growing garnet changes in composition with time. There are several processes or mechanisms that may result in changes to the composition of material added to the rim of a growing grain:

- Changes in P-T conditions.
- Changes in the mineral assemblage through loss of a reacting phase.
- Fractionation of material into the core of a zoned crystal, which changes the effective bulk composition of the matrix as the mineral grows.
- Changes in the bulk composition by infiltration or metasomatism.
- Disequilibrium partitioning of material at the rim by limitations of diffusion at the garnet rim surface.

In order to produce compositional zoning intracrystalline diffusion must be sufficiently slow that compositions are not reset as grains grow. As must be commonly the case, several of the above mechanisms may be acting simultaneously to produce growth zoning. In addition, these mechanisms can act independently for different elements. It has been shown that major element growth zoning can produce very different patterns from trace element zoning (Hickmott and others, 1987; Lanzirotti, 1995; Welch and others,1998.). Whereas growth zoning is produced by elemental fractionation during progressive growth of garnet, the spatial distribution of elements can be modified either subtly or dramatically both during and after growth by diffusion processes.

Diffusion zoning is the post-growth modification of the compositions of preexisting crystals. Unlike growth zoning, diffusion zoning may take place any time during or after the growth of a mineral. This may be an especially important process for garnet consumption reactions where certain elements may be preferentially removed (or left behind) as the garnet rim recrystallize. Diffusion zoning may also be an important process during retrograde metamorphic events.

Several models for producing growth zoning in metamorphic garnets have been proposed. Hollister (1966) proposed the first quantitative model for producing growth zoning that is based on the Rayleigh fractionation or distillation process. The model proposed that as a mineral grows elements that have a high garnet-matrix K_D (Mn in the case of garnet) will be preferentially incorporated into the growing mineral and therefore removed from the matrix reservoir. If diffusion is sufficiently slow, then the composition of the growing grain is effectively "locked". As a garnet grows there is less Mn (or other high K_D element) in the matrix to draw from. This process produces compositional profiles for garnet with Mn content decreasing from core to rim or the "bell" shaped traverse patterns for Mn that are common in garnets through amphibolite grade. It is generally accepted that at temperatures less than 600 ˚ C, the zoning produced by fractionation will be preserved (Frost and Tracy, 1991).

An understanding of the zoning patterns in garnet is essential before thermobarometric calculations are done. One other very important reasons for examining mineral zoning is that it provides some details about the reaction history of the growing grains (Tracy, 1976). By the nature of zoned minerals, the composition of the core of zoned mineral is not likely to be in equilibrium with the matrix minerals. For this reason, care should be taken in choosing locations within a zoned crystal for chemical analysis to be used in thermobarometric calculations.

P-T CONDITIONS

One of the major problems with calculating P-T conditions of metamorphism for the assemblage quartz-muscovite-biotite-plagioclase-garnet is that the absence of Al-silicate precludes the use of the well calibrated GASP barometer. However, the garnet-biotite Fe-Mg exchange geothermometer of Ferry and Spear (1978) is well suited for this assemblage at amphibolite facies conditions. There still are, however, numerous uncertainties involving the thermodynamic properties for many of the minerals involved in the net transfer reactions used as geobarometers (Essene, 1989). For this reason, two independent methods were used to determine P-T conditions of metamorphism.

P-T conditions were determined by simultaneously solving for both a barometer and an appropriate thermometer. Temperatures were then calculated using the garnet-biotite Fe-Mg exchange of Spear (1978) with garnet solution models of Hodges and Spear (1982) for those areas within a thin section where garnet and biotite were clearly involved in a reaction or appeared to be in equilibrium. For those samples that contain staurolite, temperatures were calculated using the garnet-staurolite Fe-Mg exchange geothermometer of Perchuk and others (1991). The garnet-chlorite Fe-Mg exchange geothermometer of Dickenson and Hewitt (1986) was also used for samples that show reactions involving garnet and chlorite as a check for relative P-T conditions for the stability of garnet with chlorite. Pressures were determined using the combined net transfer and exchange thermobarometer for the assemblage garnet-plagioclase-muscovite-biotite-quartz (GPMBQ) of Hodges and Crowley (1985). A list of the reactions used as thermometers and barometers for calculating P-T conditions is given below.

Garnet-biotite thermometer

$Fe_3Al_2Si_3O_{12} + KMg_3AlSi_3O_{10}(OH)_2 = Mg_3Al_2Si_3O_{12} + KFe_3AlSi_3O_{10}(OH)_2$

Garnet-Chlorite thermometer

$5\ Mg_3Al_2Si_3O_{12} + 3Fe_5Al_2Si_3O_{10}(OH)_8 = 5\ Fe_3Al_2Si_3O_{12} + 3Mg_5Al_2Si_3O_{10}(OH)_8$

Garnet Staurolite thermometer

$Fe_2Al_9Si_4O_{22}(OH)_2 + Mg_3Al_2Si_3O_{12} = Mg_2Al_9Si_4O_{22}(OH)_2 + Fe_3Al_2Si_3O_{12}$

GPMBQ thermobarometer

$Fe_3Al_2Si_3O_{12} + Ca_3Al_2Si_3O_{12} + KAl_3Si_3O_{10}(OH)_2 = 3CaAl_2Si_2O_8 + KFe_3AlSi_3O_{10}(OH)_2$

Typically several areas within a given thin section were analyzed where appropriate textures were found. The thermometers and barometer listed above were then used for the appropriate assemblage to determine P-T conditions of equilibrium for that set of minerals. Figures 23 A-E show P-T conditions for all of the thermometric calculations used for the samples analyzed in detail. Median P-T conditions were calculated using both the garnet-biotite thermometer and garnet-chlorite thermometer along with the GPMBQ thermobarometer and are shown in Figures 24 and 25.

Figure 23 A.

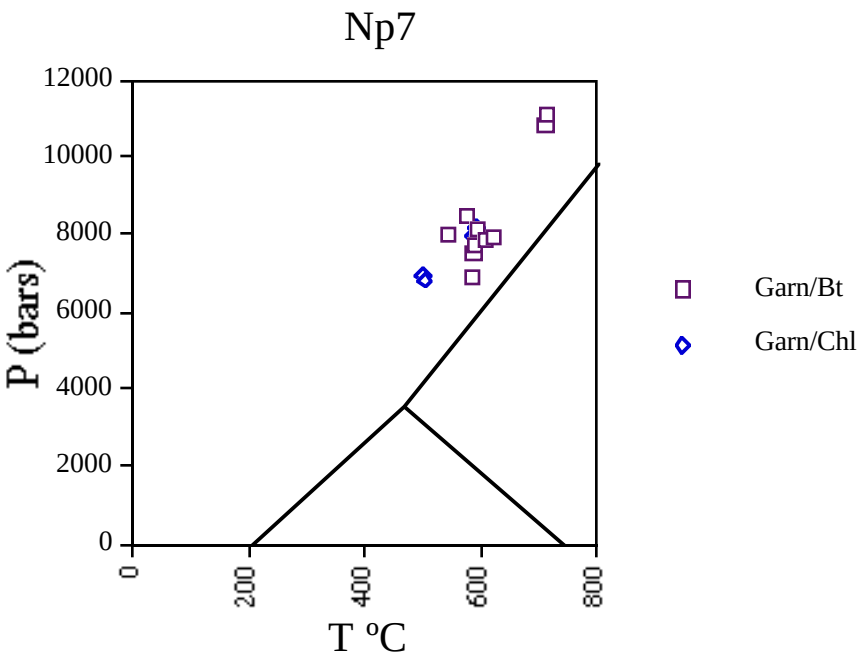

Figure 23 B.

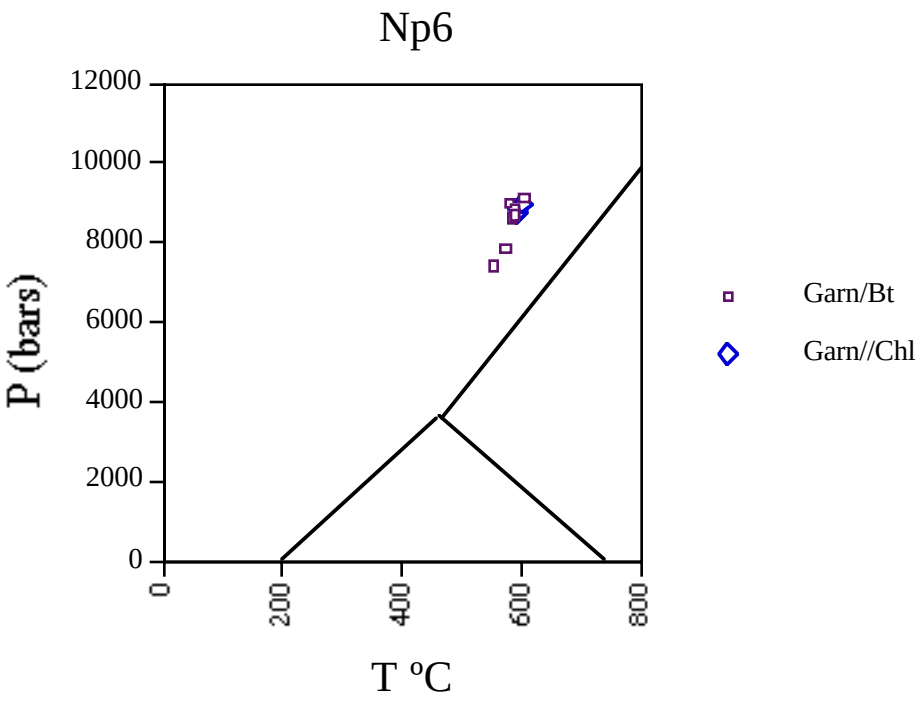

Figure 23 C.

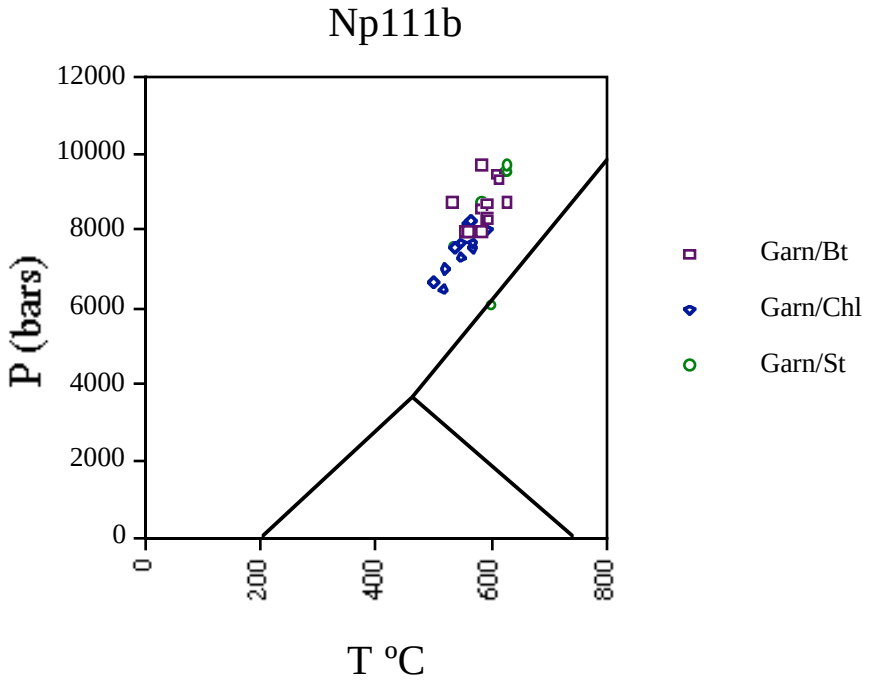

Figure 23 D.

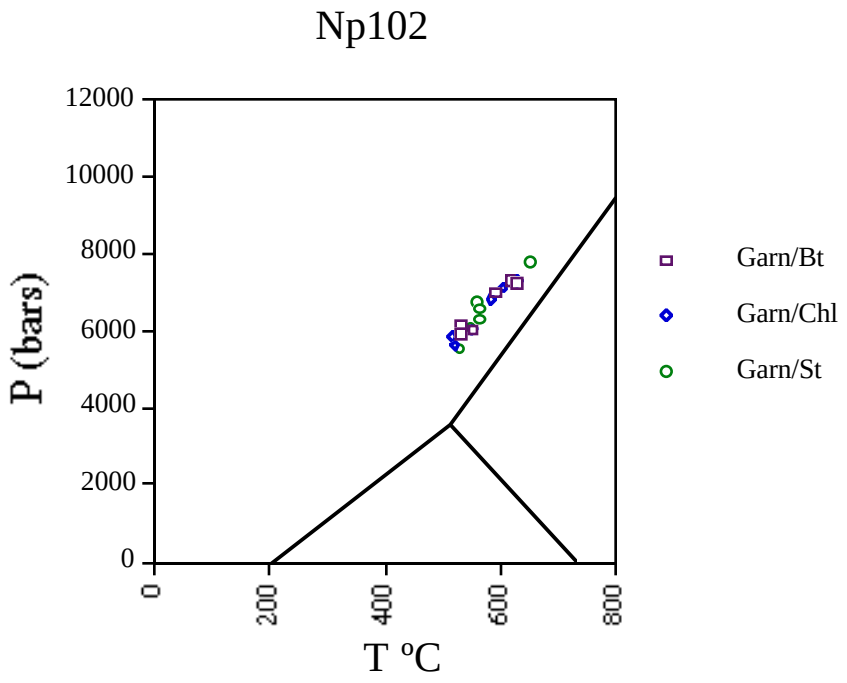
Np102
12000
10000
8000
6000
4000
2000
0
P (bars)
0
200
400
600
800
T ºC
Garn/Bt
Garn/Chl
Garn/St

Figure 23 E.

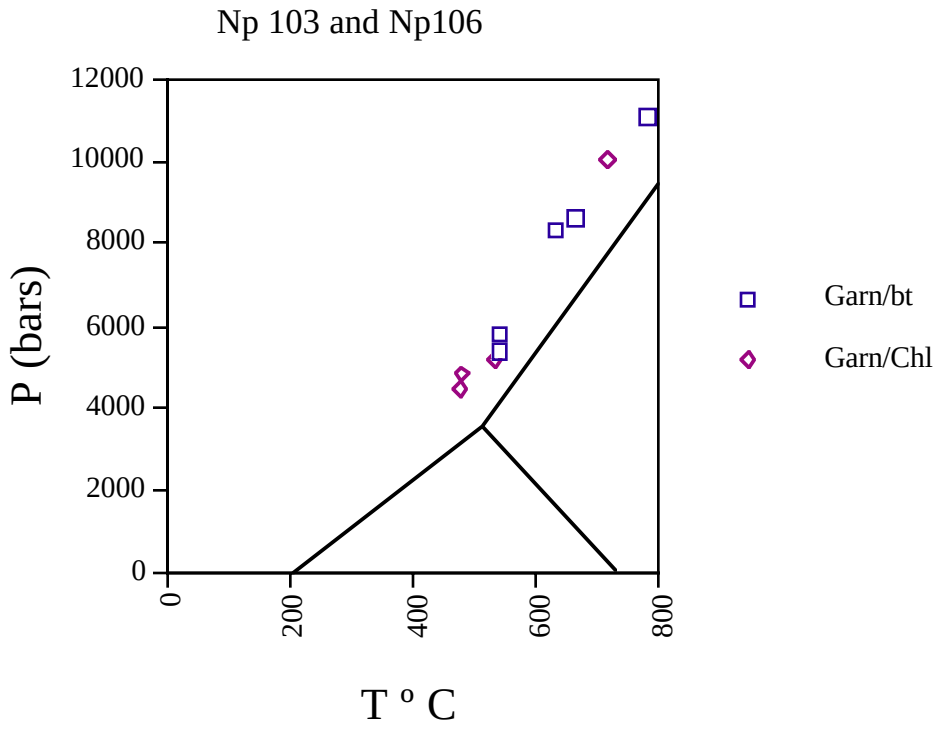
Np 103 and Np106
12000
10000
8000
6000
4000
2000
0
P (bars)
0
200
400
600
800
T º C
Garn/bt
Garn/Chl

Figure 23 A-E. P-T plots for samples within the New Preston quadrangle. Geothermometers and geobarometers were plotted for the appropriate assemblage for each sample.

Figure 24.

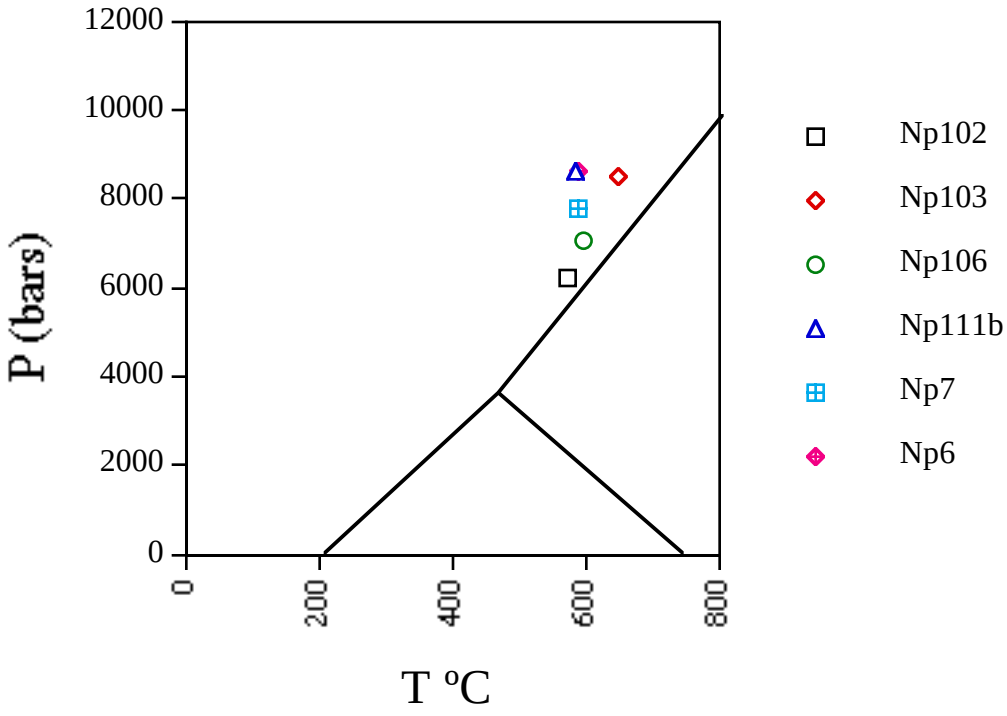

Figure 24. Summary P-T diagram for data in Figures 23 .A-E. Average P and T conditions were calculated for each sample using Grt/bt thermometer after Hodges and Spear (1982) and GPMBQ barometer of Hodges and Crowley (1985)

Table 4. Median P-T data with 1 σ estimates for the samples plotted in figure 24.

	T ˚C	1σ	P (bars)	1 σ
Np7	587	25	7861	515
Np111	585	25	8562	580
Np6	588	13	8740	475
Np102	587	39	6180	783
Np103	648	22	8463	134
Np106	541	0	5582	305

Figure 25.

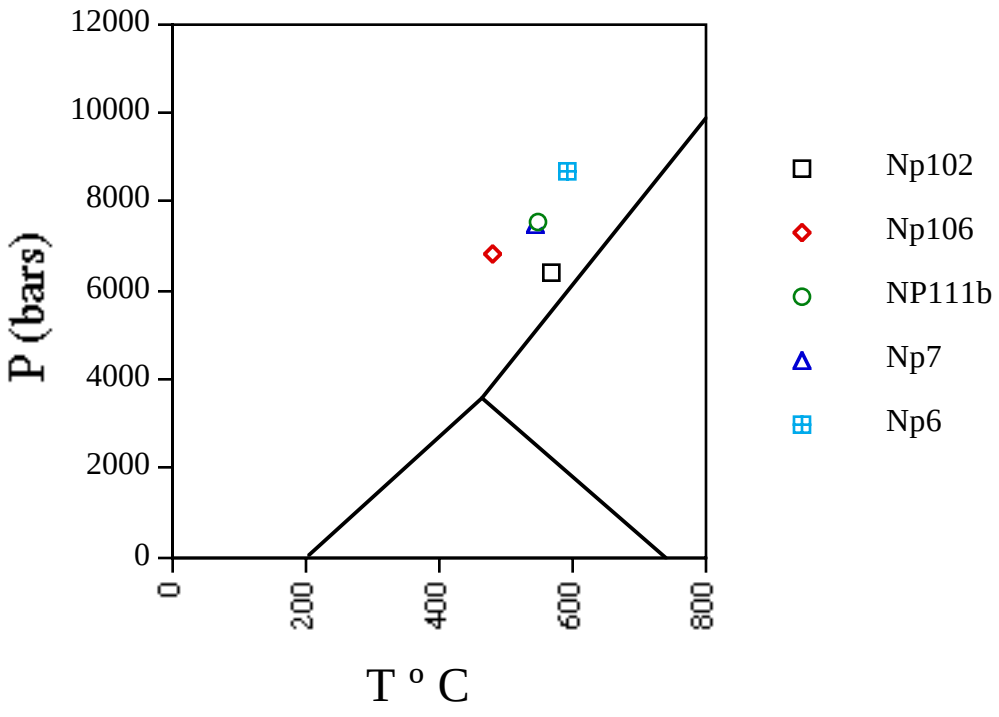

Figure 25. Summary P-T diagram for data in Figures 23.A-E. Average P and T conditions were calculated for each sample using Grt/Chl thermometer after Dickenson and Hewitt (1986) and GPMBQ barometer of Hodges and Crowley (1985)

Table 5. Median P-T data with 1 σ estimates for the samples plotted in Figure 25.

	T º C	**1 σ**	**P (bars)**	**1 σ**
Np102	566	46	6400	700
Np106	479	31	4820	350
Np111b	547	27	7550	600
Np7	544	50	7450	720
Np6	589	16	8700	590

The second approach that was used was to solve for all possible equilibria for a given assemblage using an internally consistent thermodynamic database. This was done using the software TWEEQU (thermobarometry with estimations of equilibria) and the methods outlined in Berman (1991). This method provides an independent means for determining P-T conditions for a given assemblage. Using an internally consistent thermodynamic database also provides a method for testing whether or not all or some of the minerals within a given assemblage equilibrated at the same P-T conditions.

For each sample, equilibria were calculated within the Na-Ca-K-Fe-Mg-Al-Si-O-H system using the internally-consistent thermodynamic database of Berman (1988). The following solution models for all phases that exist as solid solutions were used in the calculations: garnet - Berman (1991), muscovite - Catterjee and Froese (1975), plagioclase - Fuhrman and Lindsey (1988), biotite - McMullin and others (1991). As a first approach all possible equilibria were calculated for the total mineral assemblage in each rock. This typically would lead to far too many calculated net

transfer exchange equilibria to calculate P-T conditions with geologic significance for the assemblage. Phases were then systematically removed from the calculations one by one until meaningful intersections of equilibria were obtained. The sets of net transfer reactions and exchange equilibria were examined to confirm that they agree with petrographic observations.

Equilibria involving chlorite produced intersections across a wide range of pressures and temperatures. Chlorite was then generally removed from the calculation because petrographically it appears to postdate formation of the porphyroblasts and foliation and therefore is likely a late phase. Chlorite is also known to re-equilibrate compositionally down to low temperatures. Staurolite was also removed from the calculation because the set of equilibria involving staurolite also did not produce meaningful intersections. Equilibria were then calculated for the assemblage quartz, muscovite, biotite, plagioclase and garnet. The equilibria for representative thin sections are shown in Figures 26.A-D. The assemblage; quartz-muscovite- biotite-plagioclase-garnet produced good intersections that are consistent with results from thermobarometric calculations. .

Figure 26 A.

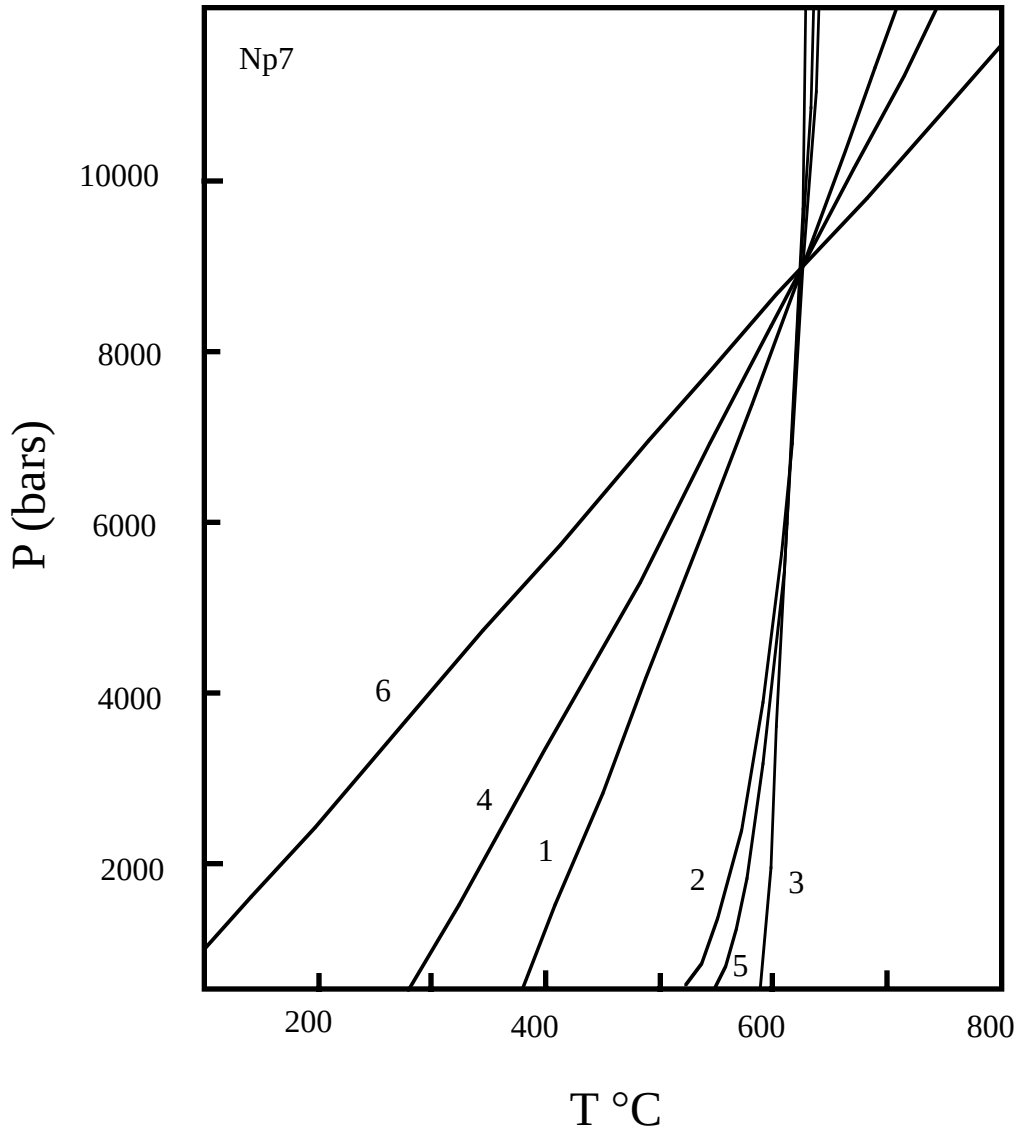

Figure 26 B.

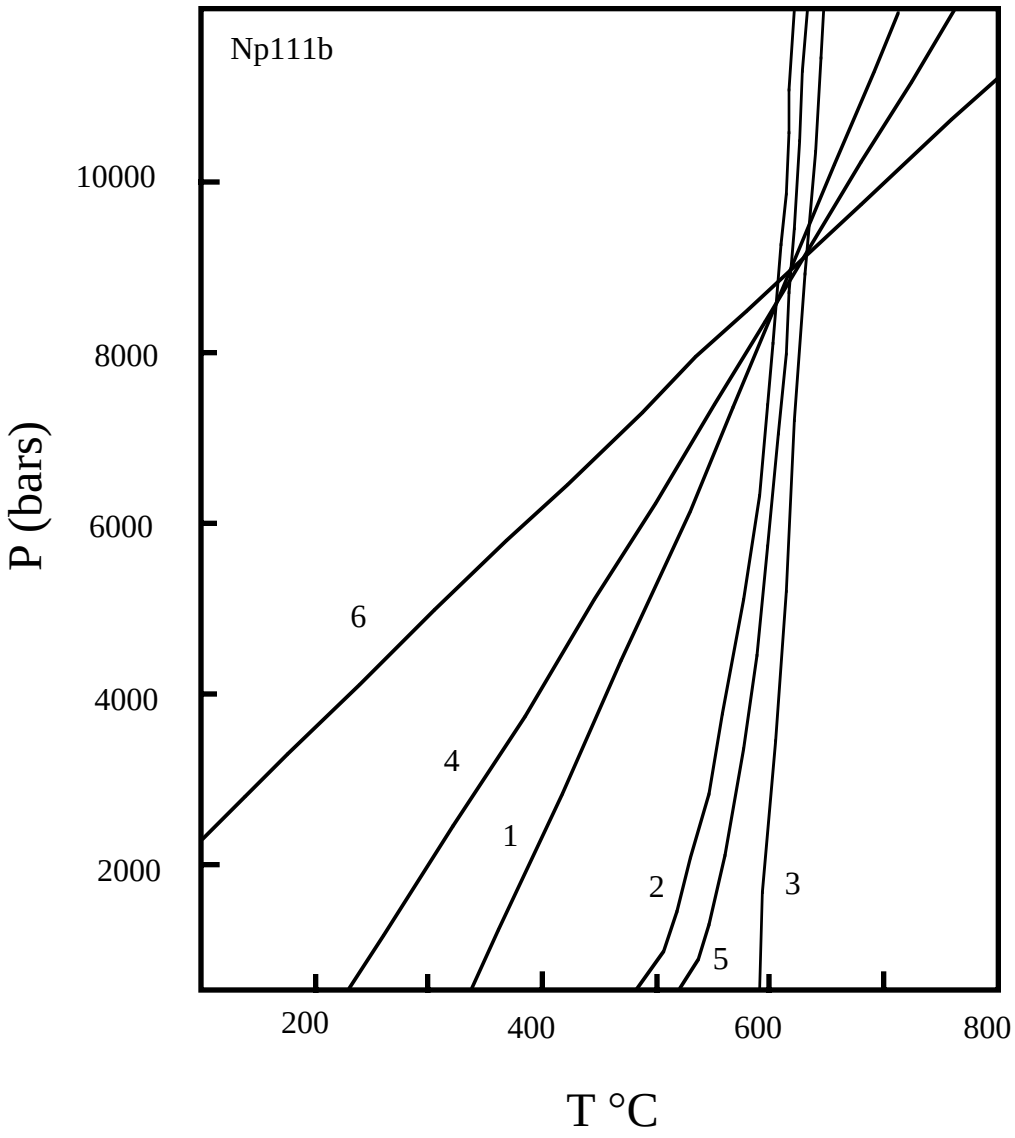
Np111b
10000
8000
6000
4000
2000
P (bars)
6
4
1
2
3
5
200
400
600
800
T °C

Figure 26 C.

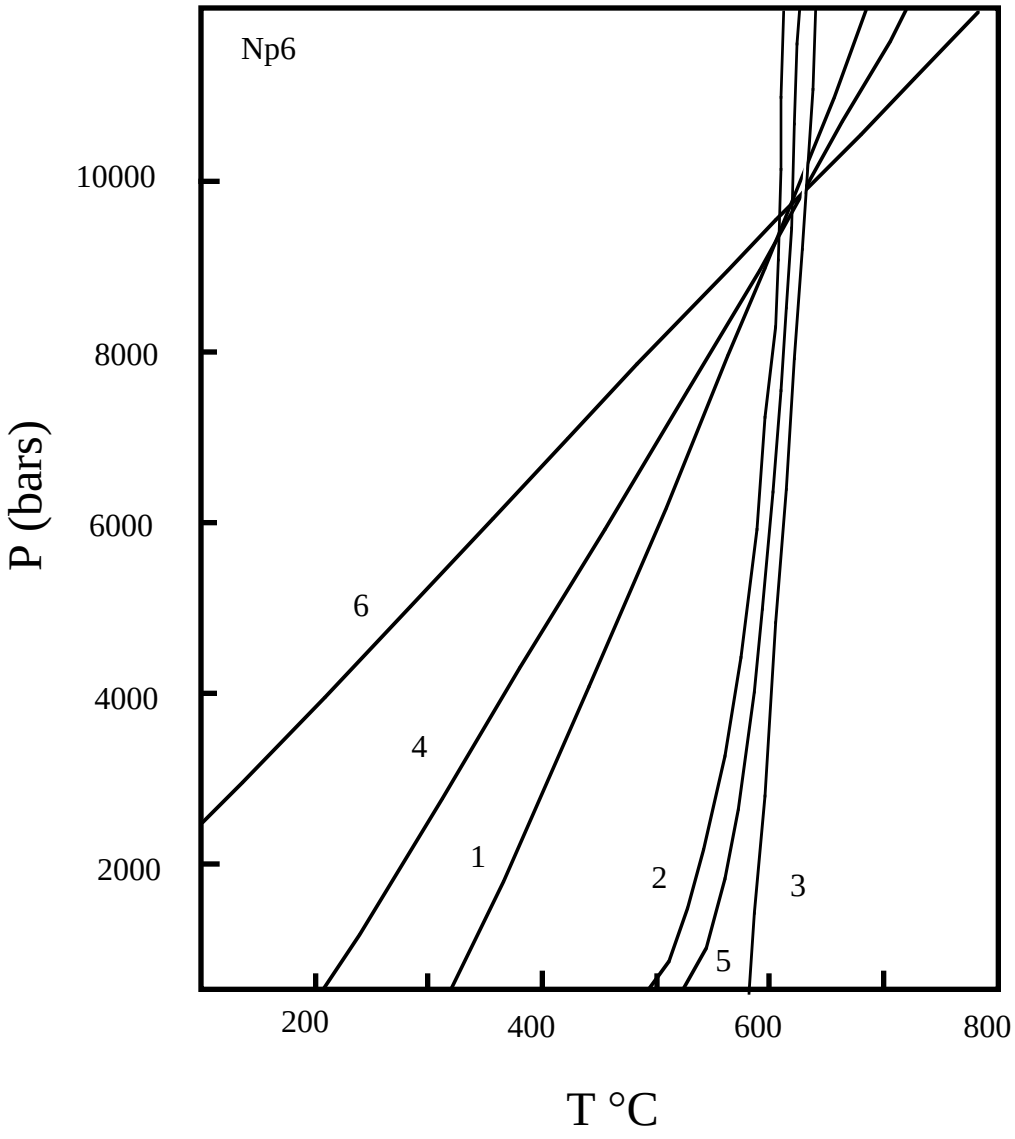

Figure 26D.

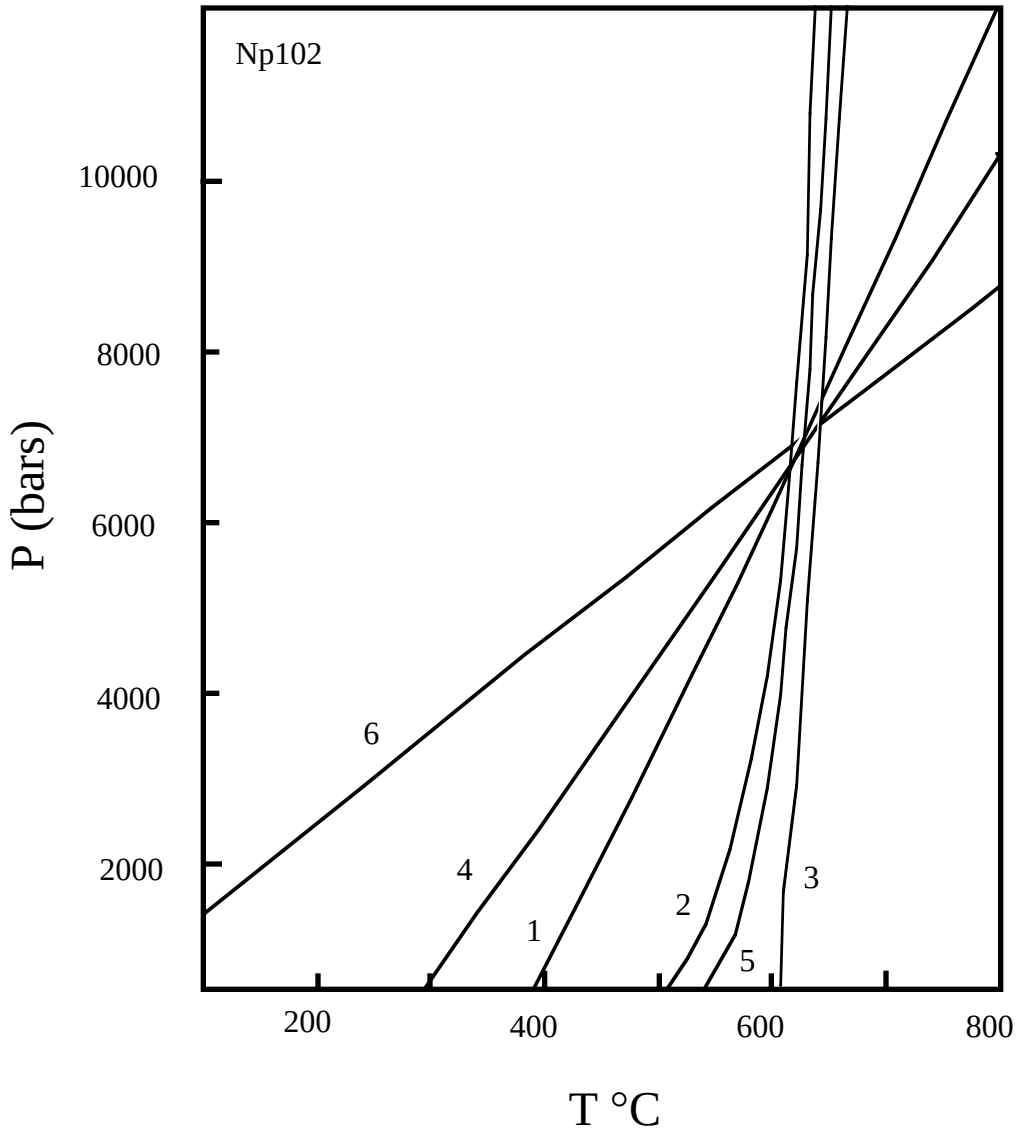

Figure 26.A-D. TWEEQU plots for the system Na-Ca-K-Fe-Mg-Al-Si-O-H for representative samples within the New Preston quadrangle. The set of equilibria plotted are for the phases plagioclase, garnet, biotite, muscovite and quartz. The net transfer reactions and exchanges for the plots are listed in Table 7.

Table 6. P-T conditions with 1σ variations calculated from intersections of substantially non-parallel equilibria

	T ˚C	**1 σ**	**P (bars)**	**1 σ**
Np7	605	1	8950	7
Np6	613	8	9670	146
Np111b	611	10	8460	100
Np102	624	10	6870	220

Table 7. Net transfer and exchange equilibria used for TWEEQU calculation.

- Grs + 2 Pg + 3Qtz = 3An + 2Ab + $2H_2O$
- Ann + 2 Pg + 3Qtz = Ms + Alm + 2Ab
- Phl + Alm = Prp + Ann
- Ms + Grs + Alm = Ann + 3An
- 2Pg + Phl + 3Qtz = Prp + Ms + 2Ab + $2H_20$
- Prp + Ms + Grs = 3An +Phl.

DISCUSSION OF MINERAL ZONING

Three unique zoning patterns have been observed in garnets from the New Preston quadrangle. One of the most striking features about the compositional zoning in garnets from this area is the generally euhedral nature of the zoning. This type of pattern suggests a relatively simple growth history with very little post-growth diffusion. Samples Np7, Np111b and Np102 have major element zoning profiles that are clearly characteristic of prograde growth (Tracy 1976). Compositional profiles are shown in Figures 16A-C and 18A and B. All the major elements show smooth bell-shaped curves in the compositional profiles and euhedral compositional images (Figures 6A and B, 8 and 10 with Mn and Ca decreasing from core to rim and Fe and Mg increasing from core to rim. These profiles lack inflection points except within a few microns of the rim where Mn increases slightly and Mg decreases slightly. Fe/(Fe + Mg) (Fe#) profiles show similar trends with Fe# decreasing from core to near the rim and then increasing within a few microns of the rim, primarily caused by a decrease in Mg. This trend in decreasing Fe# with no inflection points is characteristic of garnet growth from continuous reactions (Tracy, 1976). There are two possible explanations for the change in Fe# accompanied by an increase in Mn at the rim of these grains. One interpretation is that these reversals resulted from retrograde reequilibration during cooling. Mn is preferentially incorporated into remaining garnet as garnet rims are resorbed and recrystallize. The other is through production of a more Mg-rich secondary phase such as biotite or chlorite. The latter is a more likely explanation given that these sample show varying degrees of biotite or chlorite replacement at garnet rims. Figure 4C shows a photomicrograph of a garnet porphyroblast that has been partially overgrown by biotite and porphyroblastic chlorite. In sample Np111b most of the garnet grains show nearly complete replacement of garnet rims by biotite (Fig. 4F.).

Compositional images show euhedral zoning patterns for these samples (Figures 6, 8, and 10) suggesting that garnet growth was the result of a single continuous reaction and diffusion was very limited during and after growth. Biotite and chlorite overgrowths truncate compositional zoning at garnet rims in samples Np7 and Np111b and must therefore postdate porphyroblastic mineral growth. Sample Np7 also has several porphyroblasts that have garnet cores apparently replaced by coarse-grained quartz, plagioclase, biotite and chlorite that also truncate compositional zoning indicating that these textures must also postdate porphyroblastic mineral growth. Several continuous reactions have been proposed for the prograde growth of garnet that can produce such profiles (Thompson, 1976; Spear and Cheney 1989). All of these reactions involve chlorite and biotite as reactants breaking down to form garnet.

Compositional zoning in the Straits Schist shows similar patterns to those discussed above in that the zoning in the cores is probably the result of prograde growth. Compositional images and profiles are shown in Figure 11and 20 A-B for comparison. However, euhedral zoning patterns for elements other than Ca that are characteristic for garnets in the Ratlum Mountain and Rowe Schists are not preserved in garnets from the Straits Schist. Straits Schist garnets appear to have been at high-enough T (> 650 ˚ C) for long enough to significantly relax original growth zoning. Fe# profiles for garnets from the Straits Schist show similar but more pronounced trends to those in the Rowe and Ratlum Mountain Schists, with Fe# decreasing from core with the same inflection near the rim.

A second type of zoning pattern was observed in sample Np111a. Compositional profiles and images for this sample are shown in Figure 9B and 19 A-B. This sample has nearly homogeneous garnet cores with respect to all major elements. Towards the rim Fe, Mg and Ca decrease slightly and Mn increases. The compositional profile for Fe# is flat from core to rim and can not be explained by any

single continuous reaction involving Mg and Fe exchange (Tracy, 1976). This sample contains large porphyroblasts of both staurolite and sodic plagioclase with some garnet porphyroblasts that are completely enclosed by staurolite. Figure 4G shows a photomicrograph of garnet, plagioclase and biotite that are completely enclosed by staurolite. This type of zoning pattern is more easily explained by a discontinuous reaction, such as

$$Grt + Chl + Ms \rightarrow Staurolite + Bt + H_2O$$

rather than any continuous reaction involving Fe and Mg exchanges.
As garnet is consumed in this reaction the rim will continue to recrystallize and preferentially incorporate Mn. Compositional images for this sample (Figure 9B) show Mn enrichment parallel to the garnet edges but not in a euhedral pattern.

The third type of zoning observed is in garnets that have distinct high-Ca overgrowths. Compositional images and profiles for Np106 are shown in Figures 7 and 17 A-C respectively. Fe, Mg, and Mn show trends similar to those samples that contain garnets produced by continuous reactions. Fe and Mg increase from core to rim and Mn decreases from core to rim. Changes in Ca content cannot be correlated with changes in Fe, Mg and Mn. Rounded, high-Ca overgrowths surround euhedral cores with relatively homogeneous Ca content. At the interface between core and rim in these grains there is a narrow band of Ca depletion. The complexity of the compositional texture preserved here may be due in part to the fact that Ca diffusion is sufficiently slow relative to Mn, Mg and Fe in amphibolite facies rocks to preserve more complex zoning patterns. Chernoff and Carlson (1997) cited other examples of complexly zoned garnets where Fe, Mn and Mg zoning patterns can be correlated but which do not spatially correspond to zoning patterns for Ca. They attributed this lack of correspondence with very local dissequilibrim for Ca. Ca compositional images for sample Np6 are patchy and likely represent very localized equilibrium, perhaps at the micron scale. High resolution images for other samples also show very complex zoning for Ca with the general trend of Ca content decreasing from core to rim. The

high-Ca rims for this sample are thought to represent a second phase of garnet growth at high pressure in response to anorthite breakdown in plagioclase which will have little effect on the Fe# if the almandine and pyrope components decrease equally in response to an increase grossular content.

Trace element zoning patterns may also provide some insight into the growth history of metamorphic garnet. Hickmott and others (1987) was the first to look in detail at the trace element zoning patterns in metamorphic garnets. Hickmott found that several trace element patterns show either smooth zoning profiles from core to rim or display spikes in concentration that could be correlated to spikes in Ca content that were attributed to a P-T reversal. The two samples (Np7 and Np6) that were analyzed in detail for trace elements in this study show very similar Y zoning patterns to those in a sample from the Straits Schist reported by Lanzirotti (1995). Figures 12-15 show compositional images for these two samples. Both of the samples show strong enrichment in the garnet cores that decreases toward the rim. This type of zoning is likely caused by the same Rayleigh fractionation process that causes zoning for major elements like Mn with very high K_D. The most noticeable feature in both of these samples is a narrow band of Y enrichment near the rim. Hickmott (1989) presented several models for trace element enrichment although there is still much debate about which process may be operating to produce this kind of zoning. Zoning of this type could be produced for an element with a constant K_D by changes in growth rates. If intercrystalline diffusion in the matrix sufficient to supply a constant supply of an element to the garnet rim as it grew then very rapid porphyroblast growth should produce crystals that have relatively low concentrations for that element. However, if the growth rate is very slow then such slowly grown crystals may be enriched in that element. Episodic changes in growth rate could then produce oscillatory zoning for a given element. If the initial stages of porphyroblast growth is very rapid followed by very slow growth at the final stage then this process could produce this type of zoning.

In sample Np7 this band of Y enrichment is very sharp and close to the rim. If the model for a single prograde growth history is valid then this sharp band of Y enrichment coincides with the last stages of garnet growth. This band also lies just inside the area of the garnet that has re-equilibrated with matrix in response to later growth of chlorite and biotite In sample Np6, this narrow band lies inside the high calcium overgrowth and likely represent the last stage of garnet growth for the core of this grain that was subsequently overgrown in a separate garnet growth event.

DISCUSSION OF EQUILIBRIA AND P-T CONDITIONS

One very important aspect of calculating P-T conditions of metamorphism for rocks that have likely undergone multiple episodes of metamorphism is to ascertain whether or not the minerals being used for thermobarometric calculations are in equilibrium. All of the possible equilibria for the assemblages present in each rock were calculated using an internally consistent thermodynamic database using the methods of Berman (1991). Plots for the data of representative samples are shown in Figures 26 A-D. The plotted equilibria involve the phases quartz, plagioclase, garnet, muscovite and biotite. Chlorite and staurolite were not considered in the final calculations because equilibria including these two phases did not produce the tightly clustered sets of intersections with equilibria calculated using only other phases.

The advantages of using an internally consistent database are twofold. First, it provides a means for calculating P-T conditions using multiple equilibria based on the same thermodynamic database, thus removing systematic errors in the calibrations of thermometers and barometers. The importance of this method becomes clear when P-T conditions are calculated with traditional thermobarometric methods with several different thermometers or barometers. Second it allows for some assessment of equilibrium. In the ideal case, if all of the minerals in a rock are in equilibrium and the thermodynamic data for those minerals are well defined, then all of the equilibria will intersect at a point in P-T space representing the P-T conditions of equilibrium for that assemblage (Berman, 1991). If the intersections for equilibria of a given mineral are not tightly clustered about a point then this may suggest that it is not in equilibrium with the rest of the assemblage. A significant problem with this technique is that solution models are not well defined for all minerals. Essene (1989) provided a detailed look at the status of the knowledge of the thermodynamic database for the minerals involved in the equilibria that were used for this study. No solution models are provided for either chlorite or staurolite in the multiequilibria software of Berman,

making it difficult to determine whether or not these may be in equilibrium with rest of the assemblage. Data files for the calculations were created using garnet rim compositions along with biotite that was in direct contact. Compositions for other minerals were taken from grains that were either in mutual contact or close by in the matrix.

Calculations of equilibria show the most tightly clustered sets of intersections for those samples that petrographically show biotite overgrowing garnet. These tightly clustered sets of equilibria suggests that the mineral assemblage used for the calculation represents an equilibrium assemblage. This presents strong evidence that matrix muscovite, plagioclase and biotite were in equilibrium with garnet rims. Staurolite and chlorite were likely involved in garnet-producing or breakdown reactions at some time during the reaction history but may not have re-equilibrated with the garnet rim composition or other matrix minerals during the latest thermal event.

P-T conditions calculated using the garnet-biotite thermometer and GPMBQ barometer range from 540-650 ˚C and 5.5-8.7 kbars and are shown in Table 4. There is little intra-sample variability with maximum 1σ values for T of 40 ˚ C and for P of 800 bars. Calculations for the same assemblages using the garnet-chlorite exchange are plotted in Figure 25 and the data are listed in Table 5.There is also very little intrasample variation for these estimates. Generally, temperatures calculated with chlorite are 50 ˚ C lower than those calculated with biotite. Estimates for P and T using Berman's TWEEQU method show slightly higher P and T conditions (50 ˚C and 1 bar) and are listed in Table 6. These P-T conditions are thought to represent the peak metamorphic conditions for the textures that were observed in thin section, i.e., that they represent P-T conditions for reactions at the latest thermal maximum experienced by the samples. The proposed end-member reactions for garnet breakdown to biotite in the absence of staurolite are listed below.

4) Alm + Ms + Gross = Ann + 3 An

6) Py + Ms + Gross = Phl + 3 An

Positions for these two reactions are plotted in Figures 26 A-D. Slopes for reactions 4 and 6 are ≈ 45 bars/˚ C and 10 bars/˚ C respectively. This places biotite + anorthite on the low pressure or high temperature of these lines. The predicted garnet breakdown reaction from the petrogenetic grid of Spear and Cheney (1989) is

Grt + Chl + Ms→ Bt + St +H_2O.

The stability field for garnet + chlorite increases with increasing spessartine component in garnet and the position of this reaction lies roughly at the P-T conditions calculated for these samples. Petrographically chlorite appears to be closely related to growth of biotite. The proposed reaction, Grt + Chl + Ms → Bt + St + H_2O is not likely to have been the actual garnet breakdown reaction in these samples based on the petrographic evidence that chlorite overgrows garnet and that this texture is also observed in staurolite-free assemblages. Garnet breakdown to biotite or chlorite can be considered a retrograde reaction in that it appears to be late and that hydrous minerals have replaced non-hydrous minerals.

REGIONAL IMPLICATIONS

Hames and others (1991), working to the northwest of the area in this study, documented a zone of transition from Taconian infrastructure in the northwest to a predominantly Acadian infrastructure to the southeast. The area where Hames documented an Acadian overprinting of Taconian assemblages coincides with the "zone of retrogression" of Zen (1981) that was based on albitic overgrowths on more calcic plagioclase.

Although most samples from the present study do not show a great deal of textural complexity there is evidence for more than one episode of metamorphic mineral growth. Both in thin section and in compositional images, sample Np6 shows two distinct episodes of garnet growth. Texturally the cores of garnet grains have numerous quartz inclusions surrounded by rims that have a "dusty" appearance (Figure 4 E.). This textural break coincides with the compositional break in Ca content, in which the rim shows much higher Ca content than the cores (5 % Grs vs. 10% Grs). Similar textures were reported by Hames (1990) from garnets in the Walloomsac formation to the northwest of the study area and he interpreted to be part of the Taconian-Acadian overlap zone. Hames interpreted the garnet cores to be of Taconian age with Acadian overgrowths. Whitney and Tracy (1996) have suggested that garnets from the Taconic Range in NY and CT with similar textures may have undergone substantial fluid-aided recrystallization. They argued that with sufficient fracture densities garnets can recrystallize causing both textural and compositional perturbations. The analyzed sample from this study shows sharp euhedral bands of Y enrichment that fall inside the boundary between lower-Ca cores and high-Ca overgrowths, suggesting the likelihood of two separate episodes of garnet growth. The second phase of garnet growth was likely at higher pressure because it involved the breakdown of the anorthite component of plagioclase to produce grossular that was concentrated in the overgrowths.

Figure 27. Typical metamorphic field gradients for Eastern NY, western CT and MA

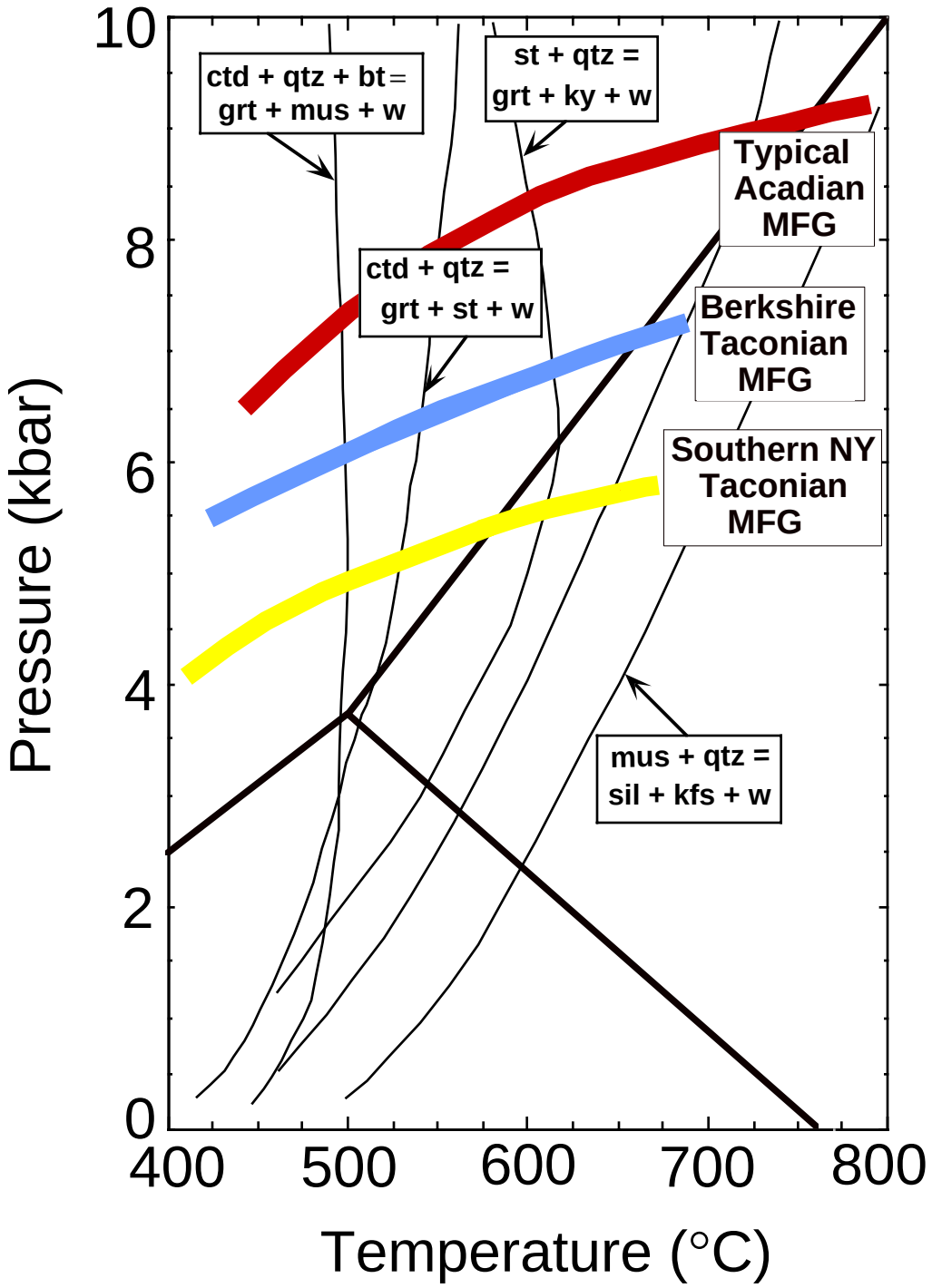

The majority of the garnet-bearing samples from the study area have garnet porphyroblasts that have been partially to completely overgrown by biotite and chlorite. This texture was also described by Agar (1936) and was interpreted to be a retrograde texture. These textures clearly postdate garnet growth, however, garnet rims have re-equilibrated with matrix minerals as discussed above. It is unclear whether or not this reaction was the result of a late stage Acadian metamorphism or if it may be an Acadian overprint on Taconian garnets.

Figure 27 shows typical Taconian and Acadian metamorphic field gradients for eastern NY State, Connecticut and Massachusetts (Tracy, 1996). P-T estimates for re-equilibration of garnet rims in the study area lie along the typical Acadian metamorphic field gradient. Sutter and others (1985) argued that along the western edge of the Acadian overprint zone metamorphic grades for both the Taconian and Acadian events are nearly equivalent and that ages of peak metamorphism can only be deciphered by Ar/Ar thermochronology. P-T estimates from this study show that typical Acadian high pressure overprinting is preserved as far west as Cameron's line.

CONCLUSIONS

A detailed analysis of mineral equilibria and compositional zoning for rocks east of Cameron's Line in western Connecticut indicates that garnet porphyroblast rims equilibrated with matrix minerals between 575-650 ˚ C and 6-9 kbars. These P-T conditions lie along a typical Acadian metamorphic field gradient for this area. Garnet porphyroblasts have been modified either by addition of overgrowths of biotite or by a second phase of garnet growth. For those grains that show two phases of growth, compositional images reveal patchy Ca content in rounded overgrowths surrounding more homogeneous euhedral cores. This is consistent with a second phase of growth of garnet at higher pressure accompanied by anorthite breakdown. Garnets that have been overgrown by biotite generally show compositional images indicative of continuous prograde growth with minor resetting along garnet rims. These overgrowths are thought to be the result of the compositionally complex reaction,

Grt + Ms → An + Bt.

Biotite overgrowths truncate compositional zoning for both major and trace elements and therefore postdates porphyroblast growth. Compositional images for these samples generally show euhedral zoning patterns suggesting that diffusion was very limited both during and after growth. Hames 1991 and others reported a very rapid initial uplift rates following peak Acadian metamorphism in this area

These data are consistent with those of Sutter and others in that they suggest a predominantly Acadian metamorphic signature. However, there is strong evidence that garnet porphyroblast predate these textures and thus may represent a resetting of Taconian garnet cores with matrix minerals during the Acadian.

Maximum P-T conditions (600 ˚ C and 9 kbars) were calculated for sample Np6 which lies in close proximity to Cameron's Line. If these P-T conditions represent the thermal maximum accompanying Acadian metamorphism, using a

geobarometric gradient of 300 bars/km this places a minimum of 30 km of overburden at the time of the Acadian metamorphism. Amenta and Mose (1985) argued that final movement on Cameron's Line could not have been any later than 440 Ma based on Rb-Sr isotopic evidence of cross-cutting plutons. These suggest; lack of motion during the Acadian and high P-T conditions during the Acadian suggest that there may also be considerable Acadian overprinting of Taconian T-3 isograds to the west of Cameron's Line as well.

REFERENCES

Agar, W.M., (1932) The petrology and structure of the Salisbury-Canaan district of Connecticut. American Journal of Science, v. 223, p.31-48.

Amenta, R.V. and Mose, D.G., (1985) Tectonic Implications of Rb-Sr ages of granitic plutons near Cameron's Line in Western Connecticut. Northeastern Geology, v. 7, n. 1, p. 111-19.

Armstrong, T.R., Tracy, R.J. and Hames, W.E. (1992) Contrasting styles Taconian, Eastern Acadian and western Acadian metamorphism, central and western New England. Journal of Metamorphic Geology, v. 10 p. 415-426.

Berman, R.G. (1988) Internally-consistent thermodynamic data for stoichiometric minerals in the system Na_2O-K_2O-CaO-MgO-FeO-Fe_2O_3-Al_2O_3-SiO_2-TiO_2-H_2O-CO_2. Journal of Petrology. V. 29 p. 445-522

Berman, R.G. (1991) Thermobarometry using multiequilibrium calculation: a new technique with petrologic applications. Canadian Mineralogist, v.29, pp. 833-855.

Berman R.G. (1990) Mixing properties of the Ca-Mg-Fe-Mn garnets. The American Mineralogist, v. 75, pp. 328-344.

Chatterjee, N.D. and Froese, E.F. (1975) A thermodynamic study of the pseudobinary join muscovite-paragonite in the system KALSi3O8-NaAlSi3O8-Al2O3-SiO2-H2O. American Mineralogist, v. 60, pp. 985-993.

Chernoff, C.B. and Carlson, W.D. (1997) Dissequilibrium for calcium during growth of pelitic garnet. Journal of Metamorphic Geology, v. 15, n. 4, p. 421-438.

Dickenson, M. P. and Hewitt, D.(1986) A garnet-chlorite geothermometer: Geol. Soc. Am. Abstracts with Programs, v. 18, p. 584.

Dietrich, J.H., (1968) Multiple folding in western Connecticut: A reinterpretation of structure in the Naugatuck-New Haven-Westport Area: Connecticut State Geological and Natural History Survey Guidebook 2, p. D-2, 1-13

Dietsch, C.W., (1988) The Geology of the Waterbury Dome, west-central Connecticut. Ph.D. dissertation, Yale University, 333p.

Dietsch, C.W. (1988) The Waterbury Dome, west-central Connecticut; a triple window exposing deeply deformed , multiple tectonic units. American Journal of Science. v. 289, n. 9, p. 1070-1097

Essene, E. J. The current status of thermobarometry. Cliff, J.S., Yardley, B.W.D. eds. Evolution of Metamorphic Belts. Geological Society Special Publication. N. 43, p. 1-44.

Ferry , J.M. and Spear, F.S. (1978) Experimental calibration of the partitioning of Fe and Mg between biotite and garnet. Contributions to Mineralogy and Petrology, v.66, p. 113-117.

Frost, R.B. and Tracy, R.J. (1991) P-T paths from zoned garnet: some minimum criteria. American Journal of Science, v. 291, pp.917-939.

Furman , M.L. and Lindsey, D.H., (1988) Ternary-feldspar modeling and thermometry. The American Mineralogist, v.73, pp. 201-216.

Gates R. M. (1952) The bedrock geology of the New Preston quadrangle; Connecticut Geologic and Natural History Survey Misc. Series 5. 46 p.

Hames, W.E. (1991) Multidisciplinary analysis of a polymetamorphic terrain, western New England. Ph. D. Dissertation, Virginia Tech. P. 249.

Hames, W.E., Tracy, R.J., Ratcliffe, N.M. and Sutter, J.S. (1991) Petrologic, structural and geochronologic characteristics of the Acadian metamorphic overprint of the Taconide Zone in part of southwestern New England. American Journal of Science. v. 291, pp. 887-913.

Hatch, N.L. Jr. (1988) Some revisions to the stratigraphy and structure of the Connecticut Valley trough, eastern Vermont. American Journal of Science, v. 17, p 727-730.

Hatcher, R.D. Jr. (1989) Tectonic synthesis of the U.S. Appalachians, in Hatcher, R.D. Jr., Thomas, W.A., and Viele, G.W., editors, The Appalachian-Ouachita orogen in the United States: Geological Society of America, The Geology of North America, v. F-2, p. 511-535.

Heinrich, Kurt F.J. (1981) Electron Beam X-ray Microanalysis. New York: Van Nostrand Reinhold and Company, 578 p.

Hickmott, D.D, Shimizu, N., Spear, F.S. and Selverstone, J. (1987) Trace-element zoning in a metamorphic garnet. Geology, V.15 pp. 573-576.

Hodges, K.V. and Crowley, P.D. (1985) Error estimation and empirical geothermometry for pelitic systems , American Mineralogist, v. 70 p.702-709.

Hodges, K.V. and Spear, F.S. (1982) Geothermometry and Geobarometry and the Al2SiO5 triple point at Mt. Mousilauke, New Hampshire. American Mineralogist, v.67, p. 1118-1134.

Hollister, L.S. (1966) Garnet Zoning: An interpretation based on Rayleigh fractionation model. Science, v. 154, p. 1747-1751.

Kretz, R. (1983) Symbols for rock-forming minerals. American Mineralogist, v. 68, p. 277-279

Lanzirotti, A., (1995) Yttrium zoning in metamorphic garnets, Geochimica et Cosmochimica, v. 59, n. 19, pp. 4105-4110.

Merguerian, C., (1983) Tectonic significance of Cameron's Line in the vicinity of the Hodges Mill complex: an imbricate thrust model for western Connecticut. American Journal of Science, v. 283, n. 4, pp. 341-368.

McMullin, D., Berman, R.G., and Greenwood, H.J. (1991) Calibration of the SGAB thermobarometer for pelitic rocks using data from phase equilibria and natural assemblages. Canadian Mineralogist, v.29, pp. 889-908.

Miller S.J. (1990)High pressure Acadian metamorphism of the Straits Schist, western Connecticut. MS Thesis, Virginia Tech. P. 90.

Perchuk, L.L., Podlesskii, K.K. and Aranovich, L.Y.(1991) Thermodynamics of some framework silicates and their equilibria: application to geothermobarometry, *In* Perchuk, L.L., ed. Progress in Metamorphic and Magmatic Petrology, A memorial volume in honor of D.S. Korzhinskiy: Cambridge Univ. Press, Cambridge, p. 131-164.

Rodgers, J. compiler (1985) Bedrock Geologic Map of Connecticut. Connecticut geologic and Natural History Survey, Scale 1:125,000. Two sheets.

Spear, F.S. and Cheney, J.T. (1989) A petrogenetic grid for pelitic schists in the system SiO2-Al2O3 - FeO - MgO - K2O - H2O. Contributions to Mineralogy and Petrology. V. 101, p. 149-164.

Stanley. R.S. and Ratcliffe, N.M., (1985) Tectonic synthesis of the Taconian Orogeny in western New England. Geological Society of America Bulletin, v.96, p. 1227-1250.

Sutter, J.F., Ratcliffe, N.M., and Mukasa, S.B. (1985) 40Ar/39Ar and K/Ar data bearing on the metamorphic and tectonic history of western New England. Geological Society of America Bulletin, v. 96, pp. 123-136.

Tracy, R. J. (1982) Compositional zoning and inclusions in metamorphic minerals. In Characterization of metamorphism through phase equilibria. Review in Mineralogy. V. 10, p. 355-397

Tracy, R.J, Hames W.E. and Whitney D.L. (1996) Ages, grade and extent of Taconian metamorphism from New York City to the Vermont-Massachusetts boundary. Geological Society of America, Northeast Section. Abstracts with Programs. V. 28, n.3, p.105

Tracy R.J., Robinson, P and Thompson, A.B. (1976) Garnet composition and zoning in the determination of temperature and pressure of metamorphism, central Massachusetts. American Mineralogist, v.61, pp. 762-775.

Thompson, A.B., (1976) Mineral reactions in pelitic rocks: II. Calculation of some P-T-X (Fe-Mg) phase relations. American Journal of Science, v. 276 p. 425-454.

Welch P.W., Tracy, R.J. and Solberg, T.N. (1998) Correlation of major and trace element zoning in metamorphic garnets. EOS, Transactions,American Geophysical Union.. v. 78, n. 6, p. F783

Whitney D.L. and Tracy, R.J. (1995) Garnets as open systems during metamorphism. Geological Society of America, Abstracts with Programs. V. 27, n. 6, p. 263

Zen, E-an (1972) The Taconide Zone and the Taconian Orogeny in the western part of the northern Appalachian Orogen. Geological Society of America, Special Paper 135, 72p.

Zen, E-an, editor, Goldsmith, R. Ratcliffe, N.M. Robinson, P. Stanley, R.S., compilers, (1983) Bedrock geologic Map of Massachusetts. : U.S. Geologic Survey, scale 1:250,000, 3 sheets.

Zen, E-an (1981) Metamorphism of slightly calcic pelitic rocks in and around the Taconic allochthon, southwestern Massachusetts and adjacent Connecticut and New York: U.S. Geologic Survey Professional Paper 1113, p.128.

VITA

Peter W. Welch was born in Nashua, New Hampshire on 31 August 1965. After many years at university he received a BS in geology from the University of New Hampshire in 1993 and was awarded the Tech Alumni Award for outstanding contributions to the Dept. of Earth Sciences. He remaimed at U.N.H. for one year to teach geology before he moved south and began graduate studies in metamorphic petrology at Virginia Tech. He was awarded an MS in geology form Virginia Tech in 1999. From there he moved to the deep south to continue his graduate studies at James Cook University in Queensland, Australia.